DOT/FAA/AR-95/85

Office of Aviation Research
Washington, D.C. 20591

ADVANCED PAVEMENT DESIGN: Finite Element Modeling for Rigid Pavement Joints Report I: Background Investigation

April 1997

Final Report

U.S. Department of Transportation
Federal Aviation Administration

NOTICE

Technical Report Documentation Page

1. Report No.	2. Government Accession No.	3. Recipient's Catalog No.
DOT/FAA/AR-95/85		

4. Title and Subtitle	5. Report Date
ADVANCED PAVEMENT DESIGN: Finite Element Modeling for Rigid Pavement Joints Report I: Background Investigation	April 1997
	6. Performing Organization Code
7. Author(s) Michael I. Hammons and Anastasios M. Ioannides	8. Performing Organization Report No.
9. Performing Organization Name and Address U.S. Army Engineer Waterways Experiment Station 3909 Halls Ferry Road Vicksburg, MS 39180-6199	10. Work Unit No. (TRAIS)
	11. Contract or Grant No. DTFA03-94-X-00010
12. Sponsoring Agency Name and Address U.S. Department of Transportation Federal Aviation Administration Office of Aviation Research Washington, DC 20591	13. Type of Report and Period Covered Final Report
	14. Sponsoring Agency Code AAR-410

15. Supplementary Notes

FAA William J. Hughes Technical Center Contract Officer (COTR) Technical Representative is Xiaogong Lee

16. Abstract

The objective of this research project is to develop an analytical model for rigid pavement joints that can be implemented into advanced pavement design models. This report documents a background investigation including a comprehensive review of rigid pavement joint models with particular emphasis on their joint and foundation modeling capabilities. The major historical developments in airport rigid pavement design are discussed. Closed-form solutions akin to those by Westergaard were derived in this study for the maximum responses on the unloaded side of a rigid pavement slab edge capable of a degree of load transfer. When used together with Westergaard's own closed-form equations for the free-edge problem, the formulae derived in this study constitute a complete solution of the edge load transfer problem, recognized over the years as a critical consideration in rigid pavement design. The newly derived solution is presented in convenient form for routine engineering application and is compared to earlier finite element data. The improvement in ease of application and precision is considerable.

17. Key Words		18. Distribution Statement
Analysis	Response models	Document is available to the public through the National Technical Information Service, Springfield, VA 22161
Design	Rigid pavements	
Joints	Testing	

19. Security Classif. (of this report)	20. Security Classif. (of this page)	21. No. of Pages	22. Price
Unclassified	Unclassified	107	

Form DOT F 1700.7

PREFACE

The research reported herein was sponsored by the U.S. Department of Transportation, Federal Aviation Administration (FAA), Airport Technology Branch, under Interagency Agreement DTFA03-94-X-00010 by the Airfields and Pavements Division (APD), Geotechnical Laboratory (GL), U.S. Army Engineer Waterways Experiment Station (WES), Vicksburg, Mississippi. Dr. Xiaogong Lee, Airport Technology Branch, FAA William J. Hughes Technical Center, was technical monitor. Dr. Satish Agrawal is Manager, Airport Technology Research and Development Branch.

This study was conducted under the general supervision of Dr. W. F. Marcuson III, Director, GL, and Dr. Albert J. Bush, Acting Chief, APD. This report was prepared under the direct supervision of Mr. T. W. Vollor, Chief, Materials Analysis Branch (MAB), APD. The project principal investigator was Mr. Michael I. Hammons, MAB. This report was written by Mr. Hammons. Dr. Anastasios M. Ioannides, Engineering Consultant to APD, assisted in the preparation of the chapter entitled "A Westergaard-Type Solution for the Load Transfer Problem." The assistance of Mr. Dan D. Mathews, APD; Ms. Vikki Edwards, APD; and Mr. Marlin Jones, contract student to APD, in preparing the manuscript for this report is gratefully acknowledged. The expert technical guidance of Dr. Raymond S. Rollings, Jr., APD, is also gratefully acknowledged.

The Director of WES during the preparation of this publication was Dr. Robert W. Whalin. The Commander and Deputy Director was COL Bruce K. Howard, EN.

TABLE OF CONTENTS

LIST OF ILLUSTRATIONS

LIST OF TABLES

EXECUTIVE SUMMARY

A rigid pavement system consists of a number of relatively thin Portland cement concrete slabs, finite in length and width, over one or more foundation layers. When a slab-on-grade is subjected to a wheel load, it develops bending stresses and distributes the load over the foundation. However, the response of these finite slabs is controlled by joint or edge discontinuities. By their nature, joints are structurally weakening components of the system. Thus, the response and effectiveness of joints are primary concerns in rigid pavement analysis and design.

Current FAA structural design criteria are based either upon the Westergaard response model or the layered elastic response model. Although available Westergaard solutions have been extensively used, they are limited by two significant shortcomings: (a) only a single slab panel is accommodated in the analysis; therefore, load transfer at joints is not accounted for, and (b) the layered nature of the pavement foundation is not explicitly reflected in the Winkler foundation model. Multilayered, linear elastic models, as used in the new FAA design method released in 1994, consider the complete layered system in the vertical direction, thereby addressing the second limitation. In the horizontal direction, however, the layers are assumed to be infinitely long with no discontinuities such as edges or joints. Consequently, the load transfer limitation remains unresolved.

Over the past two decades, several two-dimensional (2D) finite element analysis programs have been developed which incorporate load transfer at joints. These programs use a thin-plate element formulation for the slab. Some programs allow the user to choose from a library of foundation models. A few researchers have attempted to use three-dimensional (3D) finite element models for rigid pavement analysis including some load transfer mechanisms at the joint. Even state-of-the-art 2D finite element modeling involves, at least implicitly, assumptions which limit the precision of estimates concerning the load carried by each dowel. This problem is even further complicated by the interaction of loads from multiple-wheel landing gears. Adopting a 3D finite element model may clarify such issues further.

Closed-form solutions akin to those by Westergaard were derived in this study for the maximum responses on the unloaded side of a rigid pavement slab edge capable of a degree of load transfer. When used together with Westergaard's own closed-form equations for the free-edge problem, the formulae derived in this study constitute a complete solution of the edge load transfer problem, recognized over the years as a critical consideration in rigid pavement design. The newly derived solution is presented in convenient form for routine engineering application and is compared to earlier finite element data. The improvement in ease of application and precision is considerable.

INTRODUCTION

BACKGROUND.

The commercial aviation industry has responded to increased demand for air travel by developing longer, wider, and heavier aircraft with increasing numbers of wheels to support the aircraft while in ground operation. In order to maximize usable space for passengers and cargo, as well as to reduce weight, aircraft designers are developing landing gear layouts that are quite different from those on previous commercial aircraft. A new generation of such aircraft debuted in 1995 with the introduction of the Boeing B-777. The 2,630-kN (592,000-lb) B-777 features two main landing gear assemblies, each in a triple-tandem configuration. The McDonald-Douglas MD-12, which has growth versions of up to 5,780 kN (1,300,000 lb), is also envisioned in an effort to meet future air travel demands. These new generation aircraft may precipitate the requirement for adjustments to airport pavement thickness to ensure serviceable pavements over design lives of 20, 30, or even 40 years.

Many design criteria used by the Federal Aviation Administration (FAA) for rigid airport pavement thickness design have their origin in research conducted by the U.S. Army Corps of Engineers between 1941 and 1955. Current methods of selecting pavement thicknesses are based upon theoretical studies, small-scale model studies, full-scale accelerated traffic tests, and various other field studies, including monitoring of performance of in-service rigid airport pavements (Hutchinson, 1966). However, since 1955 aircraft landing gear geometry has become more complex as loads have continued to increase. In the 1970's, a series of accelerated traffic tests were conducted to verify extrapolations beyond the original experimental database for specific loads and conditions (Ahlvin, 1971). Recent development of new-generation aircraft has caused some concerns regarding the adequacy and applicability of current methods of structural design for airport pavements.

The response model which forms the basis for the FAA rigid pavement structural design procedure is the Westergaard idealization. In 1926, Westergaard developed a method for computing the response of rigid pavement slabs-on-grade subjected to wheel loads by modeling the pavement as a thin, infinite or semi-infinite plate resting on a bed of springs (Westergaard, 1926). Although available Westergaard solutions have been extensively used, they are limited by two significant shortcomings: (a) only a single slab panel is accommodated in the analysis; therefore, load transfer at joints is not accounted for, and (b) the layered nature of the pavement foundation is not explicitly reflected in the Winkler foundation model. Multilayered, linear elastic models, as used in the new FAA design method released in 1994, consider the complete layered system in the vertical direction, thereby addressing the second limitation (Parker et al., 1979). In the horizontal direction, however, the layers are assumed to be infinitely long with no discontinuities such as edges or joints. Consequently, the load transfer limitation remains unresolved.

Advances in electronic computing have revolutionized modern society, and the practice of engineering has benefited from much of this revolution. The finite element modeling technique has matured as a powerful and efficient analysis tool for boundary value problems in engineering. For over twenty years, pavement engineers have realized the potential of three-dimensional (3D) finite element analyses of jointed concrete pavements. The slab-joint-foundation system for

a rigid pavement is 3D in nature; thus, comprehensive representation of this system requires a 3D analytical approach.

OBJECTIVE.

The objective of this research is to develop an analytical model for concrete pavement joints that can be readily implemented into advanced pavement design models currently under development by the FAA. The basic criteria to be used for this model development will be (a) soundness of the theory and (b) precision of the model consistent with the requirements of the FAA pavement design model. The model developed should be capable of modeling the slab-joint-foundation system and serve as an analytical stepping stone to increased understanding of the behavior of rigid pavement systems. By judiciously applying this increased understanding of behavior, improved design criteria can be developed resulting in enhanced rigid pavement performance in the field.

The objectives listed above will be accomplished by completing the following tasks:

1. Task 1: Review and Evaluation of Existing Joint Models.
2. Task 2: Perform a Response and Sensitivity Analysis of Rigid Pavement Systems.
3. Task 3: Develop a General 3D Analytical Model.
4. Task 4: Perform Laboratory-Scale Testing.
5. Task 5: Model Application.
6. Task 6: Model Simplification for Implementation into FAA Design Procedures.

SCOPE.

This report describes the Task 1 effort to review and evaluate existing rigid pavement models with particular emphasis on their joint and foundation modeling capabilities. Also, yet unpublished small-scale model data developed by the Corps of Engineers in the 1950's is documented and analyzed using modern techniques. A closed-form solution for rigid pavement response based upon the Westergaard assumptions coupled with an elastic connection at the joint is presented and discussed.

PROBLEM STATEMENT

THE RIGID PAVEMENT SYSTEM.

A rigid pavement system consists of a number of relatively thin Portland cement concrete slabs, finite in length and width, over one or more foundation layers. Figure 1 shows a representation of a typical rigid pavement system subjected to a static loading. When a slab-on-grade is subjected to a wheel load, it develops bending stresses and distributes the load over the foundation. However, the response of these finite slabs is controlled by joint or edge discontinuities. By their nature, joints are structurally weakening components of the system. Thus, the response and effectiveness of joints are primary concerns in rigid pavement analysis and design.

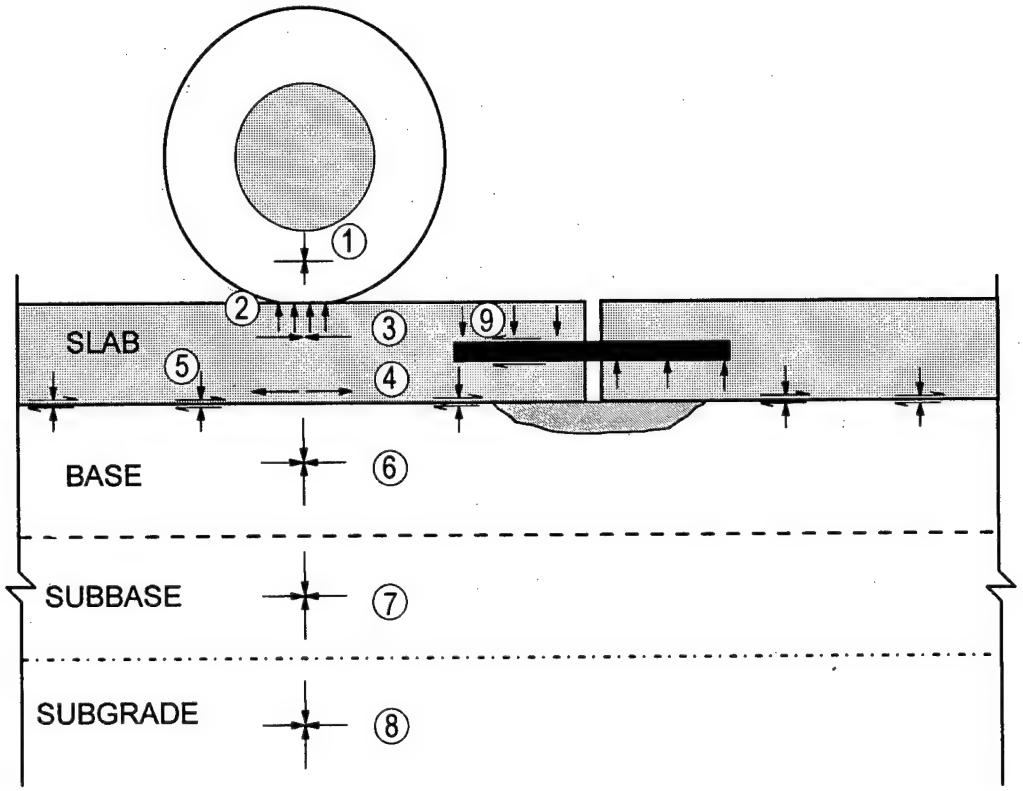

1. Tire Pressure
2. Bearing Stresses Caused by Tire
3. Flexural Stresses (Compression)
4. Flexural Stresses (Tension)
5. Stresses at the Slab-Base Interface
6. Vertical and Horizontal Stresses (Base)
7. Vertical and Horizontal Stresses (Subbase)
8. Vertical and Horizontal Stresses (Subgrade)
9. Stresses at Concrete-Dowel Interface

FIGURE 1. TYPICAL RIGID PAVEMENT SYSTEM
(AFTER LARRALDE AND CHEN, 1985)

Figure 2 presents a conceptual view of the mechanism of load transfer at a joint. The concept of load transfer is very simple: stresses and deflections in a loaded slab are reduced if a portion of the load is transferred to an adjacent slab. Load transfer is very important and fundamental to the FAA rigid pavement design procedure. Load transfer is a complex mechanism that can vary with concrete pavement temperature, age, moisture content, construction quality, magnitude and repetition of load, and type of joint (Hammons, Pittman, and Mathews, 1995).

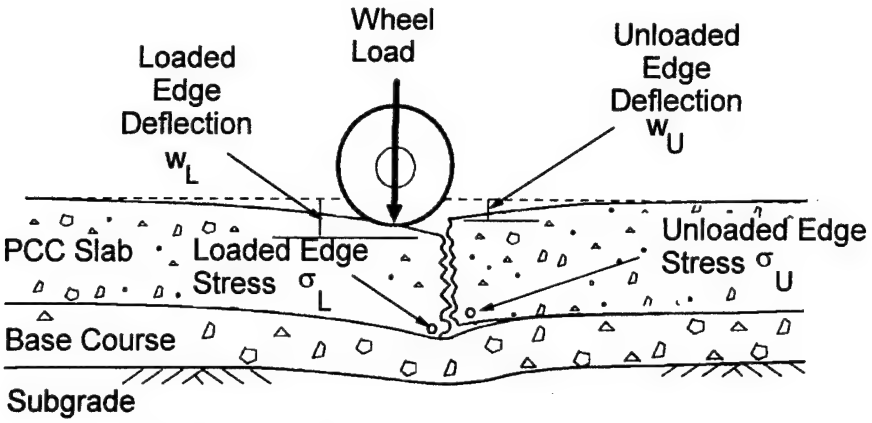

FIGURE 2. CONCEPT OF LOAD TRANSFER

When a joint is capable of transferring load, statics dictate that the total load (P) must be equal to the sum of that portion of the load supported by the loaded slab (P_L) and the portion of the load supported by the unloaded slab (P_U), i.e.,

$$P_L + P_U = P \tag{1}$$

Load may be transferred across a joint by shear or bending moments. However, it has been commonly argued that load transfer is primarily caused by vertical shear. In either case the following relationship applies:

$$\sigma_L + \sigma_U = \sigma_f \tag{2}$$

where σ_L is the maximum bending stress in the loaded slab, σ_U is the maximum bending stress in the adjacent unloaded slab, and σ_f is the maximum bending stress for the free-edge loading condition.

Because maximum slab deflections are also directly proportional to applied load under the stated conditions, it follows from equation 1 that

$$W_L + W_U = W_f \tag{3}$$

where w_L is the maximum edge deflection of the loaded slab, w_U is the maximum edge deflection of the adjacent unloaded slab, and w_f is the maximum edge deflection with no joint.

LOAD TRANSFER DEFINITIONS.

Deflection load transfer efficiency (LTE_δ) is defined as the ratio of the deflection of the unloaded slab (w_U) to the deflection of the loaded slab (w_L) as follows:

$$LTE_\delta = \frac{w_U}{w_L} \tag{4}$$

Similarly, stress load transfer efficiency (LTE_σ) is defined as the ratio of the edge stress in the unloaded slab to edge stress in the loaded slab as follows:

$$LTE_\sigma = \frac{\sigma_U}{\sigma_L} \tag{5}$$

Load transfer (LT) in the FAA rigid pavement design procedure is defined as that portion the edge stress that is carried by the adjacent unloaded slab:

$$\begin{aligned} LT &= \left(\frac{\sigma_U}{\sigma_E}\right) = \left(\frac{\sigma_E \quad \sigma_L}{\sigma_E}\right) \\ &= \left(1 \quad \frac{\sigma_L}{\sigma_E}\right) \end{aligned} \tag{6}$$

It should be noted from the above equations that the range of LTE_δ and LTE_σ is from zero to one, while the range of LT is from zero to one half. Equation 6 can be related to equation 5 as follows:

$$LT = \frac{LTE_\sigma}{1 + LTE_\sigma} \tag{7}$$

The FAA design procedure prescribes $LT = 0.25$, effectively reducing the design stress and allowing a reduced slab thickness. This accepted value is primarily based upon test sections trafficked from the mid-1940's to the mid-1950's. If the load transfer assumption is violated through a degradation of the joint system, the pavement life can be significantly reduced as illustrated by the example shown in figure 3.

Load transfer at joints is accomplished by three primary load transfer mechanisms: dowel bars, aggregate interlock, and keyways. *Dowel bars* are often placed across a joint to provide load transfer through dowel action and to maintain slab alignment. Dowels are smooth, round bars with the bond intentionally broken on one end to allow longitudinal movement of the slabs. As shown in table 1, FAA Design Circular AC 150/5320-6C prescribes the diameter, length, and spacing of dowel bars based upon pavement thickness (FAA, 1978). *Aggregate interlock* is a load transfer mechanism that relies on shear forces developed at the rough vertical interface of a concrete pavement joint. These shear forces are caused by mechanical interlock between the rough vertical surfaces of the joint and by sliding friction. Specially designed *keyways* may be formed in adjacent slabs at a joint to augment load transfer caused by aggregate interlock. The dimensions of the keyway depend upon the slab thickness. The FAA does not allow keyed joints for pavements less than 23 cm (9 in.) thick or for pavements on low strength subgrades (foundation modulus less than 54 MPa/m (200 pci)) when the traffic mix contains wide-body jet aircraft (FAA, 1978).

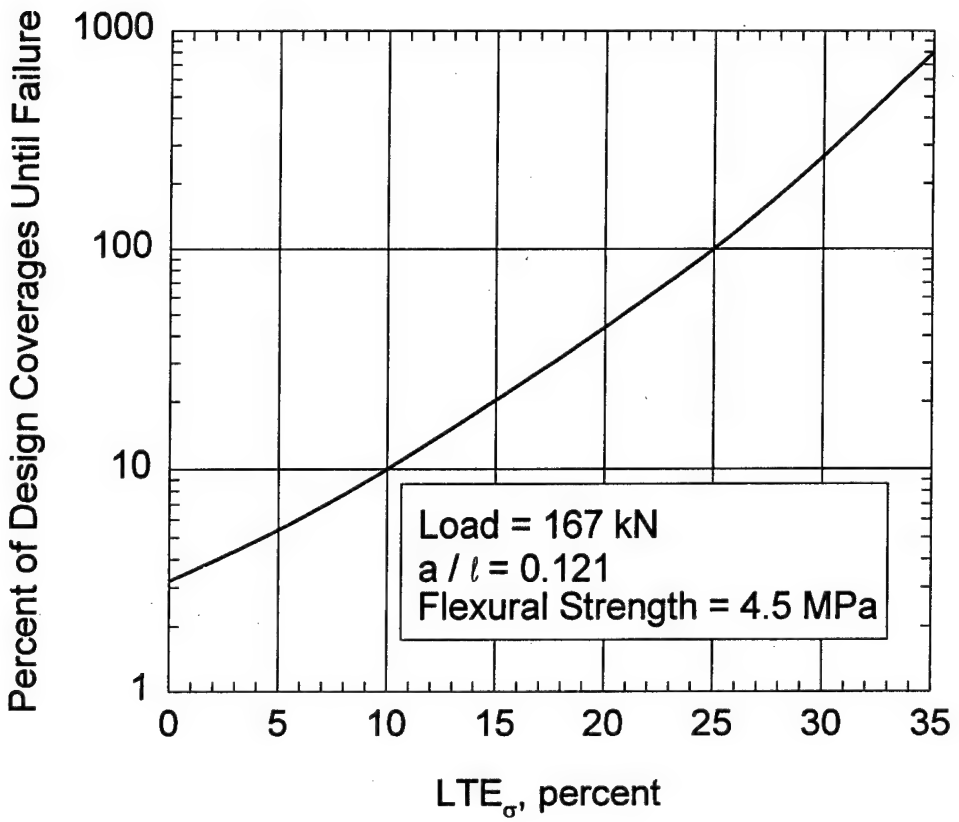

FIGURE 3. EFFECT OF LOAD TRANSFER EFFICIENCY ON PAVEMENT PERFORMANCE (HAMMONS, PITTMAN, AND MATHEWS, 1995)

TABLE 1. DIMENSIONS AND SPACINGS OF STEEL DOWELS (FAA, 1978)

Thickness of Slab	Diameter	Length	Spacing
6-7 in. (15-18 cm)	3/4 in. (20 mm)	18 in. (46 cm)	12 in. (31 cm)
8-12 in. (21-31 cm)	1 in. (25 mm)	19 in. (46 cm)	12 in. (31 cm)
13-16 in. (33-41 cm)	1 1/4 in. (30 mm)	20 in. (51 cm)	15 in. (38 cm)
17-20 in. (43-51 cm)	1 1/2 in. (40 mm)	20 in. (51 cm)	18 in. (46 cm)
21-24 in. (54-61 cm)	2 in. (50 mm)	24 in. (61 cm)	18 in. (46 cm)

Deformed steel bars, often called *tie bars*, can be placed across the joint (normal to the plane of the joint) to hold the slab faces in intimate contact. The bond between the concrete and the bar develops in both slabs; thus movement normal to the joint is restrained. Diameter, length, and spacing of tie bars is fixed by the FAA design criteria. Design Circular AC 150/5320-6C

prescribes that tie bars shall be 16 cm (5/8 in.) in diameter and 76 cm (30 in.) long and spaced at 76 cm (30 in.) on center (FAA, 1978). Load transfer due to dowel action of tie bars is small in comparison to that provided by dowel bars.

The three major types of joints are contraction joints, construction joints, and expansion joints. *Contraction joints*, used to control cracking in the concrete and to limit curling and warping stresses in the slab, are formed by introducing a weakened plane into the concrete and allowing a crack to form at the weakened plane. Typically, the weakened plane is created by sawing a groove in the concrete while it is curing. Contraction joints may be plain (often called dummy joints), doweled, or tied (often called hinged joints). *Construction joints* are required between lanes of paving or where it is necessary to stop construction within a paving lane. The two most common types of load transfer devices in construction joints are dowels and keyways. *Expansion joints* are used at the intersections of pavements with structures and in some cases within pavements. Their primary purpose is to relieve compressive stresses induced by expansion of the concrete caused by temperature and moisture changes. Expansion joints may be doweled or thickened edge. To obtain load transfer at an expansion joint, a load transfer device is required (usually a dowel bar).

RIGID PAVEMENT FOUNDATIONS.

The slab may be placed directly on the subgrade; however, most current practice has slabs placed on a unbound or bound base course. Such base course layers in airport pavements may be constructed to (a) provide uniform bearing support for the pavement slab; (b) to replace soft, highly compressible or expansive soils; (c) to protect the subgrade from frost effects; (d) to produce a suitable surface for operating construction equipment; (e) to improve foundation strength; (f) to prevent subgrade pumping; and (g) to provide drainage of water from under the pavement. An unbound base course may be a densely graded granular material or an open-graded or free-draining granular material. The base may be bound with Portland cement, a lime-fly ash blend, bitumen, or other agent.

One or more subbases may be present in the pavement system. These subbases may be a lesser quality granular material and may be chemically stabilized. The subbase provides additional strength to the pavement system, provides more uniform support over variable soil conditions, and may provide protection against frost damage and swelling.

The subgrade is the naturally occurring soil, compacted naturally occurring soil, or compacted fill. It may be subject to pumping, frost damage, or swelling. Subgrade soils will have very different values of strength depending on their soil classification, moisture conditions, and compaction.

MODEL REQUIREMENTS.

Mechanistic pavement design requires an analytical model to realistically predict the stresses, strains, and displacements of the concrete slabs and the supporting layers. The analytical model must also be able to capture the effects of various changes in the pavement features on the stresses, strains, and deflections. Tabatabaie, Barenberg, and Smith (1979) defined a list of

capabilities they deemed necessary features of an analytical model for jointed concrete pavements as follows:

1. Capability to model a rigid pavement with a stabilized base or overlay.

2. Capability to model a rigid pavement with nonuniform slab thicknesses and nonuniform subgrade support.

3. Capability to model the effect of the loss of subgrade support.

4. Capability to model the effect of different load transfer systems.

5. Capability to calculate localized stresses at the joints.

6. Capability to model the effect of slippage and separation at the joints.

7. Capability to predict partial shear and moment transfer at the joints or cracks.

Tabatabaie, Barenberg, and Smith (1979) identified the finite element method as the being capable of analyzing all seven of the conditions listed above.

In addition to the seven capabilities identified above, an eighth capability should be investigated for an analytical model for rigid pavement joints: the ability to incorporate advanced foundation models. Ioannides (1984) stated the rigid pavement problem belongs to a class of problems known as soil-structure interaction problems which lie at the interface between structural and geotechnical engineering. Chatti (1992) concluded:

> The accuracy of the total model depends strongly on the accuracy of predicting the response of the soil supporting medium. In other words, the total model will lead to erroneous results if the foundation is modeled incorrectly regardless of how good the structural (slab) model is.

HISTORICAL BACKGROUND

GENERAL.

Many of the design criteria used by the FAA for rigid airport pavements have their origin in research conducted by the U.S. Army Corps of Engineers between 1941 and 1955 (Hutchinson, 1966). When the Corps was assigned responsibility for design and construction of military airfields in November 1940, two major problems became immediately apparent. First, new heavy bomber aircraft, such as the B-17 Flying Fortress and B-24 Liberator, had maximum gross weights of 333 kN (75,000 lb) and produced single wheel main gear loadings of 156 kN (35,000 lb), three to five times greater than any highway or airport loadings previously encountered. The second and equally important problem was a lack of rational and valid design procedures by which rigid pavements could be designed to carry heavily loaded aircraft (Sale and Hutchinson, 1959). These problems were exacerbated during and after World War II as the

loadings upon rigid pavements continued to increase due to the development of even heavier bomber aircraft, including the propeller-driven B-29 and B-36 as well as the B-47 and B-52 jet bomber aircraft.

The technical issues faced by the early Corps' researchers were formidable. Many of the basic principles of airport pavement design accepted today concerning pavement response, design loadings, critical stresses, materials characterization, and others were not yet established in 1940. These technical questions included:

1. What is an appropriate response model for rigid airport pavements?

2. What are the critical stresses that the pavement must be designed to resist?

3. How should the subgrade be characterized for design? What type of tests should be conducted to characterize support provided by the subgrade?

4. Which loading is more severe: static loadings generated by fully-loaded aircraft at rest or dynamic loadings which occur at the point of touchdown during landing operations?

5. What effects do joints have on rigid pavement response and how should these be accommodated in design criteria?

6. How can pavements be designed to resist repeated heavy loads over a given design life?

7. What is an appropriate failure criteria?

8. What is the effect of aircraft wander?

To provide answers for these questions, the Corps embarked on an investigational program in 1941 with a four-tiered approach involving theoretical studies, small-scale model studies, full-scale accelerated test track and miscellaneous field studies, and condition surveys of existing rigid airfield pavements.

A review of the available design methodologies revealed that substantial variations existed in design criteria from agency to agency. Design methodologies commonly used by state agencies or foreign governments relied heavily on local experience, materials, and empiricisms developed from performance records within the agency's purview. It was apparent that research was required to develop criteria that could be universally applied for all conditions that might be encountered, whether in the United States or abroad. The criteria needed to be simple, practical, and uniform. The objectives of the investigational program, as stated by Sale and Hutchinson (1959), were as follows: (a) eliminate the use of untried methods; (b) insure adequately designed pavements; (c) provide methods not subject to variation occasioned by arbitrary cost differences of local competitive materials; (d) avoid reductions in pavement thickness in order to balance costs; and (e) establish procedures that would readily lend themselves to further development though tests, investigations, and study of actual pavement behavior. From these studies, criteria

were developed for plain and unreinforced concrete pavements as well as rigid and flexible overlays.

RESPONSE MODEL.

One of the first requirements in developing design criteria was to select an appropriate response model for rigid airport pavements. In 1926, Professor Harald M. Westergaard (1926) published a method for calculating stresses and deflections in rigid pavements. He assumed the slab to be a thin plate, the load to be circular, and the foundation a bed of springs. By 1941, Westergaard's method of calculating stresses was considered to be the most advanced method for predicting critical stresses and deflections in rigid pavements and was adopted as the response model for design (Sale, 1977). Although Westergaard considered the interior, corner, and edge loading cases in his early works, he concentrated on interior loadings. It was not until 1948 that he published relationships that were valid for computation of stresses caused by edge loading of large wheel loads on large contact areas (Westergaard, 1948). Westergaard's theory is described in more detail in a subsequent chapter of this report.

CRITICAL DESIGN STRESSES.

In 1941, the Corps began a series of static and dynamic load tests on concrete slabs at Wright Field, Dayton, Ohio, in part, to verify Westergaard's theory for airfield rigid pavement design (Sale and Hutchinson, 1959). A set of 6-m (20-ft) square slabs were constructed on a number of subgrades of different strength and tested to failure under static circular plate loadings. Also, dynamic loadings were generated by dropping aircraft tires onto the pavement. The test slabs were instrumented with strain and deflection gages. The basic conclusions from these tests were that the Westergaard formula accurately predicted the critical stresses at structural failure and that dynamic loadings produced no greater stresses than equivalent static loadings.

The Wright Field Slab Tests conclusively demonstrated that lesser loads produced structural cracking at edges and corners. Additional traffic tests at six airfields in 1942 and 1943 further confirmed that the interior load case was unconservative. Cracks transverse to the direction of traffic and corner breaks predominated, indicating that edge and corner stresses were more critical than interior stresses. Thus the design procedure produced by the Corps in 1943 included an empirically-determined design factor of 1.75 to accommodate the differences in allowable interior and edge loadings and fatigue resulting from repetitive loadings (Sale, 1977). The 1943 criteria also required load transfer devices or thickened edges at all construction and expansion joints in an attempt to enforce a balanced design between the stresses at the interior and edge (Ahlvin, 1991).

Tests with B-26 aircraft were conducted in 1941 at Dayton Municipal Airport, Ohio, to determine whether impact loadings during landing were more critical than static loadings. The runway was dusted with lime so that the width of the tread mark of the B-26 tire could be accurately measured at the point of touchdown. The width of these tread marks was correlated with the dynamic loading drop tests at Wright Field to estimate the magnitude of impact loadings. The results came as quite a surprise to those who had argued that dynamic loading at landing would be the critical load case. However, the Dayton tests proved that under normal

landing conditions the loads were only 40 to 60 percent of the static load. Under cases of hard landings, where the aircraft was literally flown into the ground, the dynamic loads were in the range of 150 to 200 percent of static loads. However, discussions with pilots indicated that hard landings of this sort would be indeed rare (Sale and Hutchinson, 1959).

ACCELERATED TRAFFIC TESTS.

The first of a series of accelerated traffic tests under controlled conditions was initiated at Lockbourne Army Airfield, Ohio, in June 1943. These ambitious tests were designed to permit a comprehensive evaluation of many of the factors influencing rigid pavement design. Each of the test items contained extensive strain and deflection measurements at slab interiors, edges, and corners.

The concept of coverages was introduced to account for aircraft wander over the pavement. Obviously, the width of the aircraft tires or landing gear is small compared to the overall width of the pavement, and the aircraft gear do not operate in the same path for each aircraft pass over the runway. By definition, one coverage is obtained when each point of the pavement surface has been subjected to one maximum stress repetition by the operating aircraft. This process is random, and is best described by a Gaussian distribution of aircraft gear across the width of the pavement feature. Studies were conducted at military airfields to determine the distribution of aircraft across various airfield features such as aprons, taxiways, and runways. At the time of the Lockbourne tests, 5,000 coverages was considered to be representative of a design life of 10 years.

Among the conclusions of the Lockbourne accelerated trafficking tests as summarized by Sale and Hutchinson (1959) were the following:

1. Stresses produced in a pavement slab by either traffic loadings or static loadings are more severe when the loading is applied at the corners and edges of a slab than when applied at the center.

2. The Westergaard edge load equations (developed in 1943 and published in final form by Westergaard in 1948) were valid for a single loading condition, but an additional design factor must applied to properly account for stress repetitions (fatigue), temperature gradients, and other unknown variables. In fact, strain measurements from the Lockbourne tests showed that the strains calculated by the Westergaard edge loading analytical model followed the shape and form of the test track measurements and gave conservative results. Therefore, the Corps revised its design criteria to edge stresses adopting a 25 percent load transfer at the joints. A design factor of 1.3 was used to account for stress repetitions up to 5,000 coverages. The design factor (DF) was defined as the ratio of the design flexural strength of the concrete (R) to the maximum free edge stress. In its most general form, the design factor is given by

$$DF = \frac{R}{(1 - LT) \times \sigma_E} \tag{8}$$

where σ_E is Westergaard's edge stress and *LT* is load transfer from equation 6 expressed as a fraction.

The design factor is not a safety factor *per se*, but takes into account the effects of repetitive loading (fatigue), cyclic stresses due to temperature and moisture changes, etc. The philosophical underpinnings of this approach are that the design factor has an initial value greater than one for design purposes but continually decreases with time and repetitive loading until a design factor of 1.0 is reached at the end of the pavement's design life. Then, the pavement will theoretically crack under the design loading. The introduction of steerable landing gear in the 1950's gave rise to a new challenge. Major failures of rigid pavements occurred as traffic became increasingly channelized. Thus, the Corps increased the design coverages from 5,000 to 30,000 with an increase in the design factor with increasing coverages.

SUBGRADE CHARACTERIZATION.

Westergaard never proposed a test method for the determining the modulus of subgrade reaction. The results of the Wright Field Slab Tests indicated that reasonable values of *k* could be obtained by dividing the magnitude of a vertical force acting on a circular load located in the interior of a slab by the volume of the resulting deflection basin. Stresses predicted by a Westergaard analysis using a value of *k* determined by this method were in good agreement with stresses calculated from strains measured in the tests. However, this method, which came to be known as the *Volumetric Displacement Method*, was unsuitable for design purposes, because it required constructing a test slab on a representative subgrade (Hutchinson, 1966, Ahlvin, 1991). In 1942, a series of plate bearing tests were conducted on each subgrade for the Wright Field Slab Tests with plates varying in diameter from 300 mm (12 in.) to 1,800 mm (72 in.). These tests showed that *k* values determined by a 760-mm (30-in.) -diameter plate were in close agreement with *k* values determined from the volumetric displacement method (Sale and Hutchinson, 1959). This plate bearing test, with minor variations, is still in use today to determine the modulus of subgrade reaction for pavement design.

The adequacy of the plate bearing test method has been questioned repeatedly in the past. One of the primary shortcomings of the test is that it requires a representative subgrade to be prepared before an accurate subgrade modulus can be obtained. The use of thick base courses and stabilized layers presents an obvious problem. However, one of the advantages of the plate bearing test is that it is a measure of the elastic (and plastic) properties of the soil at a unit loading which is approximately equal to that which the soil will be subjected to by an aircraft loading on the pavement (Hutchinson, 1966). It can also be shown that the design pavement thickness is not particularly sensitive to typical variations in *k*, and therefore, the plate bearing value is considered adequate for pavement design purposes.

RIGID PAVEMENT JOINTS.

Early experiences with highways had shown the importance of tying rigid pavement slabs together to prevent separation at the joints. Typically, deformed steel reinforcing bars were used in highway construction. However, an additional benefit was discovered: some load transfer was provided at the joint. Because highway slabs were being designed for interior loads, this

advantage was not immediately appreciated. Later, as it became apparent that edge loadings were more critical than interior loadings, highway engineers began to construct rigid pavements with thickened slabs near edges and joints. This practice was carried over into the first Corps' rigid pavement design procedure in 1943 (Hutchinson, 1966).

Early work of the Corps showed that the design thickness of pavements was controlled by the tensile stresses that occurred at the edges of the pavement slabs. This work also indicated that the edge stresses were reduced by properly designed load transfer devices at the joints. Thus, thinner, more economical pavements could be produced that would have satisfactory performance. Because load transfer devices reduced differential vertical movements at the joints, a second benefit was realized in terms of improved surface smoothness. Table 2 summarizes some of the values of load transfer from full-scale accelerated trafficking tests and in-service pavements. These values of load transfer were calculated from analysis of deflection and strain measurements made on the slabs.

TABLE 2. SUMMARY OF CORPS OF ENGINEERS LOAD TRANSFER MEASUREMENTS FOR FULL-SCALE TEST SECTIONS AND IN-SERVICE PAVEMENTS (ROLLINGS, 1989)

Type of Joint	Number of Data Points	Load Transfer, Percent		
		Range	Mean	Coefficient of Variation
Contraction joint with aggregate interlock	46	15.6-50.0	37.2	19.2
Doweled contraction joint	4	28.2-42.8	35.1	17.3
Doweled construction joint	195	0.0-50.0	30.6	38.0
Doweled expansion joint	15	15.4-42.6	30.5	24.4
Tied contraction joint	6	23.9-34.8	29.2	13.4
Tied key joint	2	25.6-26.1	25.8	----
Keyed joint	61	5.6-49.0	25.4	41.4
Lockbourne free (butt) joint	8	5.8-24.5	15.5	40.9

Based upon the performance of the test items in the Lockbourne No. 2 Test Track and upon measured deflections and strains, the following ranking of joint types from the most to least effective in terms of load transfer was made (Sale and Hutchinson, 1959):

1. Doweled contraction joint
2. Doweled construction joint
3. Keyed construction joint with tie bars
4. Contraction joint
5. Keyed construction joint
6. Doweled expansion joint
7. Free-edge expansion joint

For doweled joints in thick concrete pavements, it was found that there was no apparent advantage in using structural shapes over conventional round bars.

Observations at the test tracks at Lockbourne and later at Sharonville, Ohio, indicated that load transfer at doweled joints varied with the methods of construction. At both Lockbourne and Sharonville, the concrete slabs were cast against forms, and the dowels were locked into place in the forms. At Lockbourne, the dowels were installed by bonding one end in the concrete, pulling the forms off over the dowels, painting and greasing the exposed half of the dowel, and then paving the adjacent lane. At Sharonville the dowels were installed by painting and greasing the end of the dowel in the first paving lane, turning and removing the dowel, removing the forms, reinserting the painted and greased end of the dowels into the same hole from which they were removed, and bonding the exposed end of the dowel into the adjacent lane. Strain gages and deflection gages were installed in the pavements on each side of the joints at both test tracks. A load cart with a twin tandem assembly was used to load the track in each case. The results of these tests can be summarized as follows:

1. The construction method used as Lockbourne provided superior load transfer to that used at Sharonville.

2. At Lockbourne the greatest load transfer was observed when the load was applied on the edge of the slab having the painted and greased dowel end. It was speculated that this was caused the void created by build up of paint under the unbonded dowel (figure 4a). When load was applied to the slab containing the bonded end, the unbonded end did not make contact with the concrete and contribute to load transfer until some amount of deflection occurred. Conversely, at Sharonville, the greatest load transfer was observed when the load was applied to slab containing the bonded end of the dowel. Again, it was speculated the turning and removal of the dowel created looseness. When the dowel was reinserted, it lay on the bottom of the hole, thus creating a void at the crown of the painted and greased end (figure 4b). As a result, the load on the slab containing the painted and greased end of the dowel deflected an amount equal to the void at the top of the dowel before any load was transferred to the adjacent slab. Thus, it was the recommended that the dowels be installed with no manipulation of the dowel after concrete was placed to maximize the load transfer obtained by the doweled joint.

3. Load transfer across doweled joints resulted in edge stress reduction greater than 25 percent.

4. The load transfer computed from deflections was more than the load transfer computed from strains.

5. The load transfer across joints in multilayer pavements is about the same as load transfer in single slab construction.

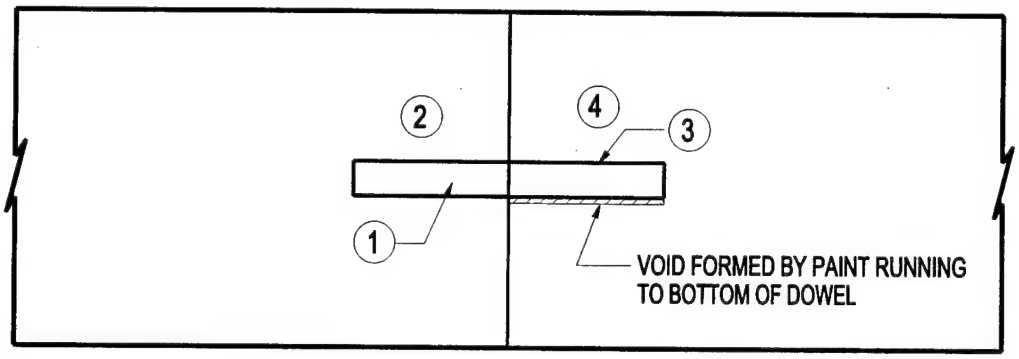

CONSTRUCTION SEQUENCE

1. DOWEL ANCHORED FIRMLY TO FORM.
2. PAVEMENT PLACED AND BONDED TO END OF DOWEL.
3. FORM REMOVED OVER DOWEL, EXPOSED END OF DOWEL PAINTED AND GREASED.
4. ADJACENT PAVEMENT PLACED.

(a) Lockbourne test track

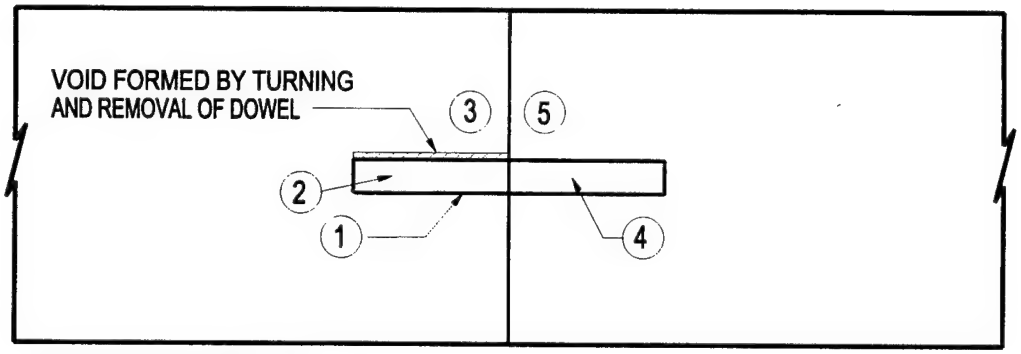

CONSTRUCTION SEQUENCE

1. DOWEL PAINTED AND GREASED.
2. DOWEL ANCHORED FIRMLY IN FORM.
3. PAVEMENT PLACED AND UNBONDED TO END OF DOWEL.
4. DOWEL TURNED TO PREVENT BOND, REMOVED, FORM REMOVED AND DOWEL REINSERTED INTO SAME HOLE.
5. ADJACENT PAVING LANE PLACED.

(b) Sharonville test track

FIGURE 4. DOWEL INSTALLATIONS AT LOCKBOURNE AND SHARONVILLE TEST TRACKS

A review of the unpublished minutes of the All-Division Meeting on Doweled Joints held at the Ohio River Division Laboratories in September 1958 revealed that it was the opinion of the Corps' rigid pavement experts that the doweled construction joint provided the best performance of the commonly used joint types. The available performance data up to that point revealed that

the 25 percent load transfer value used in design was conservative for doweled joints. Indeed, it was a topic of discussion that the load transfer assumption could perhaps be increased for doweled joints allowing a thinner pavement to be constructed. It was the opinion of these experts that perhaps load transfer values of 35 to 40 percent might be appropriate for doweled joints. However, it is important to note that these experts were cognizant of the importance of careful construction procedures in obtaining load transfer. The minutes of the meeting contain this direct quote:

> We must realize that we do not, as yet, have sufficient information to accurately evaluate the amount of load transfer that is obtained from the various methods of construction [of doweled joints], therefore, for the time being, we must be conservative and continue to use the assumed 25 percent. This does not mean, however, that we can relax our construction requirements. We must insist on good dowel installations, and we must keep the dowel looseness to a minimum if we are to ever realize the benefits of the doweled joint, because performance of the joints now being constructed will play an important role in any future work we may do along this line. Otherwise, if through looseness, we fail to obtain the better load transfer, we may as well not use the more expensive doweled joint.

After World War II, aircraft loadings continued to increase. To accommodate these increasing demands on the pavement, aircraft manufacturers added more wheels to the landing gear to achieve wheel loadings sufficient to permit usage on existing pavements. These multiple-wheel gear loadings over an entire slab raised doubts about the adequacy of the assumptions concerning interior and edge loadings on slabs assumed to extend to infinity. The advent of the Lockheed C5-A military transport and the Boeing B-747 commercial aircraft with loads twice as heavy as their predecessors lead to Multiple-Wheel Heavy Gear Load (MWHGL) Pavement Tests conducted at the U.S. Army Engineer Waterways Experiment Station in the late 1960's and early 1970's (Ahlvin, 1971; Burns, 1971; Ledbetter, 1971a, 1971b). A rigid pavement test track was trafficked as a part of the MWHGL tests. The track was constructed in two 7.6-m (25-ft) -wide lanes separated by a longitudinal keyed construction joint. The keyway was formed using metal strips. All transverse joints were weakened plane contraction joints. The following four test items were constructed so that failures would be expected from a few weeks to a few years under normal operating conditions and traffic volumes.

Item	Thickness
1	25 cm (10 in.)
2	30 cm (12 in.)
3	36 cm (14 in.)
4	20 cm (8 in.)

The subgrade was a lean clay soil compacted 95 percent of the modified density at optimum water content. The modulus of subgrade reaction was approximately 27 MPa/m (100 psi/in).

A 12-wheel load cart, each wheel loaded to 133 kN (30,000 lb) for a total load of 1,600 kN (360,000 lb), was used to traffic the test track in such a way as to obtain edge loading along the longitudinal keyed joint.

The results of these tests raised questions about the applicability of the keyed construction joint for heavy loads on low-strength subgrades. Observations made from test pits excavated after trafficking indicated that the keyed joint had failed either by shearing the key or by spalling of the bottom portion of the keyway. A distinct increase in deflection was observed when the keyway sheared. The failure of both the male and female portions of the keyed joints were taken as evidence of optimum geometry of the keyed joint. No inferences concerning the performance of keyed joints on a stiff subgrade could be made.

The performance of the transverse weakened plane contraction joints was considered adequate. Little, if any, faulting was observed. An examination of the exposed faces of the joints in the test pits did not reveal excessive deterioration of the aggregate interlock.

CLASSICAL RESPONSE MODELS

WESTERGAARD THEORY.

Professor H. M. Westergaard published a series of papers containing relationships for calculating stresses in rigid pavements based upon the theory of elasticity. His pioneering work was first published in Danish in 1923 (Westergaard, 1923). However, this work was not widely read, and in 1926, he published a method in English for calculating the stresses in a rigid pavement (Westergaard, 1926). He developed relationships for stresses

> ...by assuming the slab to act as a homogeneous, isotropic, elastic solid in equilibrium, and by assuming that the reactions of the subgrade to be vertical only and to be proportional to the deflections of the slab (Westergaard, 1926).

Westergaard characterized the subgrade by the *modulus of subgrade reaction* (k), which is a measure of the stiffness of the subgrade and has units of force per area per unit deflection or force/length^3. An important term in the Westergaard theory which quantifies the stiffness of the slab relative to that of the subgrade, called the *radius of relative stiffness*, is expressed by the following relationship:

$$\ell = \sqrt[4]{\frac{Eh^3}{12(1 - \mu^2)K}} \tag{9}$$

where

E = modulus of elasticity of concrete
h = thickness of slab
μ = Poisson's ratio of concrete

Assuming the response of the slab to be that of a plate on a bed of springs (Winkler foundation), Westergaard solved for the dimensionless ratio $\sigma h^2/P$ as a function of dimensionless ratio a/ℓ where σ is the maximum stress, P is the magnitude of the applied load, and a is the radius of the circular loaded area for the following three cases:

1. Wheel load close to the corner of a semi-infinite slab.
2. Wheel load at the interior of an infinite slab.
3. Wheel load at the edge of a semi-infinite slab.

Westergaard considered two cases for the edge load case: the tire load distributed over the area of a full circle or the entire load distributed over the area of a semicircle, as would be a more severe case if the tire were operating on the very edge of the pavement with no support under half of the tire.

In 1932, the Bureau of Public Roads conducted the Arlington Road Tests at Arlington, Virginia, using Westergaard's theory as a basis for planning the tests. Following these tests, Westergaard modified his 1926 formulae to reflect the conditions and results of the tests (Westergaard, 1933). Westergaard extended his procedures to airfield pavements in 1939. Again, Westergaard revised his formulae, this time to account for the larger contact area of aircraft tires (Westergaard, 1939). By 1941, Westergaard's method of calculating stresses was considered to be the most advanced method for predicting critical stresses and deflections in rigid pavements and was adopted as the response model for design (Sale, 1977). Although Westergaard considered the interior, corner, and edge loading cases in his early works, he concentrated on interior loadings. Ioannides, Thompson, and Barenberg (1985) found that several of the equations ascribed to Westergaard in the literature are incorrect due to typographical errors or misapplication. They also reported that the 1926 equation for edge loading was incorrect.

It was not until 1948 that he published relationships that were valid for computation of stresses caused by edge loading of large wheel loads on large contact areas (Westergaard, 1948). His revised formulas allowed the load to be characterized as an ellipse rather than being limited to a circular tire print. Ioannides, Thompson, and Barenberg (1985) recommended the use of these equations as being more accurate than the 1926 equations.

RESPONSE CHARTS. Pickett and Ray (1951) developed a graphical solution of the Westergaard theory in the form of influence charts. These graphical solutions greatly simplified the determination of theoretical deflections and moments caused by wheel loads on slabs. Influence charts were presented for four different load cases: interior loading assuming a dense liquid subgrade, interior loading assuming an elastic solid subgrade, edge loading assuming a dense liquid subgrade, and load placed at $\ell/2$ from an edge assuming a liquid subgrade. Stresses can be calculated from the moment read from the chart by dividing by the section modulus, defined as $h^2/6$. In a separate paper, Pickett et al. (1951) presented sixteen additional influence charts for deflection, moment, and reactive pressures under interior, near edge, and near center loadings on slabs for liquid, elastic solid, and elastic layer subgrades.

The first step in applying the influence chart involves solving for the radius of relative stiffness of the pavement section. The scale for the chart is then set according to the value of the radius of relative stiffness, and the tire print to be analyzed is subsequently drawn to this scale. The number of blocks (including partial blocks) covered by the tire print are counted and multiplied by the appropriate relationship to obtain either moment, deflection, or reactive pressure.

Because of their simplicity, the FAA, U.S. Army, and U.S. Air Force adopted the influence charts for the computation of maximum tensile stress for edge loading (Hutchinson 1966). Multiple-wheel gear assemblies can be analyzed with the charts simply by drawing them to the appropriate scale and counting the blocks covered by the tire print. However, it should be noted that the orientation of the gear must be positioned such that the maximum number of blocks is covered to calculate the maximum stress or deflection.

COMPUTERIZED SOLUTIONS. A few computerized solutions to the Westergaard theory have been developed, most notably the programs H-51, H51-ES, and PDILB (commonly referred to as the PCA AIRPORT program). The H-51 program, originally developed by General Dynamics Corporation and modified by WES, calculates the edge stress under multiple-wheel loads on a slab supported by a dense liquid foundation. The solution is essentially a computerized version of Pickett and Ray's response charts. The program allows the user to place the gear at any number of different orientations and positions to calculate the maximum stress condition. H-51 was modified by Ioannides (1984) by incorporating an elastic solid foundation in the program H51-ES. The PCA AIRPORT program is based upon Westergaard's theory for loads at the interior of an infinite slab supported by a dense liquid foundation. This program also allows multiple-wheel assemblies and allows the user to orient the gear to maximize the response.

Each of these programs are based upon and subject to the limitations of the Westergaard assumptions. However, as with the response charts, the computerized solutions allow the calculations of stresses caused by multiple-wheel gear.

WESTERGAARD THEORY LIMITATIONS. For nearly three-quarters of a century, Westergaard's theory has been used to calculate the response of rigid pavements to wheel loads. His theory is relatively simple to apply and has been accepted as accurate. However, there are several limitations as discussed below.

1. All pavement layers below the slab must be represented by a single parameter, the modulus of subgrade reaction. A typical pavement may have several layers of materials including unbound or bound subbases and base courses with each overlying layer having an increase in quality and stiffness. In a typical application of Westergaard's theory to such a system, these layers are modeled by an increased modulus of subgrade reaction intended to give an equivalent response. However, this clearly leads to a decrease in exactness of the analysis caused by a limitation in the model.

2. The foundation must always respond linear elastically. Few subgrade, subbase, or base materials are truly linear-elastic materials. In fact, most are nonlinear, stress dependent,

and change with time and environment. The effect of nonlinear, stress-dependent material behavior on rigid pavement foundations is obscure.

3. Westergaard assumed the slab to be in full contact with the subgrade at all points. Thus the boundary conditions are violated if a void develops due to pumping or if the slab and subgrade separate due to curling and warping.

4. Westergaard assumed that the slabs were infinite (for the interior load case) or semi-infinite (for the edge and corner load cases); that is, the slabs extend far enough from the loaded area that boundaries (discontinuities such as cracks or joints) have no effect on the solution. In actual practice this may not be the case, because rigid pavement slabs tend to be relatively narrow and have many cracks and joints.

5. Load transfer cannot be directly modeled. For airport pavement design, load transfer is set at a constant 25 percent; thus edge stresses are reduced by that amount in calculating the design factor. These values have been related to performance in field test sections to formulate design criteria. But clearly, a more rational, mechanical method of analyzing load transfer is warranted for mechanistic evaluation of rigid pavements.

6. The thickness of the slab must be uniform. This assumption makes it impossible to analyze slabs with thickened edges or other slabs of nonuniform thickness.

ELASTIC LAYER MODELS.

The elastic layer theory was first formulated for a concentrated load and one layer by Boussinesq and later generalized for a uniformly distributed load acting on a circular area and to two or more layers by others. Manual solutions of one- or two-layer elastic systems subjected to one circular load are cumbersome at best. Computerized solutions have made it possible to analyze a system of many layers subjected to multiple loads. Among these programs are the BISAR, CHEVRON, and JULEA programs (Barker and Gonzalez, 1991).

The basic assumptions of the elastic layer theory are as follows:

1. All materials in the system are assumed to be homogeneous, isotropic, and linear elastic; thus, each pavement layer can be represented by three parameters: thickness, modulus of elasticity, and Poisson's ratio. Each layer may have different elastic properties.

2. Each layer is infinite in horizontal extent, and the bottom layer extends vertically to infinity.

3. The load is static and is uniformly distributed over one or more circular areas. Most programs assume the load to be entirely vertical, although some can accommodate horizontal components.

4. The layers are continuously in contact. Also, the degree of restraint between adjacent layers must be assumed. Common assumptions are that adjacent layers are fully bonded or that they are frictionless. Some programs can allow any degree of restraint between these two extremes.

In the past several years, layered elastic design models for rigid pavements have been developed. The U.S. Army and Air Force have developed design guidance for elastic layered design methodologies for both rigid and flexible pavements (Departments of Army and Air Force 1988, 1989). The Federal Aviation Administration has adopted an alternative design procedure (known as LEDFAA) based on a layered elastic theory. For rigid pavements, the basic design principle is to limit the tensile stresses in the slab to a level sufficiently below the concrete flexural strength so that failure (cracking) occurs after some significant number of load repetitions. Rigid and flexible overlays of rigid pavements can be accommodated in the design model.

Because of the assumptions of the layered elastic model, certain limitations are intrinsic:

1. The model assumes each layer to be infinite in horizontal extent; therefore, joints and cracks in rigid pavements are ignored. Even the base and subbase layers in a pavement are not infinite in horizontal extent. Stabilized layers may also develop cracks which cannot be modeled.

2. The model assumes each material to be linear elastic. This assumption may lead to inconsistencies in stress calculations in the foundation layers. For example, it is not possible for an unbound granular layer to carry significant tensile stresses; yet the layered elastic model may predict such stresses.

MODELS FOR DOWEL STRESSES.

For over three-quarters of a century, dowels have been used as load transfer devices in jointed concrete pavements. Dowel bars are thought to prevent faulting, reduce pumping, and reduce corner breaks. However, the design of dowels is based mostly on experience. Most design procedure prescribe the diameter, length, and spacing of dowel bars based upon pavement thickness.

The major types of distresses exhibited by doweled joints are faulting, spalling, corner cracking, and lockup. Lockup of doweled joints causes the opening of transverse cracks which subsequently deteriorate.

Dowels located at some distance away from the point of application of the load are not as effective in transferring load as those that are closer. The number of dowels effective in distributing the load has been debated since the early developments of rigid pavement modeling. Westergaard (1928) concluded that only the first couple of dowels on either side of the load are effective in transferring load. Based upon the Westergaard's theory, Friberg (1940) noted that for loadings a considerable distance from any edge, the maximum positive moment occurs beneath the load, and the maximum negative moment occurs a distance of $1.8\,\ell$ from the point of loading. Beyond $1.8\,\ell$, sometimes referred to as the effective length (e), the moment changes very little.

Friberg concluded, therefore, that the influence of dowel shear beyond that point is negligible as follows:

> The effective dowel shear decreases inversely as the distance of the dowel from the point of loading, to zero at a distance of 1.8ℓ. No dowels beyond that point influence the moment at the load point.

Friberg's assumption of linear decrease of transferred shear force with distance appears realistic and has been widely accepted (Ioannides and Korovesis, 1992). Kushing and Fremont (1940) accepted Friberg's linear assumption but postulated that the effective length, e, could be as great as $\pi\ell$. Finite element studies led Tabatabaie (1978) to conclude that the linear assumption of Friberg was appropriate but that the effective length was 1.0ℓ. The above conclusions are appropriate for a single-wheel loading only; multiple wheel gear configurations will lead to different values of the effective length.

It is thought that bearing stresses under the dowel are responsible for spalling and looseness of the dowels. Analytical models for determining the bearing stresses in dowel bars have been in existence since the late 1930's. Several investigators have presented formulae for calculating the concrete bearing stresses (Friberg, 1940; Tabatabaie, 1978; Ioannides et al., 1990). According to Ioannides et al. (1990), all of these formulations for bearing stress (σ_b) may be represented by the following relationship:

$$\sigma_b = A\ (structural) \times B(load) \tag{10}$$

The first term, A, is determined from the structural characteristics of the pavement system, while the second term, B, quantifies the transferred load.

Friberg (1940) presented an analysis of stresses in doweled joints based upon the work of Timoshenko and Lessels (1925). His analysis was based upon considering the dowel as a semi-infinite beam on a Winkler foundation. His basic relationship for dowel stresses was

$$\sigma_b = Ky_o \tag{11}$$

where K is the modulus of dowel support and y_0 is the deflection of the dowel with respect to the concrete at the face of the joint. Friberg's analysis of dowel bar support is shown in figure 5.

Friberg's relationship for the maximum deformation of concrete under a dowel bar with a shear force P is

$$y_o = \frac{P}{4\beta^3 E_d I_d}(2+\beta\omega) \tag{12}$$

where

ω = joint opening
E_d = modulus of elasticity of the dowel
I_d = moment of inertia of dowel bar
β = relative stiffness of the dowel-concrete system.

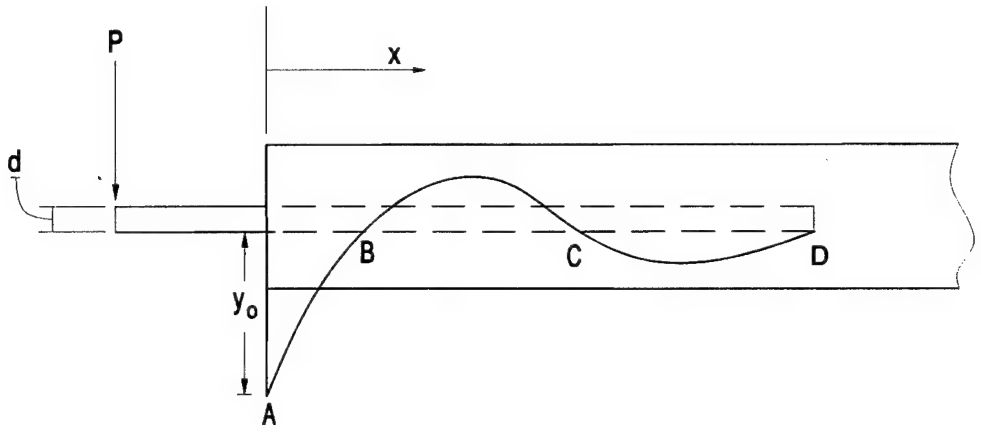

(a) Deflection diagram

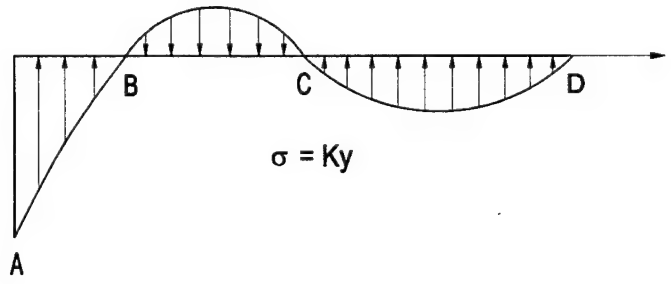

(b) Stress diagram

FIGURE 5. FRIBERG'S (1940) ANALYSIS OF DOWEL BAR SUPPORT

Friberg adopted Timoshenko's definition of the relative stiffness of a bar embedded in concrete as

$$\beta = \sqrt[4]{\frac{K\omega}{4 E_d I_d}} \qquad (13)$$

The bearing stress on the concrete at the joint face then becomes

$$\sigma_b = \frac{KP}{4\beta^3 E_d I_d}(2+\beta\omega) \tag{14}$$

Grinter (1931) reported that the value of K depended on the modulus of the slab concrete, the thickness of the slab, and the modulus of subgrade reaction. Reported values of K vary greatly. Tabatabaie (1978) reported finding values in the literature from 0.08×10^6 to 8.6×10^6 MPa/m (0.3×10^6 to 32 x 10^6 psi/in.). The value typically assumed is 0.41×10^6 MPa/m (1.5×10^6 psi/in.). Ioannides and Korovesis (1992) developed a procedure for backcalculating K from measured values of LTE_δ obtained using the a falling-weight deflectometer (FWD), Benkelman beam, etc.

FINITE DIFFERENCE MODEL.

Although not as general and flexible as the finite element method, finite difference techniques have been used in the analysis of rigid pavements. Prior to the 1960's, the finite difference technique was a commonly used numerical technique. One of the more attractive features of the finite difference technique is that it generally requires fewer computer resources than the finite element method. With the coming of faster computers with additional memory, this feature has become less important.

Ioannides (1988) described a finite difference solution for a plate on an elastic foundation. His program, called FIDES, is based on the Boussinesq equation for the deflection due to a concentrated load on the surface of an elastic half space. The upper surface of an elastic solid foundation is divided into a number of squares. Concentrated loads can be applied at the center of each square, and the equations of equilibrium for a plate on an elastic solid are enforced. Using this method slab bending stresses, subgrade stresses, and deflections can be calculated. Ioannides used this approach to develop predictive equations for deflection, subgrade stress, and bending stress in the slab for the edge and corner loading conditions.

The finite difference model lacks some of the basic attributes necessary for contending as a powerful rigid pavements analysis method. Cracks and joints cannot be modeled. The pavement foundation is modeled as an elastic solid; thus nonlinear response is not considered. The various layers in the pavement (subgrade, subbase, base course) must be modeled as a single material, characterized by a single modulus of elasticity and Poisson's ratio. There are also no provisions to allow separation of the slab and the underlying foundation, as may happen due to curling and warping of the slab.

FINITE ELEMENT RESPONSE MODELS

GENERAL.

The finite element method is a powerful numerical analysis technique that has been successfully used to solve a broad class of boundary value problems in engineering. With the development of the high-speed digital computer, finite element techniques have been applied to a variety of problems in pavement analysis. The finite element method's ability to model joint and edge discontinuities has led to its emergence as the analysis method of choice for rigid pavement research (Chatti, 1992).

Table 3 presents an overview of certain key attributes of the more common finite element programs applied to rigid pavements as reported in the literature. These finite element programs can be characterized in two general categories by their representation of the slab model as either (a) 2D medium-thick plate elements or (b) 3D continuum elements.

TABLE 3. OVERVIEW OF FINITE ELEMENT MODELS FOR RIGID PAVEMENTS

Program Name	Slab Model	Load Transfer	Foundation Model(s)
ILLI-SLAB (Tabatabaie, 1978)	2D medium-thick plate	Linear spring, beam element on spring foundation	Dense liquid, Boussinesq, nonlinear resilient, two- and three-parameter models
JSLAB (Tayabji and Colley, 1984)	2D medium-thick plate	Linear spring, beam element on spring foundation	Dense liquid
WESLIQID (Chou, 1981) and KENSLABS (Huang and Wang, 1973)	2D medium-thick plate	Linear springs	Dense liquid
WESLAYER (Chou, 1981) and KENLAYER (Huang, 1993)	2D medium-thick plate	Linear springs	Layered elastic
FEACONS III (Wy et al., 1973)	2D medium-thick plate	Linear and torsional springs	Dense liquid (linear and nonlinear springs)
GEOSYS (Ioannides et al., 1986)	3D brick element	None	3D brick elements with stress-dependent subgrade model
ABAQUS (Kuo, 1994)	2D shell element 3D brick element	Linear and nonlinear springs, interface elements, gap elements, multipoint constraints, explicit models	Dense liquid, 3D brick element with linear and nonlinear elastic, plastic, and viscoelastic constitutive models, user-defined models

TWO-DIMENSIONAL FINITE ELEMENT MODELS.

A number of finite element programs featuring the use of a 2D medium-thick plate model for the concrete slab have been developed and reported in the literature in recent years. These include ILLI-SLAB, JSLAB, KENSLABS, WESLIQID, FEACONS III, KENLAYER, WESLAYER, and RIGMUL. Each of the programs has similarities, yet certain key features (such as mechanics of the joint and available foundation models) vary. Some of the programs allow the user to choose the foundation model from a library of available models. Each of the programs incorporates load transfer capabilities with some differences in the philosophy and mechanics of the load transfer model.

All of the 2D plate programs model the slab using a 2D medium-thick plate element. A number or references describe the formulation of this element, such as Zienkiewicz and Cheung (1967) and Tabatabaie (1978). This four-noded plate bending element has dimensions of $2a$ by $2b$, as illustrated in figure 6. Each node has three degrees of freedom: a displacement w in the z direction, a rotation θ_x about the x axis, and a rotation θ_y about the y axis. The following assumptions are made for this element:

1. The plate element is assumed to be isotropic, elastic, and homogeneous.

2. Transverse loads are carried by flexure rather than by in-plane forces (thin-plate theory) or by transverse shear (thick-plate theory).

3. Lines normal to the middle surface in the undeformed plate remain straight, unstretched, and normal to the middle surface of the deformed plate.

4. Each lamina parallel to the middle surface is in a state of plane stress, and no axial or in-plane shear stress develops due to loading.

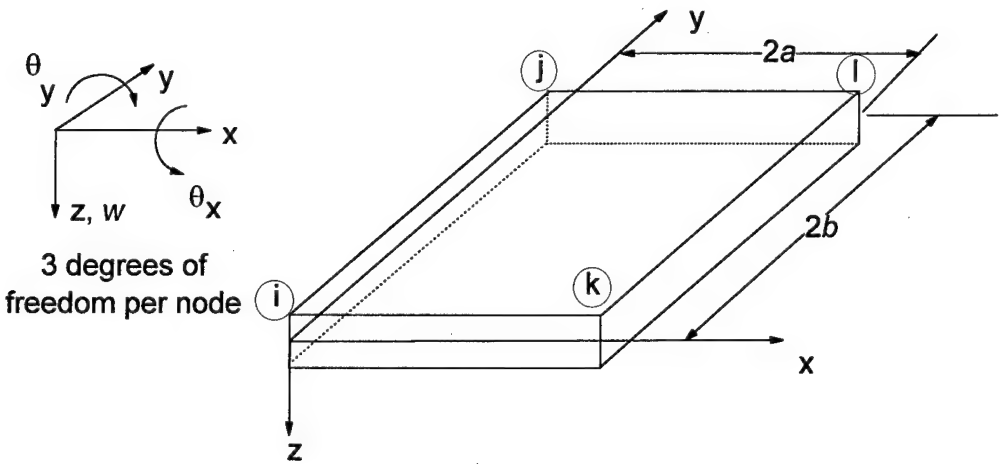

FIGURE 6. FOUR-NODE PLATE BENDING ELEMENT

ILLI-SLAB. ILLI-SLAB is the most widely used and verified of the 2D medium-thick plate finite element programs. Originally developed at the University of Illinois by Tabatabaie (1978), ILLI-SLAB has been enhanced by adding a variety of foundation models (Ioannides, 1984; Khazanovich and Ioannides, 1993) and by adding the capability to include temperature loadings (Korovesis 1990). It was extended by Chatti (1992) at the University of California at Berkeley to a new dynamic computer program called DYNA-SLAB for the analysis of jointed concrete pavements with load transfer systems at joints subjected to moving transient loads. Larralde and Chen (1985) presented a method of analysis including fatigue based on ILLI-SLAB. Majadzadeh et al. (1981) coupled the slab and load transfer models in ILLI-SLAB with a three-layer elastic foundation model developed by Huang (1974) to formulate the finite element program RIGMUL.

The basic assumptions made by Tabatabaie (1978) in the initial development of ILLI-SLAB are as follows:

1. Medium-thick plate theory (as previously described) can be used to model the slab, overlay, or stabilized base.

2. The subgrade behaves as a Winkler foundation.

3. In case of a bonded stabilized base or overlay, there is full strain compatibility at the interface. In the case of an unbonded base or overlay, the shear stresses at the interface are neglected.

4. The dowel bars at joints behave like a linear-elastic material and are located at the neutral axis of the slab.

5. When an aggregate interlock or a keyway is used as the load transfer system, the load is transferred from one slab to an adjacent one by means of shear. However, when dowel bars are used as the load transfer system, moment as well as shear may be transferred across the joints.

Figure 7 shows the finite element model used by Tabatabaie. The rectangular plate element was employed to model the two-layer slab system (figure 7a). For the case in which the two layers are bonded, the transformed section technique was used to develop an equivalent layer (figure 8). The subgrade modeled was a dense liquid or Winkler foundation characterized by the modulus of subgrade reaction (k). The value of k can be varied spatially from node to node by the user.

Figure 9 shows the concept of how ILLI-SLAB models joint load transfer. A pure shear (aggregate interlock) load transfer mechanism is modeled by a linear spring element at each node along the joint face (figure 7c). The spring element features one degree of freedom per node: w, the displacement in the z direction. The spring constant (called an aggregate interlock factor, AGG) is input by the user and is indicative of the stiffness of the joint. The value of the aggregate interlock factor can be estimated by backcalculating it from field tests. Ioannides and Korovesis (1990) presented an S-shaped curve defining a relationship between joint efficiency and a dimensionless joint stiffness ($AGG/k\ell$) shown in figure 10. This curve shows that any

value of joint efficiency from zero to 100 percent can be calculated with an appropriate choice of aggregate interlock factor or vice versa. Dowel bars are modeled by a two-node bar element (figure 7b) having one, two, or three degrees of freedom per node: a displacement w in the z direction and a rotation θ_y about the y axis, and a torsion θ_x about x axis. A vertical spring element (figure 7c) is employed to model the relative deformation of the dowel bar and the surrounding concrete. The spring element extends between the dowel bar and the surrounding concrete at the joint face. The dowel bars are located at the neutral axis of the slab and are assumed to have the same deflection and slope at the joint face as the slab's neutral axis.

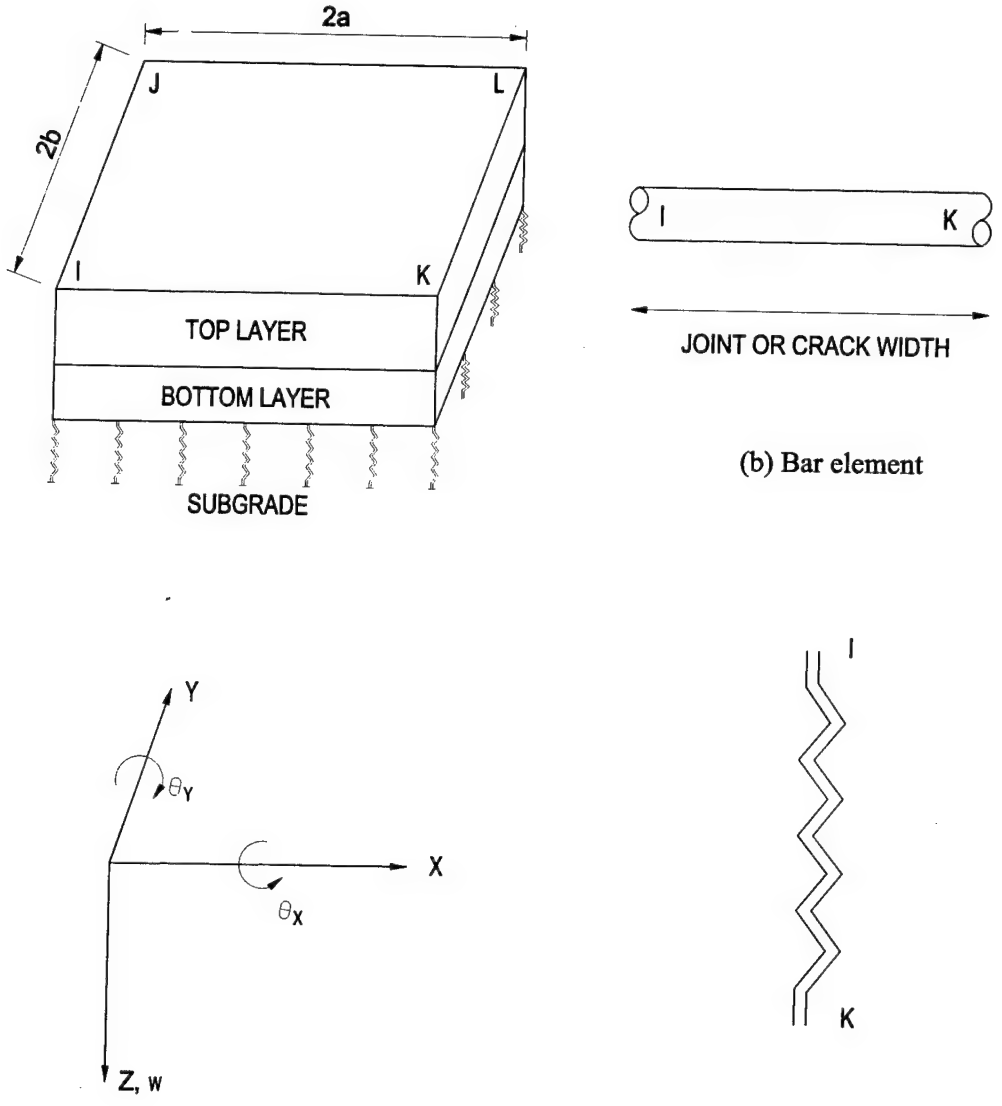

FIGURE 7. FINITE ELEMENT MODEL IN ILLI-SLAB
(AFTER TABATABAIE, 1978)

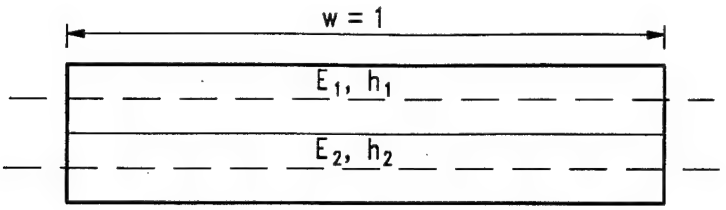

(a) Two bonded layers

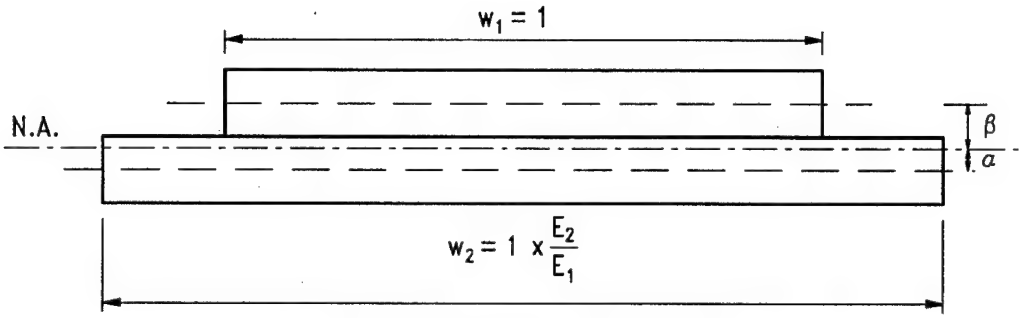

(b) Equivalent section of modulus E_1

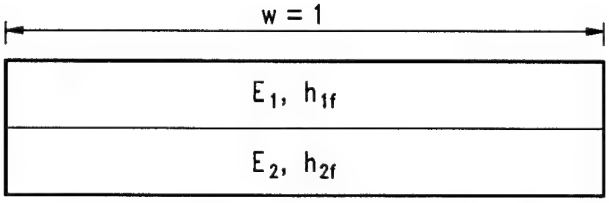

(c) Equivalent system of two unbonded layers

FIGURE 8. EQUIVALENT SECTIONS FOR A TWO-LAYER SYSTEM (AFTER KOROVESIS, 1990)

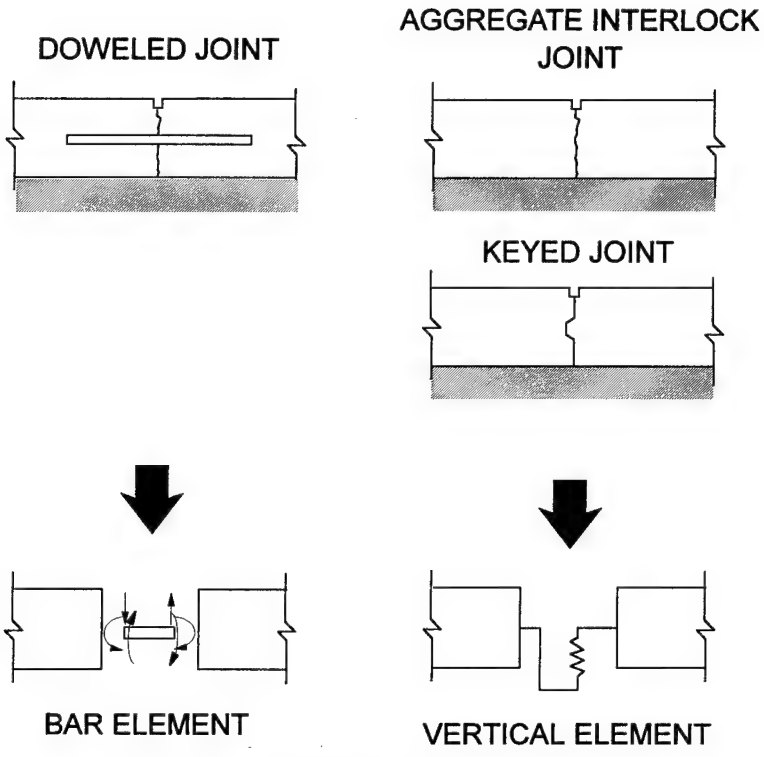

FIGURE 9. ILLI-SLAB JOINT MODEL
(AFTER LARRALDE AND CHEN, 1985)

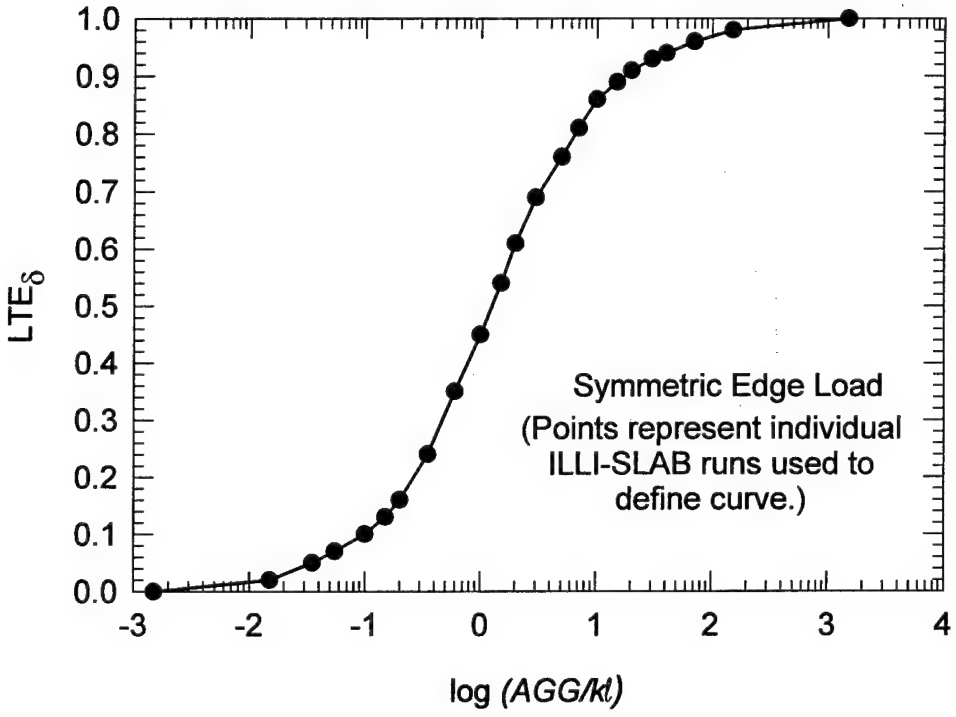

FIGURE 10. JOINT EFFICIENCY AS A FUNCTION OF DIMENSIONLESS JOINT STIFFNESS FOR AGGREGATE INTERLOCK JOINT
(AFTER IOANNIDES AND KOROVESIS, 1990)

Ioannides and Korovesis (1992) also developed the concept of a dimensionless joint stiffness for the doweled joint expressed by the quotient $D/sk\ell$ where s is the dowel spacing and D is the stiffness of the vertical spring element. The value of D depends upon the vertical stiffness caused by the support by the concrete, called the dowel-concrete interaction (DCI), and a vertical stiffness caused by beam bending. These two spring stiffnesses are summed as springs in series as follows:

$$D = \frac{1}{\frac{1}{DCI} + \frac{1}{12C}} \tag{15}$$

The value of DCI is based on assuming the dowel to be a beam on a spring foundation (Friberg analysis) and is given by the following relationship:

$$DCI = \frac{4\beta^3}{(2+\beta\omega)} E_d I_d \tag{16}$$

where ω is the width of the joint opening. Comparing this relationship with equation 12 reveals that DCI is identical with the ratio P/y_o in the Friberg analysis and has units of force/length. The term β is defined by Friberg in equation 13. The term C in equation 15 is defined by the relationship

$$C = \frac{E_d I_d}{\omega^3(1+\phi)} \tag{17}$$

where

$$\phi = \frac{12 E_d I_d}{G_d A_z \omega^2} \tag{18}$$

G_s is the shear modulus of the dowel bar as defined by

$$G_d = \frac{E_d}{2(1+\mu_d)} \tag{19}$$

The term A_z is the effective cross-sectional area in shear and is assumed to be 0.9 times the circular area as follows:

$$A_z = 0.9\left(\frac{\pi d^2}{4}\right) \tag{20}$$

A plot of joint efficiency as a function of dimensionless doweled joint stiffness is presented in figure 11. As with the aggregate interlock factor, any value of joint efficiency from zero to 100 percent can be obtained by appropriate choice of the joint stiffness.

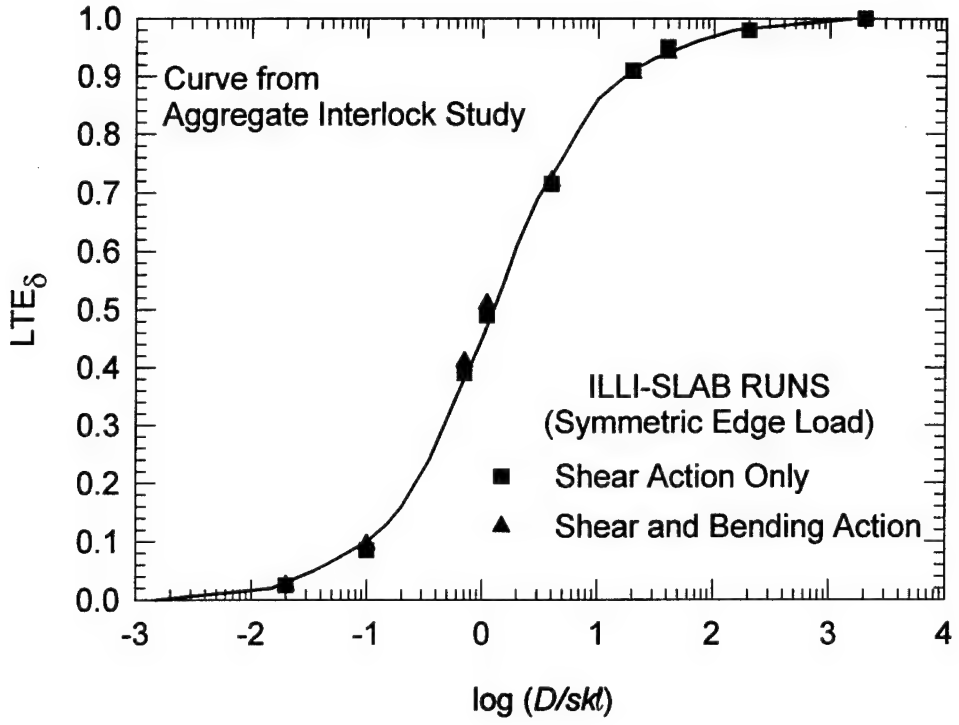

FIGURE 11. JOINT EFFICIENCY AS A FUNCTION OF DIMENSIONLESS JOINT STIFFNESS FOR DOWELED JOINT
(AFTER IOANNIDES AND KOROVESIS, 1992)

Ioannides, Lee, and Darter (1990) retained Friberg's *A* term in equation 10, but proposed an alternative *B* or loading term. Their relationship for critical bearing stress is given by

$$\sigma_b = \frac{K(2 + \beta\omega)}{4\beta^3 E_d I_d} \times P \times TLE \times f_{dc} \tag{21}$$

where f_{dc} is a dimensionless term quantifying the portion of the load carried by the critical dowel. The critical dowel is the dowel carrying the largest shearing force. Approximations for f_{dc} were given by,

$$f_{dc} = \begin{cases} \left(\frac{s}{e}\right) & \text{for edge load} \\ \dfrac{2\left(\frac{s}{e}\right)}{1+\left(\frac{s}{e}\right)} & \text{for corner load} \end{cases} \tag{22}$$

where e is the effective length and s is the dowel spacing. There is currently no theoretical method to determine the effective length; thus it can only be assumed. Ioannides and Korovesis

(1992) showed that e is not a constant, as postulated by Friberg (1940) and Tabatabaie (1978), and furthermore it is not simply a multiple of ℓ. Rather, e depends upon $(D/sk\ell)$ and (a/ℓ).

Equation 22 was derived on the basis of very simple geometric considerations and was intended to be used to estimate f_{dc} when a more precise analysis is not available. In fact, f_{dc} is a function of the dimensionless ratios $(D/sk\ell)$, (a/ℓ), and (s/ℓ). *TLE*, which itself depends upon the ratios $(D/sk\ell)$ and (a/ℓ), is defined as

$$TLE = \frac{P_T}{P} \tag{23}$$

where P_T is the total load transferred across the entire length of joint.

The original subgrade model used by Tabatabaie was the dense liquid or Winkler foundation. Later enhancements to ILLI-SLAB have included the addition of a library of foundation models. Currently available models include the following.

DENSE LIQUID SUBGRADE. The dense liquid or Winkler model is the classical flexible subgrade model characterized by the modulus of subgrade reaction (k) as in the Westergaard closed-form solution. This model represents the soil as a series of linear vertical springs with no shear interaction between them (figure 12a).

Two dense liquid formulations are incorporated in ILLI-SLAB. The original model incorporated by Tabatabaie (1978) was an equivalent mass formulation with a uniformly distributed subgrade. Later an additional dense liquid model was added featuring four concentrated springs at nodes of plate elements (Ioannides, 1985). The primary reason for adding this model was for direct comparison with other finite element codes which also use four concentrated springs at the nodes such as WESLIQID.

ELASTIC SOLID SUBGRADE. A one layer elastic solid (Boussinesq) foundation model is available in ILLI-SLAB (Ioannides, 1984). This model is a continuum model in which the deflection at a node depends not only on the forces on the node but also on forces and deflections at other nodes as well. The model is completely characterized by the two elastic parameters $E_{subgrade}$ and $\upsilon_{subgrade}$. When loaded with a plate the elastic solid foundation predicts deflections at a point beyond the plate as shown in figure 12b. This is in direct contrast with the dense liquid model which predicts zero deformations at points beyond the loaded plate (figure 12a). In reality, soil is a particulate material which exhibits some deformations beyond a load plate, but these will vanish faster than those predicted by the elastic solid model (Khazanovich and Ioannides, 1993).

The elastic solid model will allow the calculation of stresses and strains in the subgrade. However, the calculated values may not be realistic, especially in granular materials. Because of the linear elastic nature of the model, it cannot predict nonlinear, stress-dependent behavior. A second shortcoming of the elastic solid model it predicts infinite stresses under a free slab edge. Therefore, the use of the elastic solid subgrade to predict load transfer should be discouraged.

Also, the elastic solid foundation requires considerably more computational effort than the dense liquid formulation.

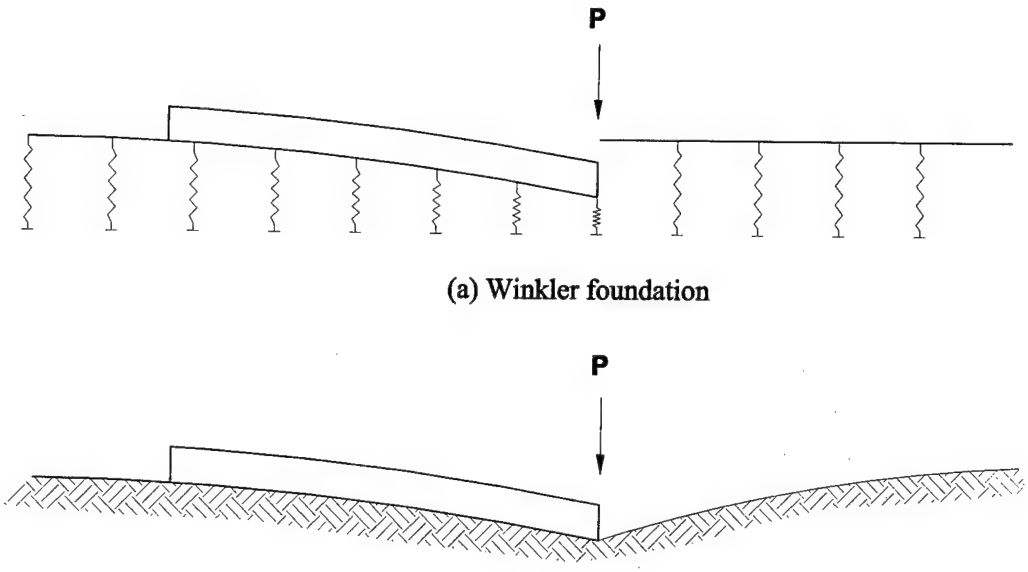

(a) Winkler foundation

(b) Elastic solid foundation

FIGURE 12. FOUND DISPLACEMENT UNDER A LOADED PLATE FOR WINKLER AND ELASTIC SOLID FOUNDATIONS (AFTER MAJADZADEH ET AL., 1981)

RESILIENT SUBGRADE MODEL. To introduce some degree of nonlinear behavior into the foundation model in ILLI-SLAB, the concept of the resilient modulus of subgrade reaction K_R was introduced (Ioannides, Barenberg, and Thompson, 1984). The resilient modulus model does not truly model stress-dependent behavior but introduces material nonlinearity through deformation-dependent response. Relationships between K_R and deflection w were developed in the form of a regression equation

$$K_R = \frac{1}{w}\left\{A_1\left[1\exp\left(A_2\left(\frac{w}{D_y}A_3\right)\right)\right] + A_4\left[\frac{w}{D_y}A_3\right] + 2\right\} \quad (24)$$

where A_1, A_2, A_3, A_4, and D_y are regression parameters determined from simulated plate load tests using the axisymmetric finite element program ILLI-PAVE. To simplify the selection of the regression parameters, ILLI-SLAB allows the user to select from four general subgrade types typical to Illinois (characterized as very soft, soft, medium, or stiff) for which the regression parameters are fixed. Alternatively, the user can enter user-determine values for the regression coefficients.

The resilient modulus foundation model is implemented in ILLI-SLAB as an iterative procedure in which the current value of K_R as determined from the calculated deflections compared against previously assumed or calculated values. If agreement is not obtained, new values of K_R are

assigned, and the calculations are repeated. This process is continued until convergence is obtained.

VLASOV TWO-PARAMETER FOUNDATION. The Vlasov or Pasternak model provides some degree of shear interaction between adjacent soil elements (Ioannides, 1994; Khazanovich and Ioannides, 1993; Kerr, 1993). Figure 13 shows a representation of the Vlasov foundation. It is characterized by the subgrade reaction pressure, q, which is a function of deflection, w, as follows:

$$q = kw \; G\nabla^2 w \tag{25}$$

where

k = modulus of subgrade reaction
G = coefficient describing the interaction of adjacent springs
∇ = Laplace operator

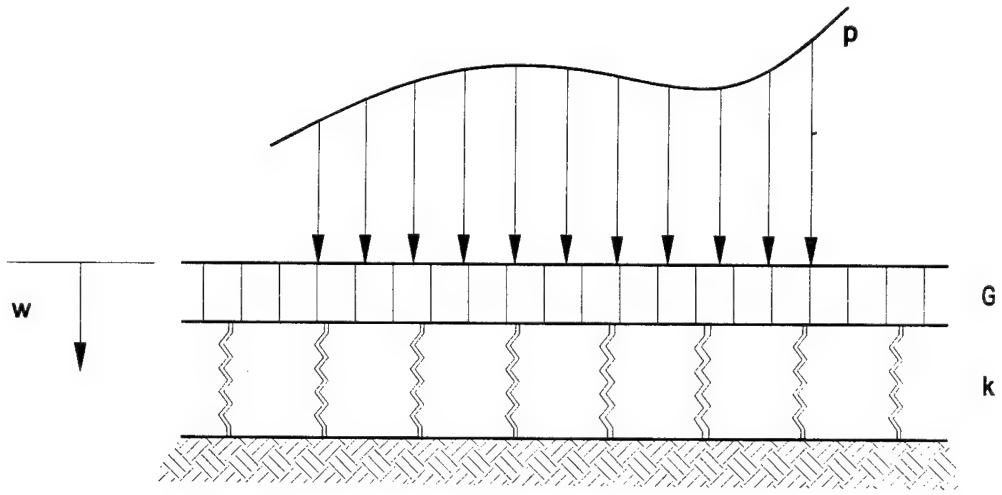

FIGURE 13. VLASOV OR PLASTERNAK FOUNDATION
(AFTER KERR, 1993)

As G approaches zero, it can be seen that the Vlasov model approaches the dense liquid foundation. To account for the influence of foundation deflections beyond the edge of the slab, ILLI-SLAB uses a strain energy approach that adds terms to the stiffness matrix to reflect the energy of soil deformation beyond the slab (Khazanovich and Ioannides, 1993).

KERR THREE-PARAMETER FOUNDATION. Kerr (1964, 1965, 1993) generalized the two-parameter model by adding a third parameter k_U which describes a second, upper layer of springs as shown in figure 14. In essence, the Kerr foundation is an in-series combination of the dense liquid foundation and the Vlasov two-parameter model. The upper dense liquid portion insures that stresses in the region of a free edge will not go to infinity. Also, the lower two-parameter portion of the model allows shear interaction.

The partial differential equation which describes the response of the Kerr model is

$$\left(1+\frac{k_L}{k_U}\right)p - \frac{G}{k_U}\nabla^2 p = kw - G\nabla^2 w$$

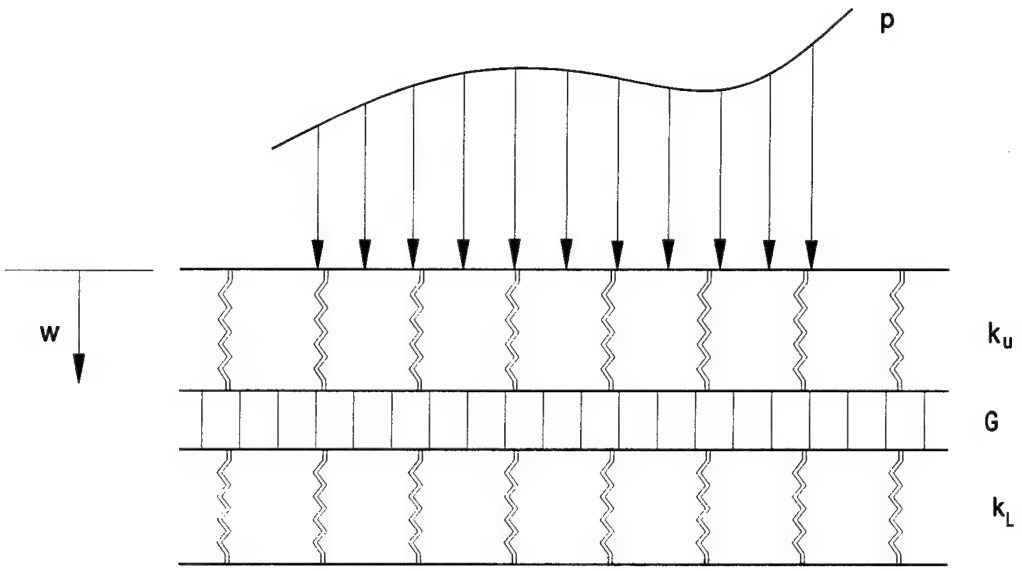

FIGURE 14. KERR FOUNDATION MODEL
(AFTER KERR, 1993)

The Kerr three-parameter model is implemented in ILLI-SLAB by introducing an eight-node, 24 degree-of-freedom element (Khazanovich and Ioannides, 1993): four nodes are placed at the top of the upper springs, while the other four nodes are positioned at the bottom of the upper layer of springs. The additional nodes in the model formulation require additional computational effort, but the resulting stiffness matrix is banded, leading to some computational benefit.

A disadvantage of the Kerr model is that it requires three parameters to calibrate the model for a subgrade material. These parameters lack the simple, convenient nature of the dense liquid *k*. However, it is possible to define an effective modulus of subgrade reaction (k_{eff}) analogous to the dense liquid case by considering k_U and k_L as springs in series:

$$k_{eff} = \frac{1}{\frac{1}{k_U} + \frac{1}{k_L}} \tag{27}$$

ZHEMOCHKIN-SINITSYN-SHTAERMAN FOUNDATION. The Zhemochkin-Sinitsyn-Shtaerman model is an in-series combination of the dense liquid and elastic solid models (Khazanovich and Ioannides, 1993). Like the Kerr model, it overcomes the elastic solid model's

shortcoming of predicting infinite stresses at a free edge. The computational effort required for the Zhemochkin-Sinitsyn-Shtaerman model is comparable to that of the elastic solid foundation.

JSLAB. JSLAB was developed by Tayabji and Colley (1984). The assumptions of JSLAB are essentially the same as ILLI-SLAB. JSLAB allows a maximum of two layers in a pavement system (slab and base or slab and overlay) on a dense liquid foundation. The slab is modeled by the same four-node plate element employed in ILLI-SLAB. No subgrade models other than the dense liquid are available in JSLAB. The formulation of the dense liquid foundation is the equivalent mass formulation.

One capability of JSLAB not found in ILLI-SLAB is the ability to consider noncircular load transfer devices. Otherwise, the basic assumptions of the mechanics of load transfer devices are identical to ILLI-SLAB. When noncircular dowels are specified, the user must input the cross-sectional area and moment of inertia of the dowel.

WESLIQID AND KENSLABS. Two computer programs were developed by Chou (1981) for calculating stresses and deflections in jointed rigid pavements: WESLIQID and WESLAYER. WESLIQID is a finite element program for jointed pavements which assumes a dense liquid foundation model. The program can analyze any number of slabs with aggregate interlock, keyways, or dowels as load transfer devices. WESLIQID is based upon the finite element programs originally developed at the University of Kentucky (Huang and Wang 1973; Huang 1985) and later developed into the computer program KENSLABS (Huang 1993).

WESLIQID employs the four-node, 2D plate bending finite element with 3 degrees of freedom per node. The slab can be either one or two layers; if two layers, the layers can be bonded or unbonded. The dense liquid foundation model, characterized by modulus of subgrade reaction k, is modeled as linear spring element attached only at the nodes. This is in contrast with ILLI-SLAB and JSLAB, which have an equivalent mass formulation with a uniformly distributed subgrade. (ILLI-SLAB also has the linear spring element attached only at the nodes as an optional foundation.)

Load transfer can be input into the model in one of four ways. The first three options are for shear transfer only: (a) efficiency of shear transfer, (b) spring constant, or (c) diameter and spacing of dowels. In the *efficiency of shear transfer*, the ratio of vertical deflections along the joint between the loaded and unloaded slab is specified by the user. This efficiency is assumed to be constant at all nodes along a joint. This method is simple but does not model actual joint behavior; that is, in reality, joint efficiencies vary along a joint.

The concept of the *spring constant* is shown in figure 15. Because load transfer is modeled solely by shear, load transfer is governed by the relative deflection w_d at the joint. The stiffness of the joint is represented by springs attached at the nodes with a stiffness C. Forces proportional to the product of the spring constant and the relative deflection are applied at the nodes.

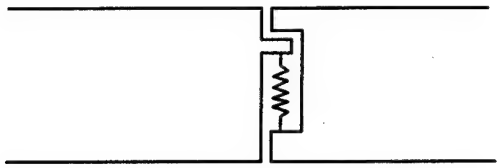

(a) Before loading

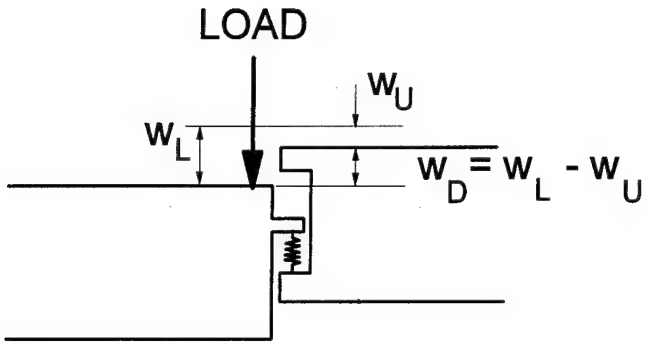

(b) After loading

FIGURE 15. JOINT MODEL IN WESLIQID AND WESLAYER
(AFTER HUANG, 1993)

The third method of specifying load transfer is to input the *diameter and spacing of the dowel bars*. Figure 16 shows the assumed geometry of shear transfer at a doweled joint. The relative deflection w_d results from the shear deformation of the dowel, *DS*, and the deformation of the concrete under the dowel such that

$$w_d = \Delta S + 2\, y_o \tag{28}$$

If the dowel bar has a shear modulus G_s and area A, the shear deformation is given by

$$\Delta S = \frac{P\omega}{G_s A} \tag{29}$$

where P is the load applied to the dowel and ω is the joint opening. The dowel is assumed to be a beam on an elastic foundation with y_o defined by equation 12. Relative displacement becomes

$$w_d = \left(\frac{\omega}{G_s A} + \frac{2 + \beta\omega}{2\beta^3 E_d I_d} \right) P \tag{30}$$

and the spring constant C becomes

$$C = \frac{1}{s\left(\frac{\omega}{G_s A} + \frac{2 + \beta\omega}{2\beta^3 E_d I_d}\right)} \tag{31}$$

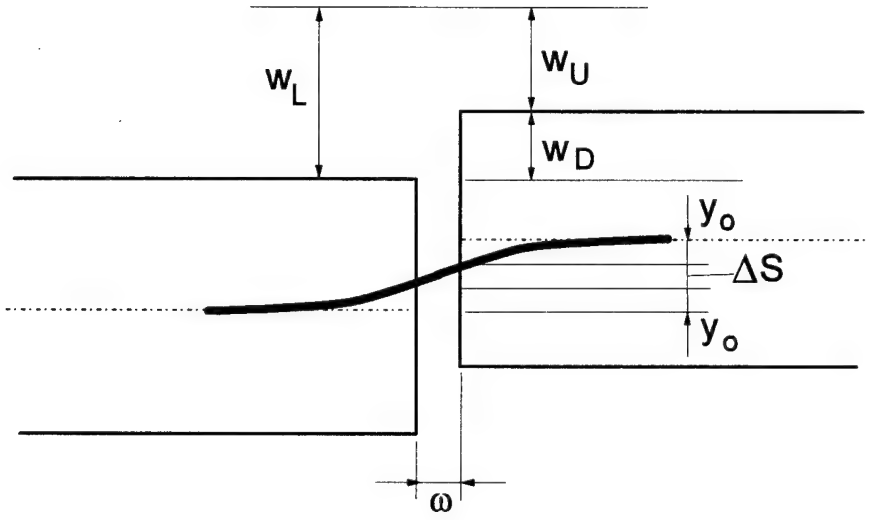

FIGURE 16. GEOMETRY OF SHEAR TRANSFER AT A DOWELED JOINT IN WESLIQID AND WESLAYER
(AFTER CHOU, 1981)

The fourth method of specifying load transfer is to specify the *efficiency of moment transfer*. It is generally agreed that moment transfer across joints with a visible opening is negligible. Nonetheless, WESLIQID allows the user this option. The efficiency of moment transfer is defined as the fraction (0.0 to 1.0) of full moment. Full moment (moment transfer efficiency of 1.0) is that moment which causes equal rotations at the nodal points on both sides of the joint. Zero moment transfer (moment transfer efficiency of 0.0) is defined as that condition in which the moments at all nodal points along the joint are zero. It should be pointed out that the rotations will not be zero at zero moment.

FEACONS III. The University of Florida has developed the finite element program FEACONS (Finite Element Analysis of Concrete Slabs) (Tia et al., 1987; Wu et al., 1993). The program has been used in a research program with the Florida Department of Transportation in the testing and evaluation of jointed concrete pavements in Florida. The third version of the program, called FEACONS III, has the following capabilities:

1. Can model either a single or two-layer concrete slab (slab and stabilized base or slab and overlay).

2. Can consider the weight of the slab in the analysis.

3. Can model subgrade voids beneath the slab.

4. Can model load transfer mechanisms at joints (including the dowel bar looseness).

5. Can model the effects of free edges.

6. Can model the effects of temperature differential between the top and bottom surfaces of a slab.

7. Can model nonlinear subgrade response.

FEACONS III uses the four-node, 12 degree-of-freedom 2D medium-thick plate bending element common to the 2D plate bending programs such as ILLI-SLAB, JSLAB, and WESLIQID. However, FEACONS III diverges from these programs in two primary features: subgrade model and load transfer model. Each of these are described below.

A three-slab pavement system as shown in figure 17 is used for the analysis of pavements in FEACONS III. Load transfer at the nodes along the joint is modeled by two springs: a shear (or linear) spring with a spring constant K_L and a torsional spring with spring constant K_T. Thus each node has two degrees of freedom: a vertical displacement w and a rotation about the y axis θ_y. For a doweled joint, both K_L and K_T are specified, while for a purely aggregate interlock joint only K_L is required.

An additional feature of the joint representation is the ability to model dowel bar looseness by varying the effective joint stiffness. Figure 18 shows a plot of the effective joint stiffness as a function of the relative displacement across the joint. Shear and moment stiffness do not become fully effective until a user-defined slip distance is obtained. The effective joint stiffness is varied linearly with relative displacement in the region where relative deflection is less the slip distance.

The subgrade model is modeled as a dense liquid with springs attached at the nodes (figure 17). At the interior nodes, the subgrade springs are characterized by a spring coefficient of K_S. However, at nodes along the edge of the slab, edge friction is modeled by an additional spring with a stiffness of K_E. Both K_S and K_E have stiffnesses governed by the linear relationship

$$K = A + Bw \tag{32}$$

where w is the deflection of the node and A and B are coefficients specified by the user. The subgrade force-deflection relationship then becomes the second-order polynomial function

$$F = Aw + Bw^2 \tag{33}$$

where F is the vertical force at the node.

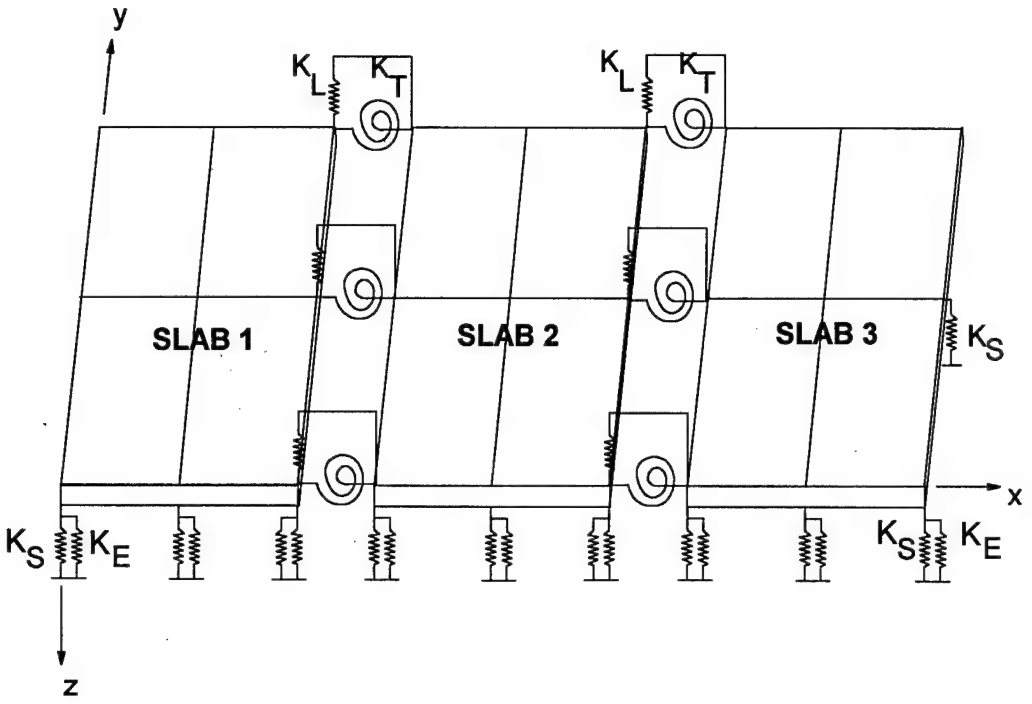

FIGURE 17. FINITE ELEMENT MODELING IN FEACONS III
(AFTER TIA ET AL., 1987)

WESLAYER AND KENLAYER. Developed by Chou (1981), WESLAYER is a coupled finite element program in which the 2D medium-thick plate bending element is coupled to either a linear elastic solid foundation or a layered elastic foundation. In many respects, WESLAYER is similar to WESLIQID, employing the same slab and load transfer model. However, the WESLAYER program is limited to two slabs because of the additional computational complexity of the layered elastic model. With modern computing technology, these limits likely are no longer required, but additional programming may be required to expand the capabilities. The program KENLAYER is very nearly identical to WESLAYER (Huang, 1993).

For the elastic solid foundation, a Boussinesq formulation is used to formulate the stiffness matrix while layered elastic theory is used for the multilayer elastic method. Each layer is characterized by the elastic modulus and Poisson's ratio. The maximum practical number of layers is five. In the case of the layered elastic foundation, the deflection of each node is not directly computed. Rather, the deflections at 21 nodes are calculated using layered elastic theory, and the deflections at other nodes are determined by interpolation. The original intent of this analysis was to reduce the demand on the computer resources required to perform the calculations. It is likely that this limitation is unnecessary given today's faster computers.

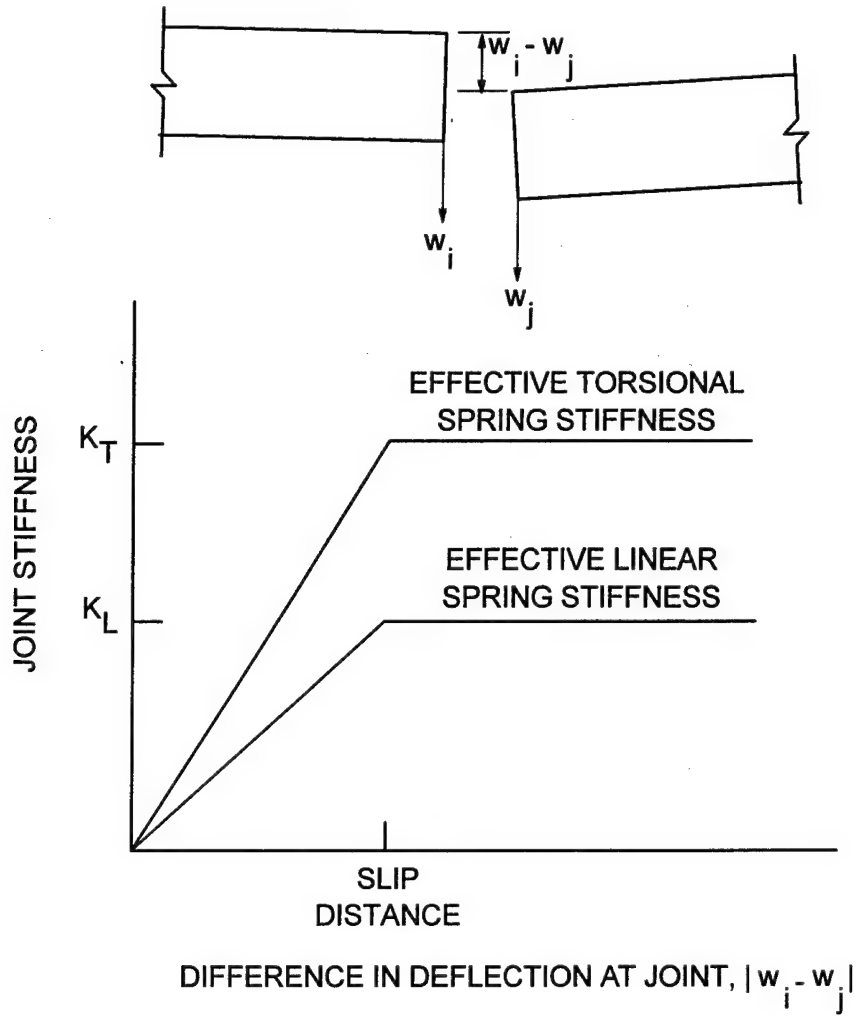

FIGURE 18. EFFECTIVE JOINT STIFFNESS WITH RELATIVE DISPLACEMENT IN FEACONS III (AFTER TIA ET AL., 1987)

THREE-DIMENSIONAL FINITE ELEMENT MODELS.

GEOSYS MODEL. Ioannides et al. (1986) developed user guidelines for a 3D finite element pavement model. GEOSYS, an existing 3D finite element program, was adopted for this study. Ioannides and Donnelly stated that their purpose was to "provide an essential guide of the effective utilization of the three-dimensional finite element approach ... and perhaps eliminate the need for conducting such preliminary and time consuming studies again."

GEOSYS is a multipurpose, 3D, finite element program developed for geotechnical applications. It has a library of several element types including beams, rods, 2D quadrilaterals and 3D brick and shell elements. Also, it is capable of time-dependent loading, gravity loading, and incremental excavation or construction. Ioannides and Donnelly (1991) modified GEOSYS for the pavement studies to simplify user input and to reduce execution times.

For the pavement studies, a 3D isoparametric brick element was used to model both the slab and foundation. The element had eight nodes with three translational degrees of freedom per node. The pavement layers were assumed to be linear elastic, isotropic, homogeneous materials.

Over 100 GEOSYS runs were executed. The effects of the finite element mesh fineness, vertical and lateral subgrade extent, boundary conditions, number of slab layers, and vertical division of the subgrade were investigated. No attempt was made to model the joints in this study. The primary findings of the study were:

1. A subgrade depth of about 10ℓ should be used to insure convergence of subgrade deflections and strains.

2. A lateral subgrade extent of about 7ℓ to 10ℓ should be used insure convergence of subgrade deflections.

3. The horizontal lower subgrade boundary should be on rollers to allow the subgrade elements to distribute loads by deforming. Similarly the lateral boundary conditions should also be rollers.

4. Maximum responses of the slab can be modeled adequately by representing the slab as two layers of 3D brick elements. Very little increase in accuracy can be gained by increasing the number of layers in the slab to five or even six layers.

5. The subgrade may be divided into three regions in the vertical direction. The upper region should extend to a depth of 1ℓ. The thickness of the finite element layers should not be greater than 0.25ℓ to 0.5ℓ. The middle region should extend from a depth of 1ℓ to 4ℓ and should be divided into at least two layers of elements. The lower region may be divided into one or more layers of elements.

6. Smaller subgrade elements are required near the slab with the element size increasing near the lateral boundaries.

7. The slab mesh fineness ratio, defined as the ratio of the shortest plan view length of the element to the element thickness should be less than 0.8. The element aspect ratio, defined as the ratio of the long plan view side of the element divided by the short plan view side of the element, should be less than four.

ABAQUS MODELS. ABAQUS is a general-purpose, nonlinear, 3D, dynamic finite element code developed by Hibbitt, Karlsson, and Sorensen, Inc. (ABAQUS, 1993). ABAQUS incorporates a comprehensive library of element types and material models including the following features:

1. Three-dimensional solid continuum (brick) elements with full and reduced integration.

2. Two-dimensional and 3D interface and gap elements.

3. Slide lines and slide surfaces with linear and nonlinear friction models.

4. Linear and nonlinear spring elements.

5. Multipoint constraints.

6. Various base, subbase, and subgrade elasticity models including linear and nonlinear elasticity.

7. Incremental plasticity models such as a modified Drucker-Prager model (with a cap) and a critical state model.

8. Dense liquid foundation models.

9. A nonlinear, fracture-based concrete model.

10. Boundary and infinite elements.

11. Capability for including user-defined element types, material models, multipoint constraints, etc.

Zaghloul and White (1993) used ABAQUS to perform nonlinear, dynamic analysis of rigid highway pavements. Their 3D model was very general and included such aspects as vertical friction between the pavement edge and the adjacent soil and the lateral passive pressure of the adjacent soil. The slab, subbase, and subgrade were modeled with 3D, eight-node brick continuum elements. The subgrade was modeled with up to five different layers. Mohr-Coulomb type friction was imposed between layers with full contact between the slab and subbase assumed as an initial condition.

Joints were modeled using gap elements with an initial opening in the range of 0.9 to 1.9 cm. Gap elements were placed between the nodes on each side of the joint to allow for the nodes to be in contact or separated, depending upon the deformed shape of the slabs. When the nodes were in contact, friction forces were developed. Dowel bars were modeled as reinforcing bars at the mid-depth of the slabs. Bond stress on one side was assumed to be zero to allow for relative horizontal movements between slabs.

Subbase and base courses were modeled using nonlinear, stress-dependent constitutive models. The subbase and granular subgrade materials were modeled with the Drucker-Prager incremental plasticity model. This model predicts elastic material behavior at stress levels below a yield criteria and plastic behavior beyond the yield criteria. All unloading is linear elastic.

Clay subgrades were modeled with a critical state plasticity model, often referred to as the modified Cam-Clay model. This model is based upon the concept of a critical state defined as that stress state for which, upon yielding, perfectly plastic flow occurs. The loci of all critical

state points forms a critical state line which effectively separates stress states for which softening behavior and hardening behavior occurs.

The load was applied in such a fashion to simulate a truck tire traveling at various velocities across the pavement. Parametric studies were conducted to investigate the effects of the load velocity, load position, load magnitude, base course, dowel bars, joint width, and slab thickness. The pavement modeled for these studies consisted of an 20-cm-thick concrete slab resting directly on a sandy subgrade. The model was loaded with an 80-KN single axle load moving at a velocity of 2.8 km/h. The results of the parameter studies were consistent with the current state of knowledge of joint behavior. The analyses indicated that dowel bars increased the joint efficiency and decreased the maximum vertical deflections. The model also predicted an increase in joint efficiency with closer dowel spacing. The effect of a stiff subbase on joint efficiency increased the joint efficiency for both doweled and undoweled joints.

Kuo (1994) attempted to realistically model some of the more complex aspects of rigid pavement behavior with a three-dimensional model developed using ABAQUS. He used this model to study the effects of various foundation supports, base thicknesses and stiffness, interface conditions between layers, temperature and moisture gradients, and load transfer at joints. One of the major objectives of his research was to investigate factors influencing the value of the modulus of subgrade reaction, particularly for pavements with stabilized layers. The second major objective was to determine the effects of base layers on slab response. Because modeling of joint load transfer was not the primary objective of Kuo's research, his modeling of the joints was somewhat simplistic, yet represents a significant step forward in the analysis of the rigid pavement system.

As a part of his research Kuo conducted an investigation into the proper element types to model the slab on grade using the ABAQUS "FOUNDATION" model. The FOUNDATION option in ABAQUS is equivalent to the dense liquid or Winkler foundation of classical analysis. In applying the FOUNDATION option, the user simply applies a spring coefficient (with units FL^{-3}) to the face of an element. Kuo found that the twenty-node isoparametric brick element with reduced integration (C3D20R) adequately approximated the theoretical Westergaard solution. This element formulation was subsequently used in more sophisticated analyses involving the modeling of the base and subgrade layers.

Kuo employed a simplistic yet effective model for aggregate interlock and doweled joints. Aggregate interlock was modeled using the ABAQUS "JOINTC" element type. The JOINTC element, which can be applied in both 2D and 3D analyses, is placed between nodes on either side of the joint. Translational and rotational springs constants can be used to define the joint stiffness in both translational and rotational degrees of freedom. The spring constants are specified as piecewise linear functions of the displacement in the active degree of freedom. Damping can also be specified in a dynamic analysis. Kuo compared the results of this ABAQUS JOINTC model with those from an ILLI-SLAB run with the same shear interlock stiffness and found that the results compared very closely for both load transfer efficiency and maximum slab stresses.

Kuo modeled doweled bars with beam elements. To account for slip of one end of the dowel bars, he invoked the "SLIDER" option in ABAQUS, one of the multipoint constraints available in ABAQUS. A multipoint constraint is a restriction imposed between degrees of freedom of a model. The SLIDER multipoint constraint allows the possibility of a node moving along a straight line defined by two other nodes and the line length of change. By invoking this restraint, Kuo was allowed one end of the dowel bar to move relative to the slab. However, Kuo did not model dowel-concrete interaction. He found that his model compared favorable with a ILLI-SLAB when a very high dowel-concrete interaction was assumed in ILLI-SLAB.

A WESTERGAARD-TYPE SOLUTION FOR THE LOAD TRANSFER PROBLEM

GENERAL.

In his 1948 paper, Westergaard provided some preliminary considerations for the solution of the edge load transfer problem. These, however, were limited by his implicit assumption that the load transfer in terms of deflection was identical to the load transfer in terms of stress, a postulate disproved by Corps model studies and full-scale tests in the 1940's and 1950's, and more recently by finite element investigations (Ioannides and Korovesis, 1990, 1992). Thus, on the prominent issue of load transfer, it has been the common understanding that Westergaard's last contribution was the very cursory treatment contained in his 1948 paper.

A recent examination of the archives of the Airfields and Pavements Division of the Geotechnical Laboratory at Waterways Experiment Station, however, has brought to light a consulting report submitted to the Corps by Westergaard in June 1949 that contains a detailed examination of the load transfer problem. This report, cited herein as Scarlatos (1949), had been prepared under contract for the Ohio River Laboratories of the Corps of Engineers, and describes analytical investigations by Mikhail S. Skarlatos under the supervision of Westergaard. As far as could be ascertained, the findings of this report have never been published elsewhere, although at least one citation of this work has been encountered in the literature (Woodhead and Wortman, 1973).

This chapter presents the results of an investigation which sought to extend and refine the load transfer solution by Skarlatos (1949) using modern computational tools. A comparison of this solution to earlier finite element solutions is also presented. Following the same approach as Skarlatos and Westergaard, closed-form equations are derived for the maximum deflection and maximum bending stress occurring on the unloaded side of an edge capable of load transfer. Together with Westergaard's 1948 edge loading equations, the two formulae derived herein effectively extend Westergaard's solutions to the case of the load transfer problem. Its effective utilization is now possible owing to the development of modern electronic computational tools, i.e., software and hardware.

GENERAL SOLUTION FOR LOAD TRANSFER.

According to Skarlatos (1949), the deflection at the origin of the coordinates (0,0) on the unloaded side of a joint caused by a point load, P, applied at (x,η) is given by

$$w_U^* = \frac{w_U\, k\, \ell^2}{P} = \frac{4}{\pi} \int_0^\infty \frac{\gamma^2}{F(4\gamma + F/f)} \cos\frac{\alpha x}{\ell}$$

$$\left(\cos\frac{\beta\eta}{\ell} + \kappa \sin\frac{\beta\eta}{\ell}\right) e^{-\gamma\eta/\ell}\, d\alpha \tag{34}$$

in which

$$\kappa = (1-\mu)\,\alpha^2 \tag{35}$$

$$F = 1 + 4\kappa\gamma^2 - \kappa^2 \tag{36}$$

$$\beta = \sqrt{\frac{1}{2}\left(\sqrt{1+\alpha^4} - \alpha^2\right)} = \frac{1}{2\gamma} \tag{37}$$

$$\gamma = \sqrt{\frac{1}{2}\left(\sqrt{1+\alpha^4} + \alpha^2\right)} = \sqrt{\alpha^2 + \beta^2}\ . \tag{38}$$

$$f = \frac{q_0}{k\,\ell} = \frac{AGG}{k\,\ell} \tag{39}$$

Equation 39 defines a dimensionless joint stiffness in terms of the slab-subgrade radius of relative stiffness, ℓ, the subgrade modulus, k, and parameter q_0 (or AGG). The last term has dimensions of force/length^2 and represents the force transferred across a unit length of joint per unit differential deflection across the joint. The slab's Poisson ratio is denoted by μ. The x-axis runs along the joint, while the η-*axis* is perpendicular to the joint and is positive in the direction of the unloaded slab. Accordingly, determination of the dimensionless deflection, w_U^*, for a loaded area of finite size involves a triple integral in dx, $d\eta$, and $d\alpha$. This integral has been evaluated using the commercial mathematical software *MATHEMATICA* (Wolfram, 1991) for square loaded areas of various sizes 2ε by 2ε. The results are plotted in figure 19 as a function of a dimensionless load size ratio, ε/ℓ. The dimensionless deflection at (0,0) caused by a load on a circular and a square-shaped loaded area can be expected to be essentially the same if their centroids coincide.

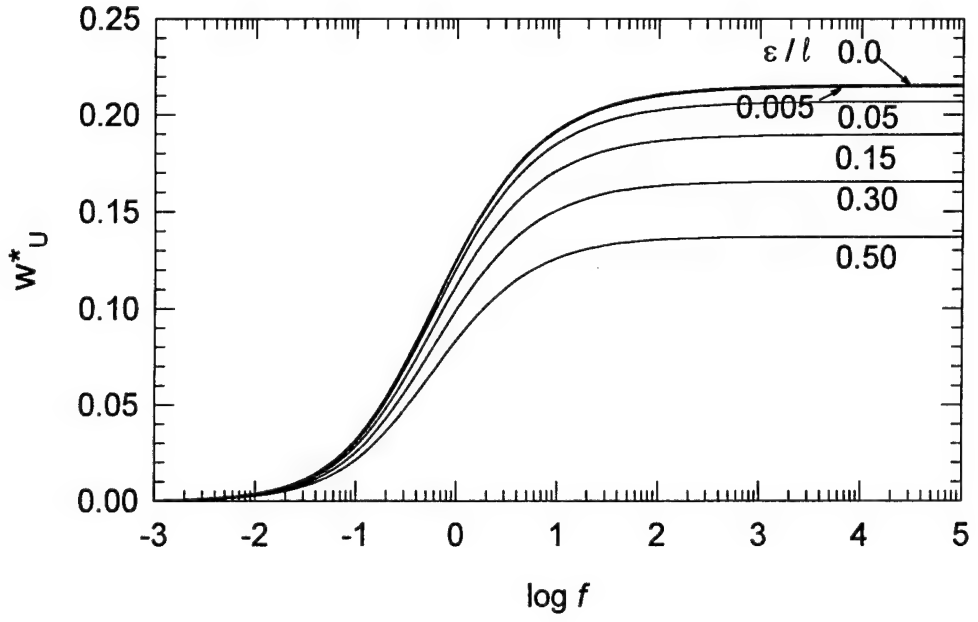

FIGURE 19. VARIATION OF UNLOADED SIDE MAXIMUM DIMENSIONLESS DEFLECTION WITH DIMENSIONLESS JOINT STIFFNESS AND ε / ℓ

Similarly, according to Skarlatos (1949), the stress at the origin of the coordinates (0,0) on the unloaded side of a joint caused by a point load, P, applied at (x,η) is given by

$$\sigma^*_U = \frac{\sigma_U \, h^2}{P} = \frac{24\,(1-\mu^2)}{\pi} \int_0^\infty \frac{\alpha^2 \, \gamma^2}{F\,(4\gamma + F/f)} \cos\frac{\alpha x}{\ell} \left(\cos\frac{\beta\eta}{\ell} + \kappa \sin\frac{\beta\eta}{\ell} \right) e^{-\gamma\eta/\ell} \, d\alpha \qquad (40)$$

Here, h denotes the thickness of the slab. Proceeding as outlined above for the unloaded deflection and setting the slab Poisson's ratio, μ, to 0.15, the curves in figure 20 were obtained. For a slab resting on a dense liquid foundation and equipped with a pure-shear load transfer mechanism, the corresponding responses on the loaded side can be obtained as follows:

$$w_L = w_f - w_U \qquad (41)$$

and

$$\sigma_L = \sigma_f - \sigma_U \qquad (42)$$

in which w_f and σ_f are the maximum responses of a free edge. Equations for the latter in integral form were given by Westergaard (1948), as follows:

$$w_f^* = \frac{w_f\, k\, \ell^2}{P} = \frac{2}{\pi} \int_0^\infty \frac{\gamma}{F} \cos\frac{\alpha x}{\ell} \left(\cos\frac{\beta y}{\ell} + \kappa \sin\frac{\beta y}{\ell} \right) e^{-\gamma y/\ell}\, d\alpha \qquad (43)$$

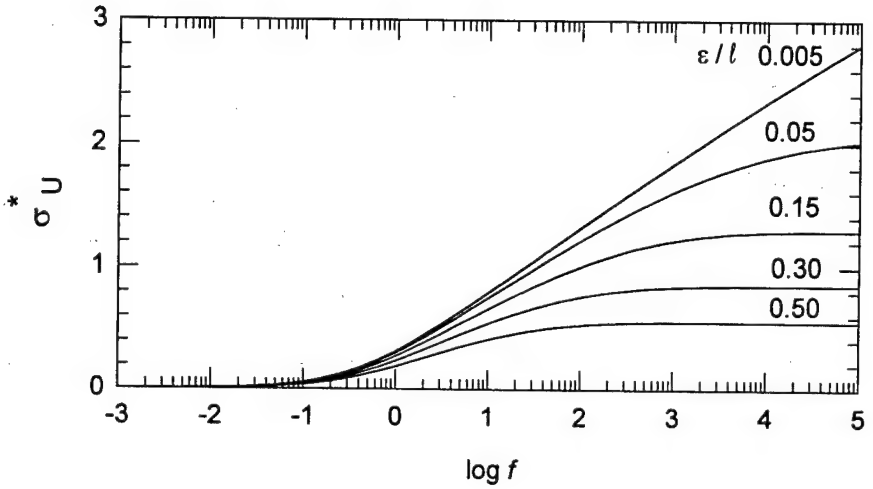

FIGURE 20. VARIATION OF UNLOADED SIDE MAXIMUM DIMENSIONLESS BENDING STRESS WITH DIMENSIONLESS JOINT STIFFNESS AND ε / ℓ

and

$$\sigma_f^* = \frac{\sigma_f\, h^2}{P} = \frac{12(1-\mu^2)}{\pi} \int_0^\infty \frac{\alpha^2\, \gamma}{F} \cos\frac{\alpha x}{\ell} \left(\cos\frac{\beta y}{\ell} + \kappa \sin\frac{\beta y}{\ell} \right) e^{-\gamma y/\ell}\, d\alpha \qquad (44)$$

In this case, the y-axis is perpendicular to the joint and is positive in the direction of the loaded slab. These formulae, which pertain to a point load, were also integrated over *dx*, *dy*, and $d\alpha$ for various square loaded areas, assuming $\mu = 0.15$. The results are shown in figures 21 and 22. It is observed that the more precise numerical integration afforded by *MATHEMATICA* reveals discrepancies of up to 8 percent for the loaded area sizes considered, when compared to Westergaard's 1948 formulae.

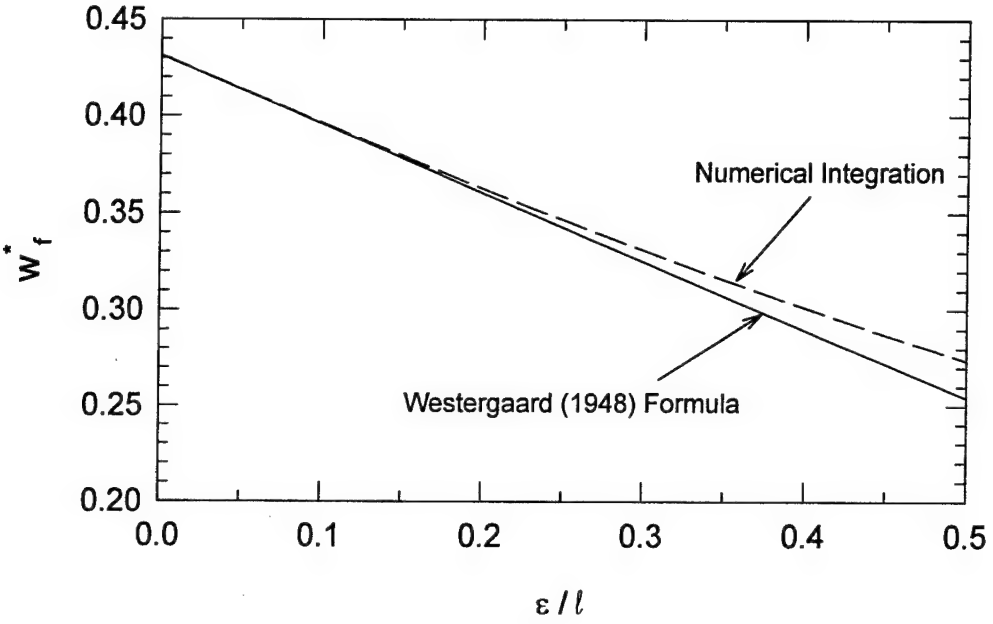

FIGURE 21. VARIATION OF MAXIMUM DIMENSIONLESS DEFLECTION FOR FREE EDGE WITH ε / ℓ

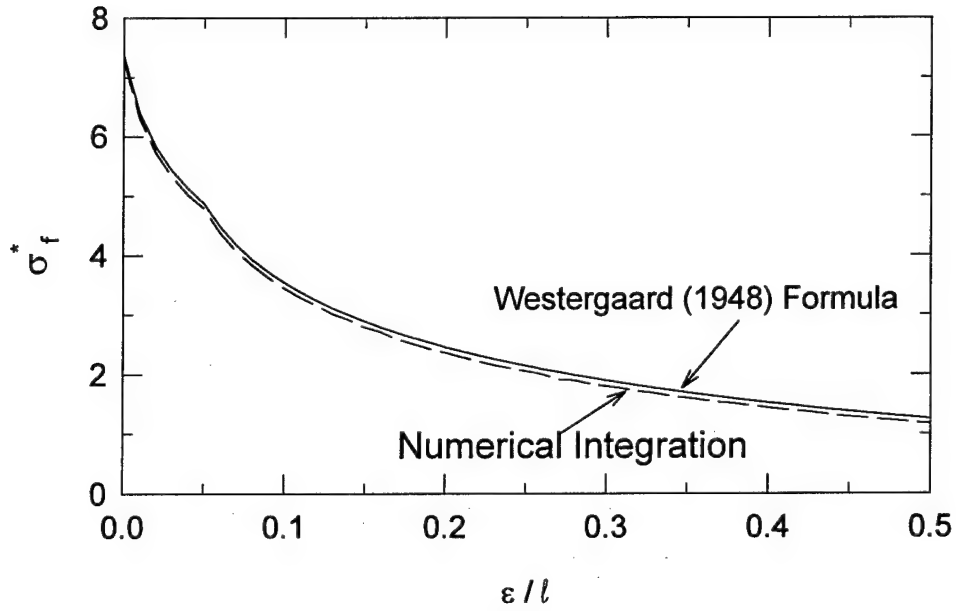

FIGURE 22. VARIATION OF MAXIMUM DIMENSIONS BENDING STRESS FOR FREE EDGE WITH ε / ℓ

INTERPOLATION FORMULAE.

It is useful to develop closed-form equations, similar to those presented by Westergaard (1948), which could be used to determine the response of a joint with load transfer in routine engineering applications. It is obvious from the above discussion that two additional formulae are necessary, namely one for w_U and one for σ_U. Due to the sensitivity of load transfer efficiency to even small shortfalls in precision, it is considered desirable to enhance the two free-edge equations presented by Westergaard (1948) as well. In the description provided below, the free edge is treated first.

FREE-EDGE DEFLECTION. Westergaard (1948) provided the following formula for the deflection at the origin of coordinates caused by a distributed load placed tangentially to the free edge with its centroid located at a distance $\bar{y}$ from the free edge:

$$w_f^* = \frac{w_f \; k \; \ell^2}{P} = \left[\; B_3 \quad B_4 \; \frac{\bar{y}}{\ell} \; \right] \tag{45}$$

In this expression, B_3 and B_4 are dimensionless constants dependent only on the value of the slab's Poisson ratio, μ. Centroidal distance $\bar{y}$ is replaced by a for a circular loaded area and by ε for a square loaded area. Equation 44 represents the Taylor series for the complete solution, with only the linear term retained. By considering the deflection and slope at the origin caused by a point load at the same location and setting $\mu = 0.15$, Westergaard evaluated B_3 and B_4 as 0.4314 and 0.3510, respectively. For other values of μ, he provided the following interpolation formulae for the two constants, which afford "quite satisfactory accuracy:"

$$B_3 = \frac{\sqrt{2 + 1.2\,\mu}}{\sqrt{12\,(1 - \mu^2)}} \tag{46}$$

$$\frac{B_4}{B_3} = 0.76 + 0.4\,\mu \tag{47}$$

It may be expected that a better approximation to the complete solution may be obtained by adding a quadratic term to equation 45:

$$w_f^* = \frac{w_f \; k \; \ell^2}{P} = \left[\; B_3 \quad B_4 \left(\frac{a}{\ell} \right) + \frac{1}{2} \; B_6 \; (a over \ell)^2 \; \right] \tag{48}$$

Using the commercial statistical software *SigmaStat* (Jandel, 1994), a comparison with the solution obtained using *MATHEMATICA* for $\mu = 0.15$, suggests that B_6 should be set to 0.1305.

FREE-EDGE BENDING STRESS. Because of a singularity in equation 44, Westergaard (1948) split into two parts the bending stress arising at the origin of coordinates under the action of a tangential distributed loaded area, as follows:

$$\sigma_f = \bar{\sigma} + \sigma_c \tag{49}$$

Making reference to his earlier work (Westergaard, 1943) and to a suggestion by Nadai (1925), Westergaard wrote the first term in equation 49 as:

$$\bar{\sigma}^* = \frac{\bar{\sigma}\, h^2}{P} = \frac{12(1+\mu)}{\pi(3+\mu)} \left[0.1159 + L + \frac{1-\mu}{4} S \right] \tag{50}$$

For a circular load, radius a:

$$L = \log_e \left(\frac{a}{\ell} \right) \tag{51}$$

and $S = 1/2$. As for the second term in equation 49, Westergaard again expressed it in terms of a Taylor series, retaining only the linear term, as follows:

$$\sigma_c^* = \frac{\sigma_c\, h^2}{P} = \frac{12(1+\mu)}{\pi(3+\mu)} \left[\frac{3-\mu}{4} B_1 + B_2 \left(\frac{a}{\ell} \right) \right] \tag{52}$$

For $\mu = 0.15$, Westergaard obtained $B_1 = 0.9544$ and $B_2 = 0.3822$. In adapting this solution for a square load, Westergaard's first term was retained (equations 50 and 51, with a replaced by ε), but quadratic and cubic terms were added to equation 52, as follows:

$$\sigma_c^* = \frac{\sigma_c\, h^2}{P} = \frac{12(1+\mu)}{\pi(3+\mu)} \left[\frac{3-\mu}{4} B_1 + B_2 \left(\frac{\varepsilon}{\ell} \right) + \frac{1}{2} B_9 \left(\frac{\varepsilon}{\ell} \right)^2 + \frac{1}{6} B_{10} \left(\frac{\varepsilon}{\ell} \right)^3 \right] \tag{53}$$

Using *SigmaStat*, a comparison with the numerical integration solution obtained using *MATHEMATICA* for $\mu = 0.15$ suggests that $B_9 = -4.225$ and $B_{10} = 24.12$.

UNLOADED SIDE DEFLECTION. The derivation of the interpolation formulae for the responses of the unloaded side follows the general approach described by Skarlatos (1949), who, in turn, had emulated Westergaard (1948). Thus, the unloaded side deflection is written as a Taylor series retaining only the linear term, as follows:

$$w_U^* = \frac{w_U\, k\, \ell^2}{P} = \left[B_3' - B_4' \frac{\varepsilon}{\ell} \right] \tag{54}$$

in which

$$B'_3 = [\ w_U\ ]_{x=\eta=0} = \frac{4}{\pi}\int_0^{\infty} \frac{\gamma^2}{F\left(4\gamma + \frac{F}{f}\right)}\, d\alpha \tag{55}$$

and

$$B'_4 = \left[\ \frac{\partial w_U}{\partial \eta}\ \right]_{x=\eta=0} = \frac{2}{\pi}\int_0^{\infty} \frac{\gamma(2\gamma^2-\kappa)}{F\left(4\gamma + \frac{F}{f}\right)}\, d\alpha \tag{56}$$

The integrals in equations 55 and 56 were evaluated in this study using *MATHEMATICA* for the case of $\mu = 0.15$ and for values of $\log(f)$ ranging between -3 and 5. Subsequently, the statistical software package *SigmaStat* (Jandel, 1994) was used to derive the following regression equations for the constants in equation 54, retaining the functional forms first suggested by Skarlatos (1949):

$$B'_3 = \frac{f - 0.6367 \log\ (1 + f)}{4.6516 f + 1.8210} \tag{57}$$

and

$$\frac{B'_4}{B'_3} = 0.6984 + 0.0441 \log\ (1 + f) - 0.00655\ f^{0.24} \tag{58}$$

Substituting equations 57 and 58 into equation 54 leads upon rounding off to

$$w_U^* = \frac{w_U k \ell^2}{P} = 0.125\left[\frac{f - 0.6\log(1+f)}{f+0.4}\right]* \left[1 - 0.7\frac{\varepsilon}{\ell}\left\{1 + 0.06\log(1+f) - 0.01 f^{0.2}\right\}\right] \tag{59}$$

The predictive ability of equation 59 deteriorates slightly as ε/ℓ and f increase. For $\varepsilon/\ell = 0.5$, the ratio of the predicted, to exact values of w_U, range between 0.91 and 0.99 for $\log(f)$ values between -3 and 5. It is, therefore, observed that equation 59 affords approximately the same precision as the free-edge deflection equation given by Westergaard (1948). By analogy to equation 47, a quadratic term is added to equation 54, as follows:

$$\Delta_U^* = \frac{\Delta_U\ k\ \ell^2}{P} = \left[\ B'_3\ \ B'_4 \left(\frac{\varepsilon}{\ell}\right) + \frac{1}{2}\ B'_6 \left(\frac{\varepsilon}{\ell}\right)^2\ \right] \tag{60}$$

in which:

$$B'_6 = \frac{1}{\pi} \int_0^{\infty} \frac{-1 + 4\gamma^4 - 4\gamma^2\kappa}{F\left(4\gamma + \frac{F}{f}\right)} d\alpha \tag{61}$$

The integral in equation 61 was evaluated using *MATHEMATICA* for $\mu = 0.15$ and for log(f) ranging between -3 and 5. Results were then fitted with a regression algorithm using commercial statistical software package *TBLCURVE*. The functional form of this regression algorithm was arbitrary from an engineering viewpoint, and was selected from among a large number of choices considered by the software. The choice was guided by the desire to keep the number of regression coefficients to a minimum, thus enhancing ease of use of the algorithm, while ensuring its high predictive ability. The resulting relationship was

$$B'_6 = \frac{0.01945 + 0.009348 \log f - 0.002093 \log^2 f - 0.001086 \log^3 f}{1 - 0.1474 \log f + 0.2666 \log^2 f - 0.02004 \log^3 f} \tag{62}$$

The functional form in equation 62 was then added to equation 59 as suggested by equation 60 and *SigmaStat* was used to compare the result with the corresponding numerical solution obtained using *MATHEMATICA*. In this manner, the following simplified expression was obtained, defining a quadratic deflection increment to be added to the value calculated using equation 59:

$$\Delta_U^{**} = \frac{1}{2}\left[\, 0.015 + 0.005 \log f \,\right]\left(\frac{\varepsilon}{\ell}\right)^2$$

UNLOADED SIDE BENDING STRESS. Similarly, retaining only the linear term in the Taylor series expansion for the unloaded side bending stress results in:

$$\sigma_U^* = \frac{\sigma_U h^2}{P} = \frac{24(1-\mu^2)}{\pi}\left[\, B'_1 - B'_2\left(\frac{\varepsilon}{\ell}\right)\right] \tag{63}$$

in which

$$B'_1 = \left[\, \sigma_U \,\right]_{x=\eta=0} = \int_0^{\infty} \frac{\alpha^2 \gamma^2}{F\left(4\gamma + \frac{F}{f}\right)} d\alpha \tag{64}$$

and

$$B'_2 = \left[\frac{\partial \sigma_U}{\partial \eta} \right]_{x=\eta=0} = \frac{1}{2} \int_0^{\infty} \frac{\alpha^2 \gamma (2\gamma^2 - \kappa)}{F\left(4\gamma + \frac{F}{f}\right)} d\alpha \tag{65}$$

The integrals in equations 64 and 65 were once again evaluated in this study using *MATHEMATICA* for the case of $\mu = 0.15$ and for values of $\log(f)$ ranging between -3 and 5. Subsequently, the statistical software package *SigmaStat* was used to derive the following regression equations for the constants in equation 63, retaining the functional forms first suggested by Skarlatos (1949):

$$B'_1 = 0.03316 + 0.07205 \log (1 + f) + \frac{0.00773\sqrt{f} - 0.03360}{f + 1} \tag{66}$$

and

$$\frac{B'_2}{B'_1} = \left[0.08281 f + 0.4790 \frac{0.000149}{f} \right]^{\frac{1}{4.209}} \tag{67}$$

Substituting equations 66 and 67 into equation 63 leads (upon rounding off the regression coefficients) to

$$\sigma_U^* = \frac{\sigma_U h^2}{P} = 0.54 \left[0.42 + \log (1 + f) + 0.1 \frac{\sqrt{f} - 4.2}{f + 1} \right] * \left[1 \; 0.54 \left(\frac{\varepsilon}{\ell}\right) \sqrt[4.1]{f + 5.0} \right] \tag{68}$$

The predictive ability of equation 68 deteriorates rapidly as f increases above 10, especially for $\varepsilon/\ell > 0.3$. To address this limitation, a second-order term in the Taylor expansion for σ_U^* was derived in this study. Thus, equation 63 is expanded to

$$\sigma_U^* = \frac{\sigma_U h^2}{P} = \frac{24 (1 \; \mu^2)}{\pi} \left[B'_1 - B'_2 \left(\frac{a}{\ell}\right) + \frac{1}{2} B'_9 \left(\frac{\varepsilon}{\ell}\right)^2 \right]$$

in which

$$B'_9 = \left[\frac{\partial^2 \sigma_U}{\partial \eta^2} \right]_{x=\eta=0} = \int_0^\infty \frac{\alpha^2 \gamma^2 (\gamma^2 - \beta^2 - \kappa)}{F\left(4\gamma + \frac{F}{f} \right)} d\alpha \qquad (70)$$

The integral in equation 70 was evaluated using *MATHEMATICA* for the case of $\mu = 0.15$ and for values of log(f) ranging between -3 and 5. Subsequently, the statistical software package *SigmaStat* was used to derive the following regression equation for coefficient B'_9:

$$B'_9 = \log^{-1} [\, 0.6671 \log f - 1.6570 \,] \qquad (71)$$

Proceeding as outlined above for the unloaded side deflection, the following simplified equation is derived for the quadratic bending stress increment $\sigma_U^{*'}$ to be added to equation 68:

$$\sigma_U^{*'} = 7.5 \log^{-1} [\, 0.74 \log f - 1.94 \,] * \frac{1}{2} \left(\frac{\varepsilon}{\ell} \right)^2 \qquad (72)$$

It is recommended that the increment in equation 72 be used for $f > 10$, subject to the constraint that the resulting unloaded side stress not exceed half the corresponding free edge stress for the case considered.

LOAD TRANSFER EFFICIENCY.

The preceding results may be consolidated into two charts as suggested by Ioannides and Korovesis (1990). Figures 23 and 24 illustrate the variation of the load transfer efficiencies with respect to deflection, LTE_δ, and with respect to stress, LTE_σ, with the dimensionless joint stiffness, f or $AGG/k\ell$, and the dimensionless loaded area size, ε/ℓ. These figures confirm the observations made by Ioannides and Korovesis (1990) on the basis of finite element results that LTE_δ is rather insensitive to ε/ℓ, whereas the sensitivity of the relationship between these two efficiencies to ε/ℓ is quite pronounced. The improvement in precision achieved using the solution by Skarlatos (1949) and modern computational tools is clearly discernible in figure 25, in which the newly derived LTE_δ versus LTE_σ relationships for two extreme ε/ℓ ratios are compared with earlier finite element results.

Nonlinear regression was used to develop an expression for dimensionless joint stiffness, f, as a function of LTE_δ and of the dimensionless load size ratio, (ε/ℓ). The resulting relationship was as follows:

$$\log f = \left[0.434829 \left(\frac{\varepsilon}{\ell} \right) - 1.23556 \right] \log \left(\frac{1}{LTE_\delta} - 1 \right) + 0.295205 \qquad (73)$$

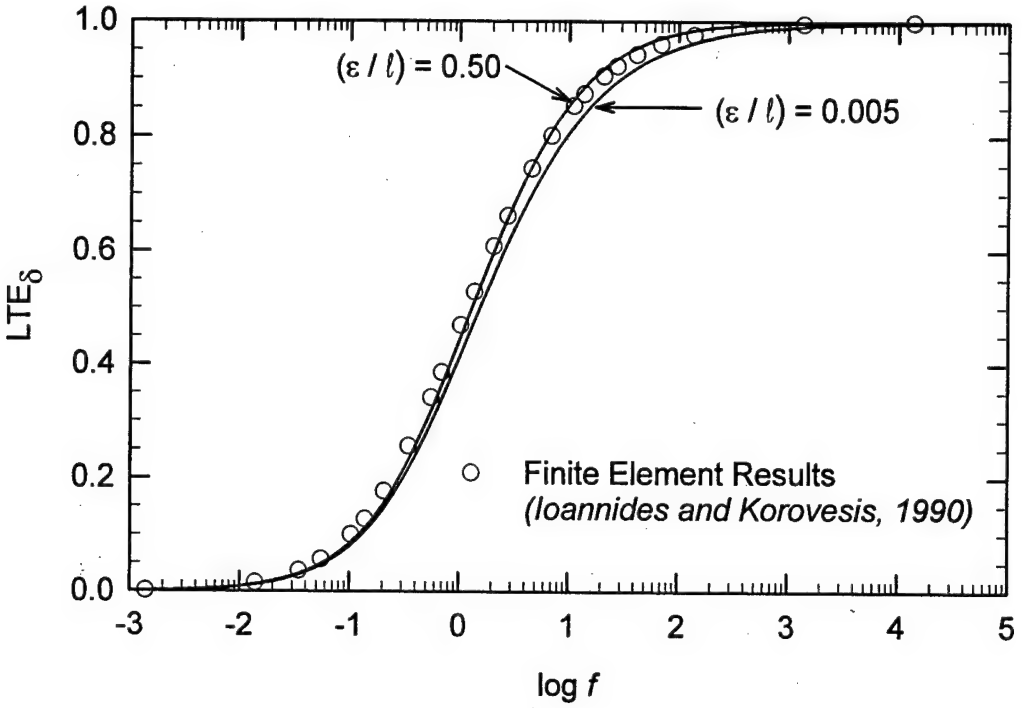

FIGURE 23. VARIATION OF LTE_δ WITH DIMENSIONLESS JOINT STIFFNESS AND ε/ℓ

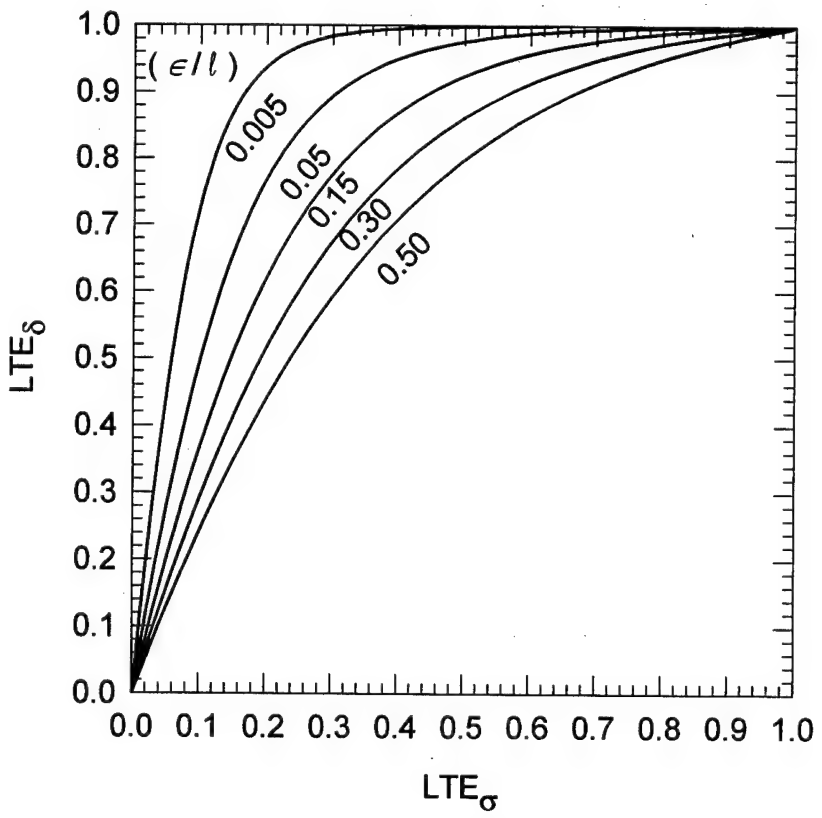

FIGURE 24. RELATIONSHIP BETWEEN LTE_δ AND LTE_σ WITH ε/ℓ

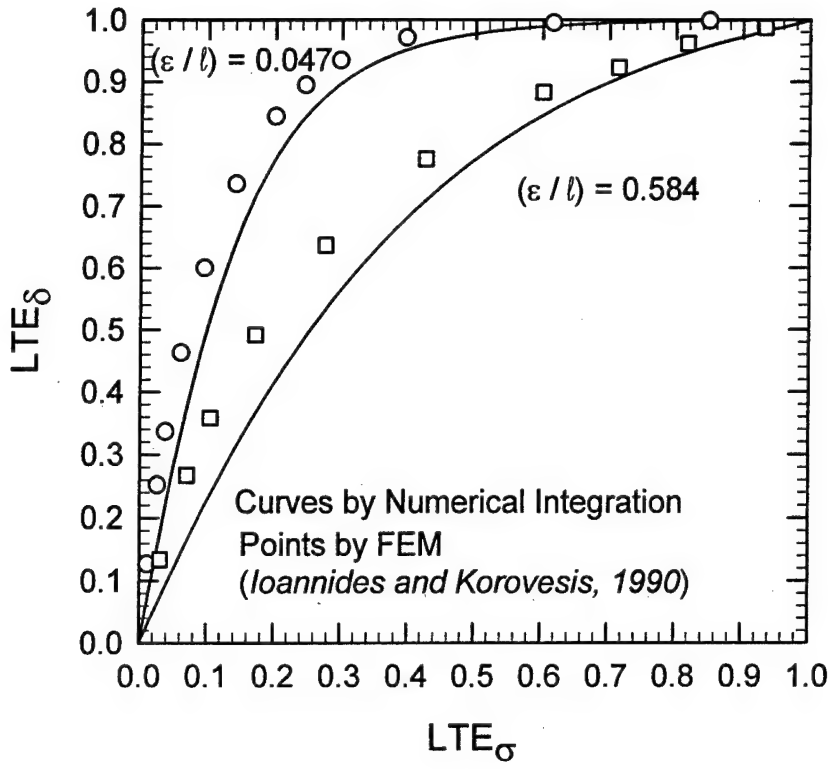

FIGURE 25. COMPARISON OF NEWLY DERIVED SOLUTION WITH EARLIER FINITE ELEMENT RESULTS

Likewise, nonlinear regression was used to develop an expression for LTE_σ as a function of LTE_δ and of (ε/ℓ). The regression formula obtained in this fashion was:

$$LTE_\sigma = \frac{\left[10.14\left(\frac{\varepsilon}{\ell}\right) + 4.00\right] LTE_\delta - \left[4.3\left(\frac{\varepsilon}{\ell}\right) + 3.98\right] LTE_\delta^2}{21.03 + \left[5.74\left(\frac{\varepsilon}{\ell}\right) - 20.98\right] LTE_\delta} \quad (74)$$

In the same fashion, a relationship was developed between LT (expressed as a percentage) and LTE_δ and (ε/ℓ):

$$LT(\%) = \frac{\left[34.3\left(\frac{\varepsilon}{\ell}\right) + 14.98\right] LTE_\delta - 14.835\ LTE_\delta^2}{1 + \left[0.686\left(\frac{\varepsilon}{\ell}\right) - 0.995\right] LTE_\delta} \quad (75)$$

SUMMARY.

The Skarlatos solution has never implemented in practical design, owing to a number of factors, including Westergaard's passing away and the repatriation of Skarlatos himself to Greece, where he continues to practice civil engineering. A report describing that investigation had been submitted by Westergaard to the Corps in 1949, but was never widely disseminated. The development of modern computational tools, in the form of high-speed personal computers and powerful mathematical and statistical software, has created new possibilities for the fruitful application of this ground-breaking achievement.

Using the commercial mathematical software *MATHEMATICA* and statistical software *SigmaStat* and *TBLCURVE*, closed-form solutions akin to those by Westergaard were derived in this study for the maximum responses on the unloaded side of a Portland Cement Concrete (PCC) pavement slab edge capable of a degree of load transfer. When used together with Westergaard's own closed-form equations for the free edge problem, the formulae derived in this study constitute a complete solution of the edge load transfer problem, recognized over the years as a critical consideration in PCC pavement design. The newly derived solution is presented in convenient form for routine engineering application, and is compared to earlier finite element data. The improvement in ease of application and precision is considerable.

SMALL-SCALE PHYSICAL MODEL STUDIES

GENERAL.

Physical modeling techniques were used by early researchers to extend the range of observations from full-scale test tracks and in-service pavement performance as well as to confirm theory developed from analytical studies. Small-scale physical models were used to verify Westergaard's theory for interior and edge loading, particularly as it related to the effects of contact pressures and multiple-wheel loadings (Mellinger and Carlton, 1955). Similarly, small-scale models were used extensively in developing and verifying design procedures for prestressed concrete pavements (Small-Scale Model Studies, 1962, 1963). The effects of sawkerfs and bored recesses of the load-carrying capacity of rigid pavements was investigated by Behrmann (1966). Perhaps of most importance to this research was a set of yet unpublished small-scale tests on doweled joints, described in more detail later in this report.

SINGLE-SLAB MODELS.

TEST DESCRIPTION. Physical model testing to verify Westergaard's theory for predicting maximum stresses acting at the interior and edge of rigid pavement slabs were conducted in the early to mid-1950's (Mellinger and Carlton, 1955; Carlton and Behrmann, 1956; Behrmann, 1972). These tests involved measuring strains resulting from static loadings on Hydrostone gypsum cement slabs resting on a solid, natural rubber pad. The materials and dimensions of the models were selected after considering several factors:

1. A natural rubber subgrade was chosen to simulate a uniform subgrade and to provide continuous support.

2. Hydrostone gypsum cement was chosen to provide a homogeneous and isotropic material to model a slab of uniform thickness.

3. The horizontal dimensions of the slab were chosen so that distant edge effects were minimal.

4. The thickness of the rubber pad was chosen so that the bottom effects were minimal.

5. Applied loads in the tests were small enough to ensure that the stresses in the models did not exceed the elastic limits of the slab and subgrade.

6. The size of the loaded area and the thickness of the slab were of such relative dimensions that the ordinary theory of bending of thin plates was applicable.

The physical material properties that were of concern were modulus of elasticity, E, Poisson's ratio, μ, and modulus of subgrade, k. The basic similitude relationship between the model and prototype was developed from Westergaard's theory:

$$\frac{a_{prototype}}{\ell_{prototype}} = \frac{a_{model}}{\ell_{model}} \tag{76}$$

where a is the radius of a circular area over which the load is applied and ℓ is the radius of relative stiffness as defined by Westergaard (1926).

The slab dimensions were approximately 380 mm (15 in.) by 380 mm (15 in.) by 3 mm (0.125 in.) thick. The slabs were constructed by placing gypsum cement mortar in a steel form between two plates of glass to insure a uniform thickness. The rubber pad had dimensions of 610 mm (24 in.) by 610 mm (24 in.) by 305 mm (12 in.) thick, and was supported by a rigid concrete table and confined on its side by a rigid box.

After a seven day curing period, 6.3-mm (0.25-in.) -long resistance wire strain gages were glued to the slab. Up to 17 gages were installed on a single slab. Experience with gages bonded opposite each other on the top and bottom of the slab had shown that the strain measurements were identical within the precision of the gages. Thus the strain gages were typically placed on the top of the slab for convenience. The slab was subsequently placed directly on the rubber subgrade. A layer of 19-mm (0.75-in.) lead cubes were uniformly distributed over the top surface of the slab to insure intimate contact between the slab and subgrade. Static loads were applied through a circular rubber pad cemented to a conforming rigid die. The static load was applied by means of a reaction beam as shown in figure 26.

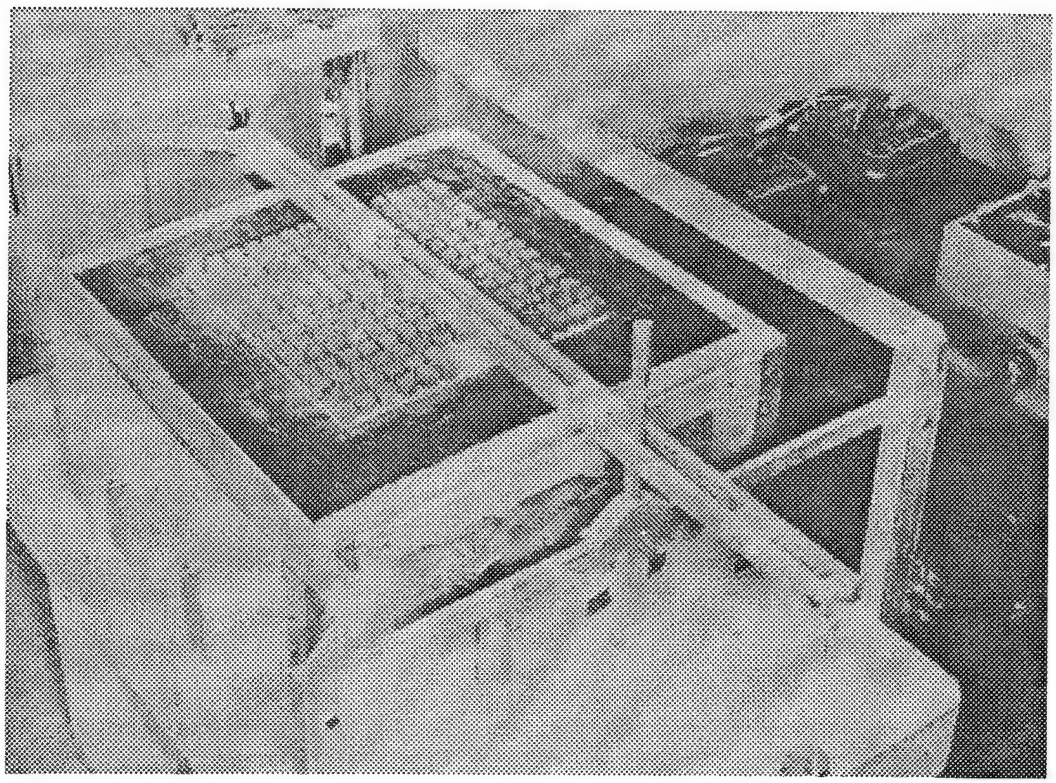

FIGURE 26. PHOTOGRAPH OF SMALL-SCALE PHYSICAL MODELS TEST SETUP

The measured elastic properties of the cured gypsum cement mortar were E = 20,700 MPa (3,000,000 psi) and $\mu = 0.25$. The flexural strength was 17 MPa (2500 psi). Themodulus of subgrade reaction of the natural rubber subgrade, k, was determined using volumetric displacement method to be 9.6 MPa/m (35 psi/in.) for interior loading and 17.8 MPa/m (65 psi/in.) for edge loading. Based upon the physical constants of the model, the physical model had a radius of relative stiffness of 50 mm (1.96 in.) for interior loading and 43 mm (1.68 in.) for edge loading.

TEST RESULTS AND ANALYSIS. Figure 27 shows a contour plot of deflections measured for a typical test under edge loading conditions (Carlton and Behrmann, 1956). Figure 28 shows the deflection basin profile from the test shown in figure 27 along with profiles obtained from finite element solutions from ILLI-SLAB. The experimental basin was obtained by carefully scaling the deflections along the edge from figure 27. The lower ILLI-SLAB deflection basin was obtained using the reported values of E = 20,700 MPa (3,000,000 psi), μ = 0.25, and k = 17.8 MPa/m (65 psi/in.). Obviously, the calculated response using these values does not approximate that of the experiment. Therefore, an iterative backcalculation procedure was used to determine the combination of E and k (holding $\mu = 0.25$) which would produce a deflection basin profile matching that of the experiment. The best match curve is shown as the upper ILLI-SLAB curve in figure 28. These backcalculated material characterization values were as follows:

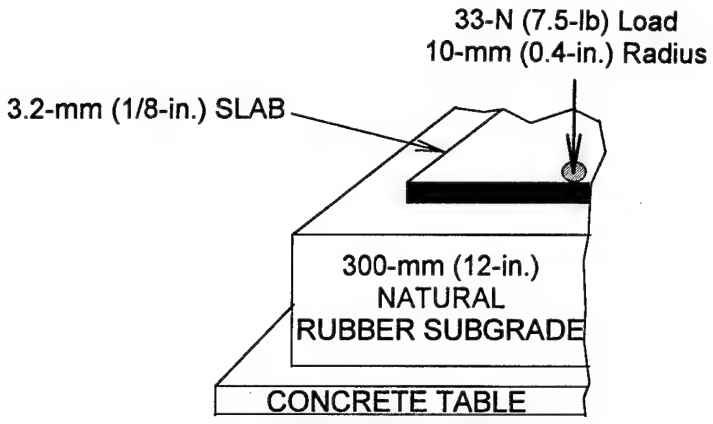

(a) Test configuration

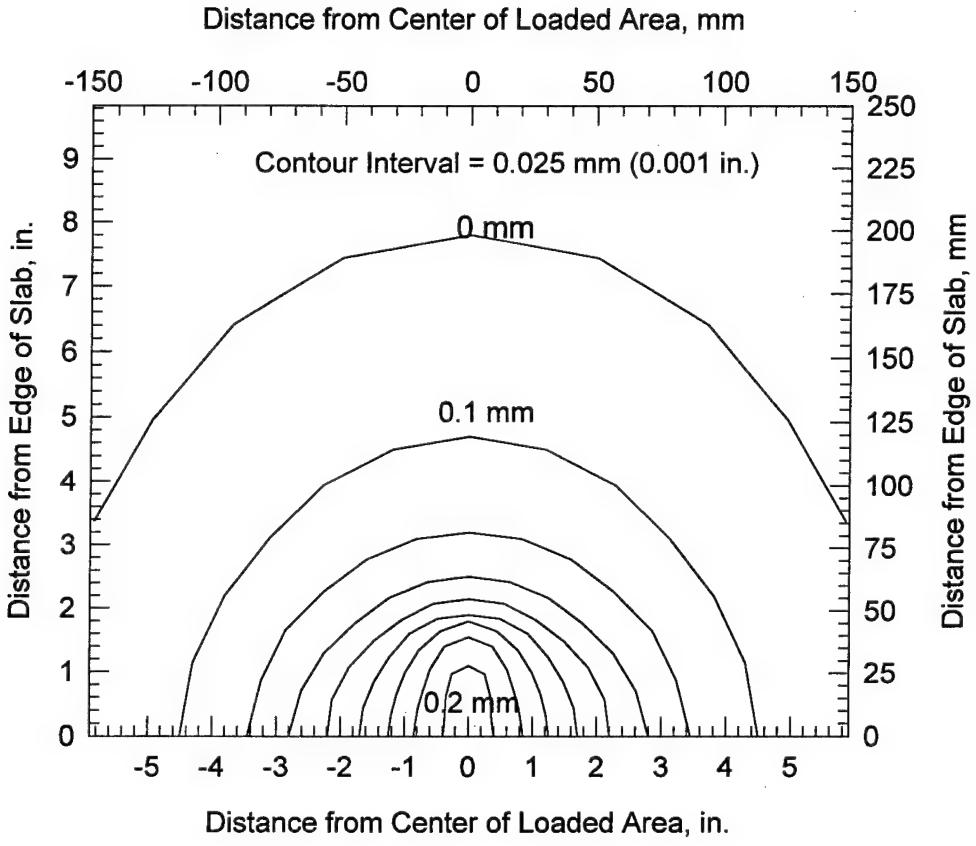

(b) Contour plot

FIGURE 27. EDGE LOADING DEFLECTION CONTOURS FROM SMALL-SCALE MODEL STUDY (AFTER CARLTON AND BEHRMANN, 1956)

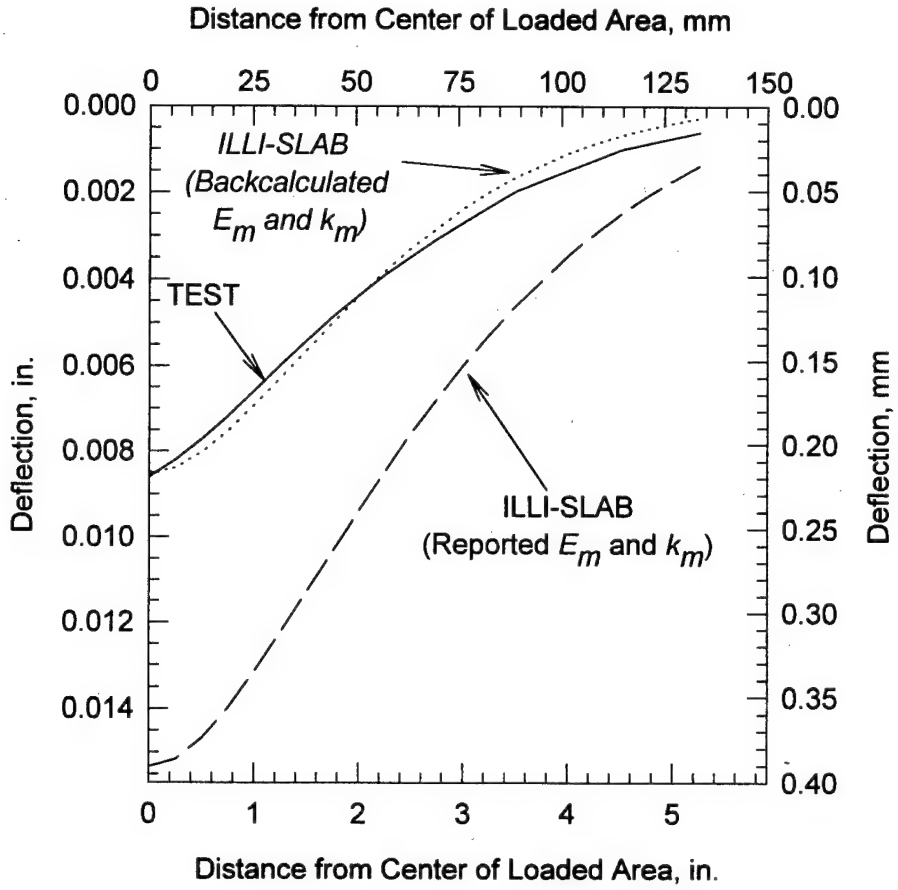

FIGURE 28. COMPARISON OF EDGE LOADING DEFLECTION BASINS FROM EXPERIMENT AND ILLI-SLAB

E = 24,340 MPa (3,530,000 psi)
k = 44.11 MPa/m (162.5 psi/in.)

These values, valid for $\mu = 0.25$, will be used in analyses of data from scaled dowel joint models.

The results of these model studies indicated that models were excellent analog devices for investigating a wide variety of problems related to rigid pavement design. Model studies can be used to study conditions for which a theoretical solution has not been developed or to verify the applicability of new theory. In fact, these small-scale models were referred to as a analog computer and were felt to be a very significant part of the Corps' investigational program.

DOWELED JOINT MODELS.

TEST DESCRIPTION. By the early 1950's certain Corps researchers felt that the thickness requirements for heavily loaded pavements had reached such proportions that the formulation of a definitive method of design for doweled joints was imperative. In an attempt to obtain basic information about the behavior of doweled joints under various loading conditions, a study using small-scale physical models was undertaken by the Ohio Division Laboratories in 1954. The

stated objective was to use these behavior data to develop criteria for use in a rational method for design of doweled joints. The techniques of model construction and data collection described for single slabs above were used to study various combinations of doweled joint designs and loading conditions.

Hydrostone gypsum cement slabs approximately 5.08-mm (0.2-in.) thick were fabricated. A single joint simulating a longitudinal construction joint divided the slabs into two halves each approximately 213 mm (8.38 in.) by 425 mm (16.75 in.). Dowels were simulated by music wire located at mid-depth. The joint design was varied by combining different dowel diameters and dowel spacings. The music wire had been straightened by passing an electrical current through the wire while it was under tension.

The subgrade was simulated by a 610-mm (24-in.) square by 300-mm (12-in.) -thick pad of natural rubber identical to the one described above for testing of single slabs. The radius of relative stiffness (ℓ) of the models was approximately 50 mm (2 in.). Loads were applied through a single circular footprint whose radii (a) were set at 19 mm (0.75 in.), 13 mm (0.50 in.), 8 mm (0.30 in.), and 5 mm (0.20 in.). Additional test variables were dowel bar diameter (d), dowel spacing (s), and joint openings (ω). The testing program followed a matrix in which several ratios, listed in table 4, were formed among the variables. For each of the three values of d/h in table 4, slabs were constructed at the three dowel spacings indicated by s/h. Finally for each combination of d/h, s/h, and ω/h, the loading radii were varied among the values indicated by the four a/ℓ ratios.

TABLE 4. SMALL-SCALE DOWELED JOINT MODEL TEST PARAMETERS

a/ℓ	d/h	s/h	w/h
0.098	0.05	1.5	0
0.156	0.07	2.5	0.025
0.244	0.10	4.5	0.10
0.366			

Each half of the model was cast separately. The first half was cast in a form consisting of steel or brass bars and glass plates. The bar was fitted with holes at the proper dowel spacings. The dowels were cleaned and secured in these holes prior to casting; dowels in this half are referred to as being bonded. The second half of the model was cast in a similar form arrangement, except the first half was used to form the joint. Dowel surfaces were treated to prevent bonding; dowels in this half are referred to as being unbonded. The slabs were allowed to set for 45 minutes before the forms were removed and to cure for 7 days before testing.

The two slabs were placed directly on the rubber pad. Two layers of 19-mm (0.75-in.) lead cubes were distributed uniformly over the surface of each slab to insure continuous contact between the slab and the rubber. Tests were conducted with the load placed directly over a dowel and with the load placed midway between dowels. The loadings were conducted on either side of the joint, referred to as loading on the bonded-dowel side of the joint or loading on the unbonded-

dowel side of the joint. Strains were measured at the surface of the slab immediately above dowels and midway between dowels using resistance wire strain gages bonded to the slab. A typical slab layout showing approximate locations of strain gages is shown in figure 29.

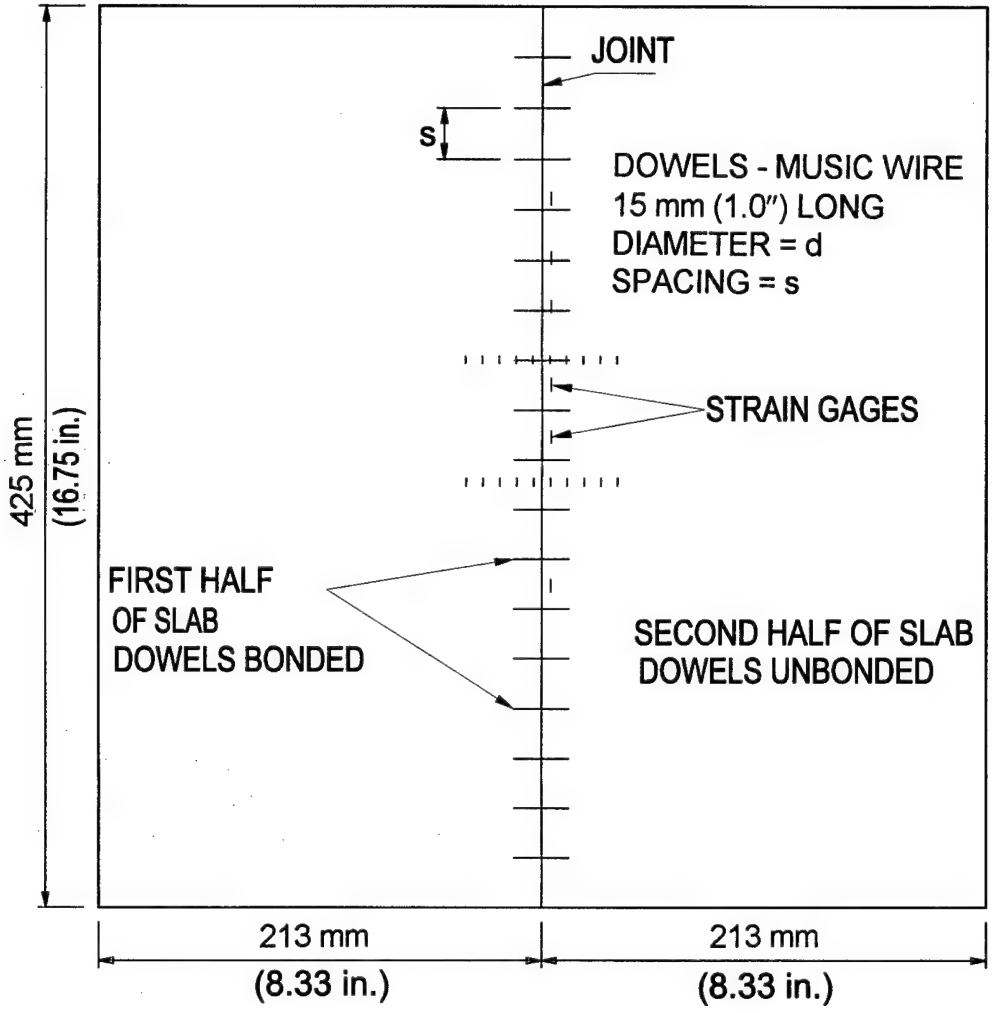

FIGURE 29. TYPICAL SMALL-SCALE DOWEL JOINT TEST SLAB SHOWING APPROXIMATE STRAIN GAGE POSITIONS

TEST RESULTS. Experimental strain curves are presented in appendix A. The values of strain measured on either side of the joint were used to estimate load transfer using the following approximation:

$$LT(\%) = \frac{\varepsilon_L}{\varepsilon_f} \, x \, 100\% \tag{77}$$

where ε_L and ε_f are the experimentally obtained strains on the loaded slab of a jointed model and for a slab with a free edge, respectively. This approximation differs from an exact measurement of *LT* because it neglects Poisson's effects; however, the error in the approximation is very small.

The estimates of *LT* are presented in appendix B. These values confirm that load transfer depends on the size of the dowel, spacing of the dowel, joint opening, and radius of the loaded area. For the various combinations of joint parameters tested, the load transfer values obtained in the experiments were mostly greater than 25 percent, supporting data obtained from the full-scale experimental slab. Upon close examination of the data, some inconsistencies are apparent. For example, if all parameters are held constant except for the dowel spacing, a smaller spacing should result in smaller maximum strain on the loaded slab side of the joint. However, these trends do not always hold true for the data. (See Tests 5-DJ, 8-DJ, and 14-DJ.) Some of these discrepancies are likely due to errors in the experimental measurements, this is justifiable considering the technology of the day. Any errors reaffirm the difficulty of such tests, the meticulous effort of the investigators, as well as their scientific integrity. Nonetheless, the trends delineated by these tests remain a great contribution to the profession.

ANALYSIS. The data were analyzed to backcalculate the joint response parameters necessary to estimate the dimensionless doweled joint stiffness $D/sk\ell$ as defined by Ioannides and Korovesis (1992) and the modulus of dowel reaction *K*. First, the basic material characterizations were assumed to be the same as those backcalculated from the experiments of Carlton and Behrmann (1956); that is,

E = 24,340 MPa (3,530,000 psi)
k = 44.11 MPa/m (162.5 psi/in.)
(for $\mu = 0.25$)

The modulus of elasticity of the dowels where set at E_d = 207,000 MPa (30,000,000 psi) and a Poission's ratio of $\mu_d = 0.25$, values typical of steel. For each combination of test parameters, LTE_δ was estimated from LTE_σ using equation 72. Finally, using equations 12, 17, 18, 19, 19, 20, and 21, estimates of the modulus of dowel reaction (*K*) were obtained by backcalculation.

Table 5 summarizes the backcalculated values of the modulus of dowel reaction and the doweled joint stiffness. These data are plotted in figures 30 and 31. In figure 30 values of K have been normalized by forming the dimensionless ratio of $K(h - d)/E$ suggested by Nishizawa et al. (1989).

Backcalculated values of dimensionless joint stiffness ranged from a low of 3.7 to a high of 996.2, a range of three orders of magnitude. In almost every case, the backcalculated values of dimensionless joint stiffness decrease as the joint opening increases and increase as the dowel diameter increases, which follows with intuition. However, modulus of dowel reaction does not appear to be as well behaved as the dimensionless joint stiffness. Backcalculated values of *K* varied from 0.3×10^6 MPa/m (1.0×10^6 psi/in.) to 598×10^6 MPa/m ($2{,}220 \times 10^6$ psi/in.). These values range from approximately equal to those values commonly reported in the literature to some two orders of magnitude greater than those commonly reported. The reasons for these discrepancies are not immediately apparent. However, it is possible that there exists a significant "size effect," similar to that observed as the size of the circular plate is varied in the plate bearing

TABLE 5. BACKCALCULATED DOWELED JOINT RESPONSE PARAMETERS

Test Name	*s/h*	*d/h*	ω/*h*	*K* 10^6 psi/in.	*K* 10^6 Mpa/m	*D/sk* ℓ
8-DJ	1.5	0.05	0	14.6	4.0	18.3
			0.025	10.3	2.8	12.8
			0.100	5.1	1.4	6.1
5-DJ	2.5	0.05	0	47.4	12.9	27.1
			0.025	14.4	3.9	10.0
			0.100	8.8	2.4	5.3
14-DJ	4.5	0.05	0	30.4	8.2	10.6
			0.025	22.3	6.0	7.5
			0.100	12.6	3.4	3.7
7-DJ	1.5	0.07	0	6.8	1.8	18.6
			0.025	4.6	1.2	13.0
			0.100	3.3	0.9	8.8
3-DJ	2.5	0.07	0	34.7	9.4	38.0
			0.025	11.8	3.2	15.6
			0.100	7.4	2.0	9.16
13-DJ	4.5	0.07	0	327.0	88.7	116.4
			0.025	52.5	14.3	26.1
			0.100	50.6	13.7	17.7
6-DJ	1.5	0.10	0	31.1	8.4	110.4
			0.025	9.7	2.6	43.3
			0.100	5.2	1.4	24.0
4-DJ	2.5	0.10	0	231.0	62.6	297.6
			0.025	94.3	25.6	134.4
			0.100	43.6	11.8	59.5
12-DJ	4.5	0.10	0	1.0	0.3	996.2
			0.025	2,220.0	598.0	554.3
			0.100	52.3	14.2	37.1

test method for determining the modulus of subgrade reaction. It should be noted that *K* is not an intrinsic material property, but rather a system parameter. Thus, *K*, like the modulus of subgrade reaction, is a useful tool for calculating system response, but can be difficult to measure even in carefully controlled experiments, and even more difficult to estimate *a priori* for design purposes.

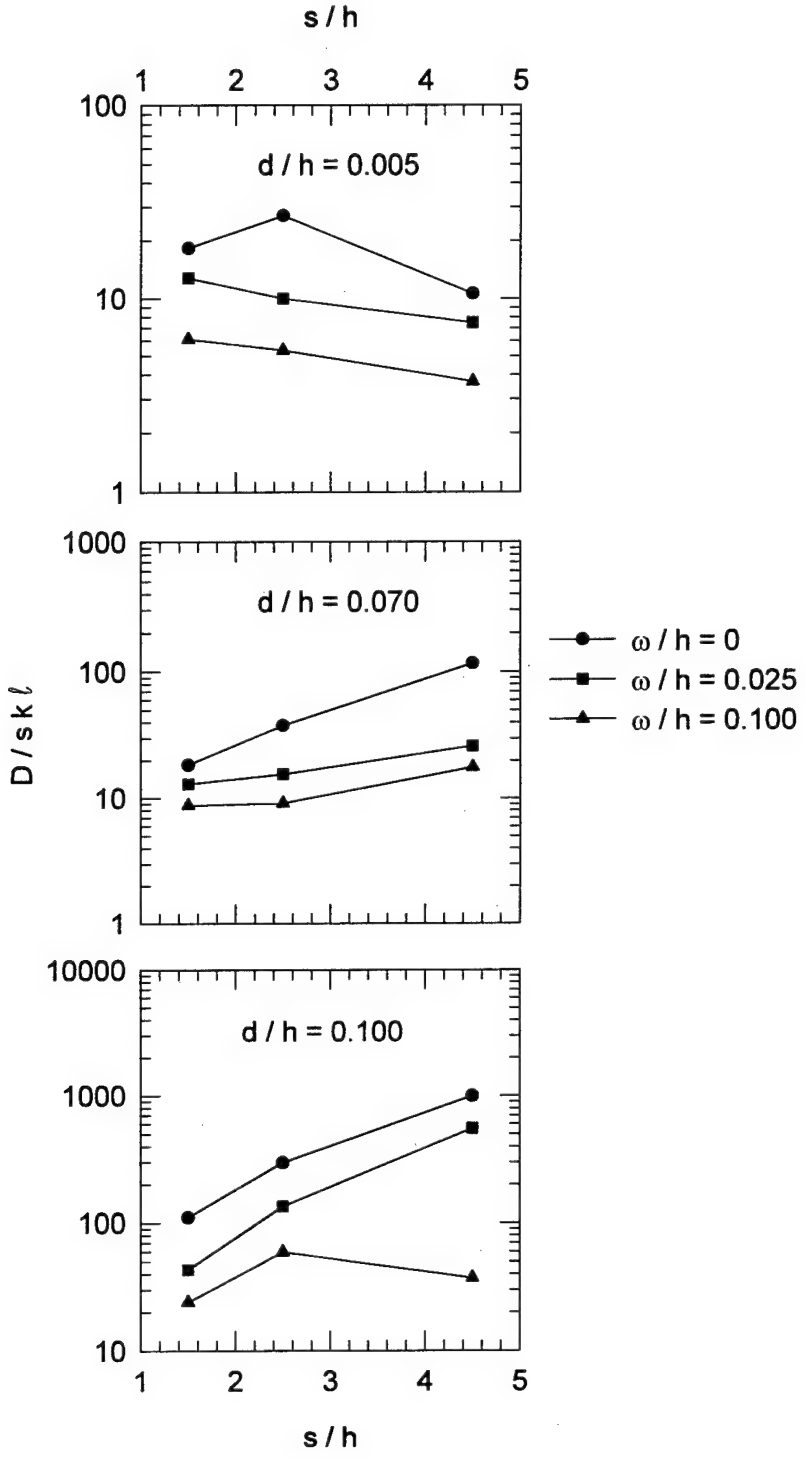

FIGURE 30. BACKCALCULATED DIMENSIONLESS JOINT STIFFNESS FROM SMALL-SCALE MODEL TESTS

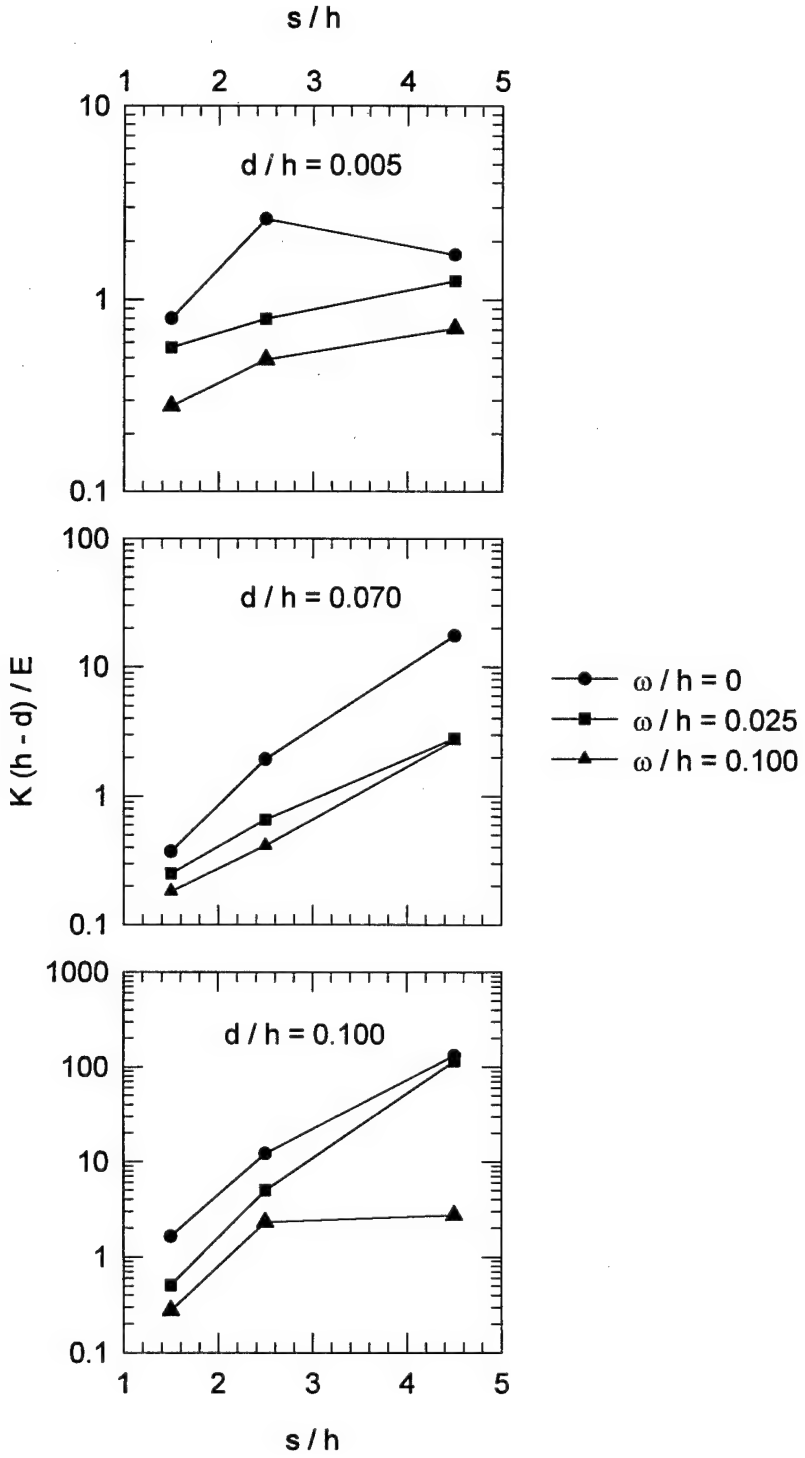

FIGURE 31. BACKCALCULATED MODULUS OF DOWEL REACTION FROM SMALL-SCALE MODEL TESTS

Despite the limitations exhibited by the modulus of dowel reaction, the experimental data confirm the usefulness of the dimensionless joint stiffness as a means of characterizing the response of the doweled joint. The use of the concept of dimensionless joint stiffness appears to be a reasonable approach for developing a mechanistic-based design approach for doweled joints.

CONCLUSIONS AND RECOMMENDATIONS

CONCLUSIONS.

A rigid pavement system consists of a number of relatively thin Portland cement concrete slabs, finite in length and width, and over one or more foundation layers. When a slab-on-grade is subjected to a wheel load, it develops bending stresses and distributes the load over the foundation. However, the response of these finite slabs is controlled by joint or edge discontinuities. By their nature, joints are structurally weakening components of the system. Thus, the response and effectiveness of joints are primary concerns in rigid pavement analysis and design.

Current FAA structural design criteria are based either upon the Westergaard response model or the layered elastic response model. Although available Westergaard solutions have been extensively used, they are limited by two significant shortcomings: (a) only a single slab panel is accommodated in the analysis; therefore, load transfer at joints is not accounted for and (b) the layered nature of the pavement foundation is not explicitly reflected in the Winkler foundation model. Multilayered, linear elastic models, as used in the new FAA design method released in 1994, consider the complete layered system in the vertical direction, thereby addressing the second limitation. In the horizontal direction, however, the layers are assumed to be infinitely long with no discontinuities such as edges or joints. Consequently, the load transfer limitation remains unresolved.

Closed-form solutions akin to those by Westergaard were derived in this study for the maximum responses on the unloaded side of a PCC pavement slab edge capable of a degree of load transfer. When used together with Westergaard's own closed-form equations for the free-edge problem, the formulae derived in this study constitute a complete solution of the edge load transfer problem, recognized over the years as a critical consideration in PCC pavement design. The newly derived solution is presented in convenient form for routine engineering application and is compared to earlier finite element data. The improvement in ease of application and precision is considerable.

Experimental data from small-scale model tests conducted on dowel joints in the 1950's by the Corps of Engineers confirm the usefulness of the dimensionless joint stiffness as a means of characterizing the response of the doweled joint. The use of the concept of dimensionless joint stiffness appears to be a reasonable approach for developing a mechanistic-based design approach for doweled joints.

Over the past two decades, several two-dimensional (2D) finite element analysis programs have been developed which incorporate load transfer at joints. These programs use a thin-plate element formulation for the slab. Some programs allow the user to choose from a library of

foundation models. Finite element analyses which treat the pavement system as 3D have not been used extensively because of the computer resources required. However, today's analytical and computational capabilities have matured to a point that a practical 3D model can be used to develop design criteria for jointed rigid pavements. Use of the available features of finite element methods such as gap elements, interface elements, boundary elements, multipoint constraints, advanced constitutive models, automated mesh generation, and enhanced pre- and postprocessing of results coupled with massively-parallel supercomputers warrants incorporation of these methods into the design process.

RECOMMENDATIONS.

The Westergaard closed-form solutions (including Westergaard's equations, Pickett and Ray's influence chart solutions, as well as their computerized equivalents), layered elastic analysis, and finite element (FE) programs based on 2D elements have proven to be useful tools in the design and analysis of rigid pavements. It is not likely that 3D FE models will summarily replace these techniques in the near future. However, several very important physical processes cannot be adequately modeled without the 3D approach; furthermore, recent developments in engineering mechanics are best suited for 3D applications. Comprehensive 3D modeling will provide a more fundamental understanding of certain aspects of pavement response that can be incorporated into the design process. A broad overview these aspects is presented below.

PAVEMENT PERFORMANCE MODELING. Performance criteria based on total (elastic plus plastic) strain energy densities in the pavement layers may well be a better indicator of pavement performance than current strain-based criteria. Fracture mechanics, a very powerful tool for analyzing crack initiation and propagation in Portland cement concrete slabs and bound base courses, can provide the tools for assessing strain energy effects. With the current state of the art, fracture mechanics has the potential to replace fatigue-based criteria as indicators of pavement performance.

MATERIAL MODELING. The performance of stabilized base courses is not well understood. Currently, layered elastic theory is the most mature analysis methodology for predicting the response of pavement structures containing stabilized bases. However, layered elastic theory treats the stabilized layer as semi-infinite and monolithic. Therefore, it is not well suited for assessing the repercussions on pavement performance of cracking which invariably develops in the stabilized base layer. Within the framework of layered elastic theory, an approximation can be achieved using a fictitious (reduced) modulus, provided a reasonable estimate for its value can be made. This, however, can be a demanding task.

The response of unbound base and subbase courses as well as of the subgrade is not adequately modeled by the simple assumptions of the dense liquid foundation. Layered elastic theory treats each layer as an elastic continuum, resulting in tensile stresses in unbound granular layers as well as ignoring plastic response in the system. Even though more sophisticated two- and three-parameter foundation models are available in some 2D FE programs, a 3D FE approach will allow the use of incremental plasticity theory, such as the modified Drucker-Prager or critical state plasticity models, to be fully implemented in predicting plastic deformations in the system.

MULTIPLE-WHEEL LOAD MODELING. The interaction of multiple wheels is a major concern in pavement analysis, more so in flexible pavements than in rigid. However, the complex interaction of these heavily-loaded wheel on rigid pavement joints is far from well understood. A 3D modeling approach will be required to understand the effects these closely spaced wheels have on jointed pavements.

JOINT MODELING. Dowels have been used as load transfer devices in jointed concrete pavements almost since the beginning of construction of such pavements. Dowel bars are thought to prevent faulting, reduce pumping, and reduce corner breaks. However, the design of dowels is based mostly on experience and theoretical abstractions. Most design procedures, including that of the FAA, prescribe the diameter, length, and spacing of dowel bars based upon pavement thickness. To broaden the understanding of the fundamental mechanics of doweled joints and to put the selection and spacing of dowel bars on a more fundamental basis, a more sophisticated modeling technique is required. The interaction between the dowel and the concrete matrix in which it is encased is a complex 3D phenomenon, ideally requiring a 3D analytical approach. It is well known that dowels located at some distance away from the point of application of the load are not as effective in transferring load as those that are closer. The number of dowels that are effective in distributing the load has been debated since the early developments of rigid pavement modeling. Even state-of-the-art 2D FE modeling involves, at least implicitly, assumptions which limit the precision of estimates concerning the load carried by each dowel. This problem is even further complicated by the interaction of loads from multiple-wheel landing gears. Adopting a 3D FE model may clarify such issues further. It is also known that the proper installation of dowels has been a problem during construction. A 3D modeling technique could accommodate misalignment and therefore provide criteria useful for quality control and acceptance testing of doweled pavements during the construction process.

The work of Kou (1994) can be used as the starting point for the analytical model to be developed in this study. ABAQUS, a general-purpose, nonlinear, 3D, dynamic finite element code developed by Hibbitt, Karlsson, and Sorensen, Inc., can be used to develop this model.

A general 3D finite element model including the joint and interfaces between the slab and base can be developed. First, a 3D model of a slab on a dense liquid foundation can be developed and the results from this model compared to the Westergaard solution for loads for the interior and edge loading case.

Next, load transfer at the joint between two adjacent slab panels can be added to the model using the concepts of the nondimensional joint stiffness developed by Ioannides and Korovesis (1992). The ABAQUS JOINTC element can be used to formulate the joint stiffness. The model parameters for the joint can be correlated to fundamental joint response parameters such as deflection or stress load transfer efficiency. The results of these analyses can be compared to the 2D finite element code ILLI-SLAB and the 3D model improved until acceptable results are obtained.

Finally, an explicit model of the base course can be added to the 3D model. The boundary between the slab panels and the base course can be modeled using interface elements. These

elements are formulated to model contact and friction of part of or all of the areas of the contact surfaces. Interpolation functions of the interface elements can be chosen to be compatible with the interpolation functions for the elements on either side of the contact surface.

REFERENCES

Ahlvin, R. G., 1971. "Multiple-Wheel Heavy Gear Load Pavement Tests, Volume I," AFWL-TR-70-113, Vol. I, Air Force Weapons Laboratory, Kirtland Air Force Base, NM.

Ahlvin, R. G., 1991. "Origin of Developments for the Structural Design of Pavements," Technical Report GL-91-26, Department of the Army, U.S. Army Engineer Waterways Experiment Station, Vicksburg, MS.

Barker, W. R. and Gonzalez, C. R., 1991. "Pavement Design by Elastic Layer Theory," Aircraft/Pavement Interaction, An Integrated System, American Society of Civil Engineers, New York, NY, pp. 21-43.

Behrmann, R. M., 1966. "Small-Scale Model Study to Determine the Effects of Sawkerfs and Bored Recesses of Load-Carrying Capacity of Rigid Pavement," Technical Report No. 4-38, Corps of Engineers, Ohio River Division Laboratories, Cincinnati, OH.

Behrmann, R. M., 1972. "Small-Scale Static Load Model Study: Behavior of Rigid Pavement Loaded Near the Edge," Technical Report No. S-4, Construction Engineering Research Laboratory, Champaign, IL.

Burns, C. D., 1971. "Multiple-Wheel Heavy Gear Load Pavement Tests, Volume II," AFWL-TR-70-113, Vol. II, Air Force Weapons Laboratory, Kirtland Air Force Base, NM.

Carlton, P. F. and Behrmann, R. M., 1956. "A Model Study of Rigid Pavement Behavior Under Corner and Edge Loadings," Proceedings, Thirty-Fifth Annual Meeting, Highway Research Board, National Research Council, Washington, DC, pp. 139 - 146.

Chatti, K., 1992. "Dynamic Analysis of Jointed Concrete Pavements Subjected to Moving Transient Loads," Ph.D. Dissertation, University of California at Berkeley, Berkeley, CA.

Crawford, J. E. and Katona, M. G., 1975. "State-of-the-Art for Prediction of Pavement Response," Contract Report S-75-8, U.S. Army Engineer Waterways Experiment Station, Vicksburg, MS.

Departments of the Army and the Air Force, 1988. "Rigid Pavement Design for Airfields, Elastic Layered Method," Army TM 5-825-3-1 and Air Force AFM 88-6, Chap. 3, Section A, Headquarters, Departments of the Army and the Air Force, Washington, DC.

Departments of the Army and the Air Force, 1989. "Flexible Pavement Design for Airfields (Elastic Layered Method)," Army TM 5-825-2-1 and Air Force AFM 88-6, Chap. 2, Section A, Headquarters, Departments of the Army and the Air Force, Washington, DC.

Federal Aviation Administration, 1978. "Airport Pavement Design and Evaluation," Advisory Circular AC 150/5320-6C, Federal Aviation Administration, Washington, DC.

Grinter, L. E., 1931. "Design of Reinforced Concrete Road Slabs," Bulletin No. 39, Texas Engineering Experiment Station, College Station, TX.

Friberg, B. F., 1940. "Design of Dowels in Transverse Joints of Concrete Pavements," Transactions of the American Society of Civil Engineers, Vol. 105, pp. 1076-1095.

Hammons, M. I.; Pittman, D. W., and Mathews, D. D., 1995. "Effectiveness of Load Transfer Devices," DOT/FAA/CT-94/54, Federal Aviation Administration Technical Center, Atlantic City Airport, NJ.

Heinrichs, K. W., Liu, M. J., Darter, M. I., Carpenter, S. H., and Ioannides, A. M., 1989. "Rigid Pavement Analysis and Design," Publication No. FHWA-RD-88-068, Federal Highway Administration, McLean, VA.

Huang, Y. H., 1974. "Finite Element Analysis of Slabs on Elastic Solids," Journal of Transportation Engineering, Vol. 100, No. TE2, American Society of Civil Engineers, New York, NY.

Huang, Y. H., 1985. "A Computer Package for Structural Analysis of Concrete Pavements," Proceedings, Third International Conference on Concrete Pavement Design and Rehabilitation, Purdue University, West Lafayette, IN.

Huang, Y. H., 1993. Rigid Pavement Analysis and Design, Prentice-Hall, Inc., Englewood Cliffs, NJ.

Huang, Y. H. and Wang, S. T., 1973. "Finite-Element Analysis of Concrete Slabs and Its Implications for Rigid Pavement Design," Highway Research Record No. 466, Highway Research Board, Washington, DC.

Hutchinson, R. L., 1966. "Basis for Rigid Pavement Design for Military Airfields," Miscellaneous Paper No. 5-7, Department of the Army, Corps of Engineers, Ohio River Division Laboratories, Cincinnati, OH.

Ioannides, A. M., 1984. "Analysis of Slabs-On-Grade for a Variety of Loading and Support Conditions," Ph.D. Thesis, University of Illinois, Urbana, IL.

Ioannides, A. M., Thompson, M. R., and Barenberg, E. J., 1985. "Westergaard Solutions Reconsidered," Transportation Research Record 1043, Transportation Research Board, National Research Council, Washington, DC, pp. 13-23.

Ioannides, A. M., Donnelly, J., Thompson, M. R., and Barenberg, E. J., 1986. "Three-Dimensional Finite Element Analysis of a Slab on Stress Dependent Elastic Solid Foundation," Air Force Office of Scientific Research, Bolling AFB, DC.

Ioannides, A. M., Thompson, M. R., Donnelly, J., and Barenberg, E. J., 1986. Three-Dimensional Finite Element Analysis of a Slab on Stress Dependent Elastic Solid Foundation, University of Illinois at Urbana-Champaign, Urbana, IL.

Ioannides, A. M., 1988. "Finite Difference Solution for Plate on Elastic Solid," Journal of Transportation Engineering, Vol. 114, No. 1, American Society of Civil Engineers, New York, NY, pp. 57-75.

Ioannides, A. M., Lee, Y. H., and Darter, M. I., 1990. "Control of Faulting Through Joint Load Transfer Design," Transportation Research Record No. 1286, Transportation Research Board, Washington, DC, pp. 49-56.

Ioannides, A. M. and Korovesis, G. T., 1990. Aggregate Interlock: A Pure-Shear Load Transfer Mechanism. In *Transportation Research Record 1286*, Transportation Research Board, National Research Council, Washington, DC, pp. 14-24.

Ioannides, A. M. and Korovesis, G. T., 1992. "Analysis and Design of Doweled Slab-on-Grade Pavement Systems," Journal of Transportation Engineering, Vol 118, No. 6, American Society of Civil Engineers, New York, NY, pp. 745-768.

Jandel, 1994. *SigmaStat* Statistical Software for Windows, User's Manual. Jandel Scientific Software, San Rafael, CA.

Kerr, A. D., 1964. "Elastic and Viscoelastic Foundation Models," Journal of Applied Mechanics, Vol. 31, No. 3.

Kerr, A. D., 1965. "A Study of a New Foundation Model," Acta Mechanic, Vol. I/2.

Kerr, A. D., 1993. "Mathematical Modeling of Airport Pavements," Airport Pavements Innovations, Theory to Practice, Proceedings, 1993 Airfield Pavement Committee Conference, Jim W. Hall, Jr., editor, American Society of Civil Engineers, New York, NY.

Khazanovich, L. and Ioannides, A. M., 1993. "Finite Element Analysis of Slabs-On-Grade Using Higher Order Subgrade Models," Airport Pavements Innovations, Theory to Practice, Proceedings, 1993 Airfield Pavement Committee Conference, Jim W. Hall, Jr., editor, American Society of Civil Engineers, New York, NY.

Korovesis, G. T., 1990. "Analysis of Slab-On-Grade Pavement Systems Subjected to Wheel and Temperature Loadings," Ph.D. thesis, University of Illinois, Urbana, IL.

Kuo, C. M., 1994. "Three-Dimensional Finite Element Analysis of Concrete Pavement," Ph.D. Dissertation, University of Illinois at Urbana-Champaign, Urbana, IL.

Kushing, J. W. and Fremont, W. O., 1940. "Design of Load Transfer Joints in Concrete Pavements," Proceedings, No. 20, Highway Research Board, National Research Council, Washington, DC, pp. 481-493.

Larralde, J. and Chen, W. F., 1985. "Computer Model for Analysis of Rigid Pavements with Fatigue," Proceedings, Third International Conference on Concrete Pavement Design and Rehabilitation, Purdue University, West Lafayette, IN.

Ledbetter, R. H., 1971a. "Multiple-Wheel Heavy Gear Load Pavement Tests, Volume IIIA," AFWL-TR-70-113, Vol. IIIA, Air Force Weapons Laboratory, Kirtland Air Force Base, NM.

Ledbetter, R. H., 1971b. "Multiple-Wheel Heavy Gear Load Pavement Tests, Volume IIIB," AFWL-TR-70-113, Vol. IBIA, Air Force Weapons Laboratory, Kirtland Air Force Base, NM.

Majidzadeh, K., Ilves, G. H., and McComb, R., 1981. "Mechanistic Design of Rigid Pavements," Proceedings, Second International Conference on Concrete Pavement Design, Purdue University, West Lafayette, IN.

Mellinger, F. M. and Carlton, P. F., 1955. "Application of Models to Design Studies of Concrete Airfield Pavements," Proceedings, Thirty-Fourth Annual Meeting, Highway Research Board, National Research Council, Washington, DC, pp. 57-64.

Nádai, A., 1925. Die Elastischen Platten (Elastic Plates). Julius Springer, Berlin (In German).

Nishizawa, T., Fukuda, T., and Matsumo, S., 1989. "A Refined Model of Doweled joints for Concrete Pavement Using FEM Analysis," Proceedings, Fourth International Conference on Concrete Pavement Design, Purdue University, West Lafayette, IN.

Corps of Engineers, 1962. "Small Scale Model Studies of Prestressed Rigid Pavements for Military Airfields, Part I, Development of the Model and Results of Exploratory Tests," Technical Report 4-13, Ohio River Division Laboratories, Cincinnati, OH.

Corps of Engineers, 1963. "Small Scale Model Studies of Prestressed Rigid Pavements for Military Airfields, Part II, Single-Wheel Loadings on Pre-tensioned and Post-tensioned Slabs," Technical Report 4-25, Ohio River Division Laboratories, Cincinnati, OH.

Pickett, G. and Ray, G. K., 1951. "Influence Charts for Concrete Pavements," Transactions, American Society of Civil Engineers, Vol. 116.

Pickett, G., Rayville, Jones, and McCormick, 1951. "Deflections, Moments, and Reactive Pressures for Concrete Pavements," Kansas State College Bulletin, No. 65, October 1951, Kansas State College, Manhatten, KS.

Rollings, R. S., 1989. "Developments in the Corps of Engineers Rigid Pavement Design Procedure," Proceedings, Fourth International Conference on Concrete Pavement Design and Rehabilitation, Purdue University, West Lafayette, IN, pp. 405-418.

Sale, J. P. and Hutchinson, R. L., 1959. "Development of Rigid Pavement Design Criteria for Military Airfields," Journal of the Air Transport Division, Vol. 85, No. AT3, 1959. American Society of Civil Engineers, New York, NY, pp. 129-151.

Sale, J. P., 1977. "Rigid Pavement Design for Airfields," Proceedings, First International Conference on Concrete Pavement Design, Purdue University, West Lafayette, IN.

Skarlatos, M. S., 1949. "Deflections and Stresses in Concrete Pavements of Airfields with Continuous Elastic Joints," Ohio River Division Laboratories, U.S. Army Corps of Engineers, Mariemont, OH.

Tabatabaie, A. M., Barenberg, E. J., and Smith, R. E., 1979. "Longitudinal Joint Systems in Slip-Formed Rigid Pavements," (3 Volumes), Report No. FAA-RD-79-4, Federal Aviation Administration, Washington, DC.

Tabatabaie-Raissi, A. M., 1978. "Structural Analysis of Concrete Pavement Joints," PhD Dissertation, University of Illinois, Urbana, IL.

Tayabji, S. D. and Colley, B. E., 1984. "Analysis of Jointed Concrete Pavements," Report No. FHWA/RD-86/041, Federal Highway Administration, McLean, VA.

Tia, M., Armaghani, J. M., Wu, C., Lie, S., and Toye, K. L., 1987. "FEACONS III Computer Program for Analysis of Jointed Concrete Pavements," Transportation Research Record No. 1136, Transportation Research Board, Washington, DC.

Timoshenko, S. and Lessels, J. M., 1925. Applied Elasticity, Westinghouse Technical Night School Press, Pittsburgh, PA.

Westergaard, H. M., 1923. "Om Beregning Af Plader Paa Elastisk Underlag Med Særligt Henblik Pass Ppørgsmaalet Om Spændinger I Betonveje," Ingeniøren, 1923, pp 513-524. (In Danish).

Westergaard, H. M., 1926. "Stresses in Concrete Pavements Computed by Theoretical Analysis," Public Roads, Vol. 7, No. 2, Highway Research Board, Washington, DC, pp. 25-35.

Westergaard, H. M., 1928. "Spacing of Dowels," Proceedings, National Research Council, Highway Research Board, No. 8, Washington, DC, pp. 154-158.

Westergaard, H. M., 1933. "Analytical Tools for Judging Results of Structural Tests of Concrete Pavements," Public Roads, Vol. 14, No. 10, Dec. 1933, pp 129-151.

Westergaard, H. M., 1939. "Stresses in Concrete Runways of Airports," Proceedings, Highway Research Board, National Research Council, Washington, DC, pp. 197-205.

Westergaard, H. M., 1948. "New Formulas for Stresses in Concrete Pavements of Airfields," Transactions, American Society of Civil Engineers, Vol. 113, pp. 425-444.

Woodhead, R. W. and Wortman, R. H., 1973. Proceedings, Allerton Park Conference on Systems Approach to Airfield Pavements: 23-26 March, 1970. *Technical Report P-5*, Construction Engineering Research Laboratory, Champaign, IL.

Wolfram, S., 1991. *Mathematica: A System for Doing Mathematics by Computer*, Second Edition, Addison-Wesley Publishing Company, Inc., Redwood City, CA.

Wu, C., Tia, M., and Larsen, T. J., 1993. "Analysis of Structural Response of Concrete Pavements under Critical Thermal-Loading Conditions," Proceedings, Fifth International Conference on Concrete Pavement Design and Rehabilitation, Purdue University, West Lafayette, IN.

Zaghloul, S. and White, T. "Non-Linear Dynamic Analysis of Concrete Pavements," Proceedings, Fifth International Conference on Concrete Pavement Design and Rehabilitation, Vol. 1, Purdue, University, West Lafayette, IN, pp. 277-292.

Zienkiewicz, O. C. and Cheung, Y. K., 1967. The Finite Element Method of Structural and Continuum Mechanics, McGraw-Hill Publishing Company Limited, London.

APPENDIX A

STRAIN PLOTS FROM SMALL-SCALE MODEL TESTS

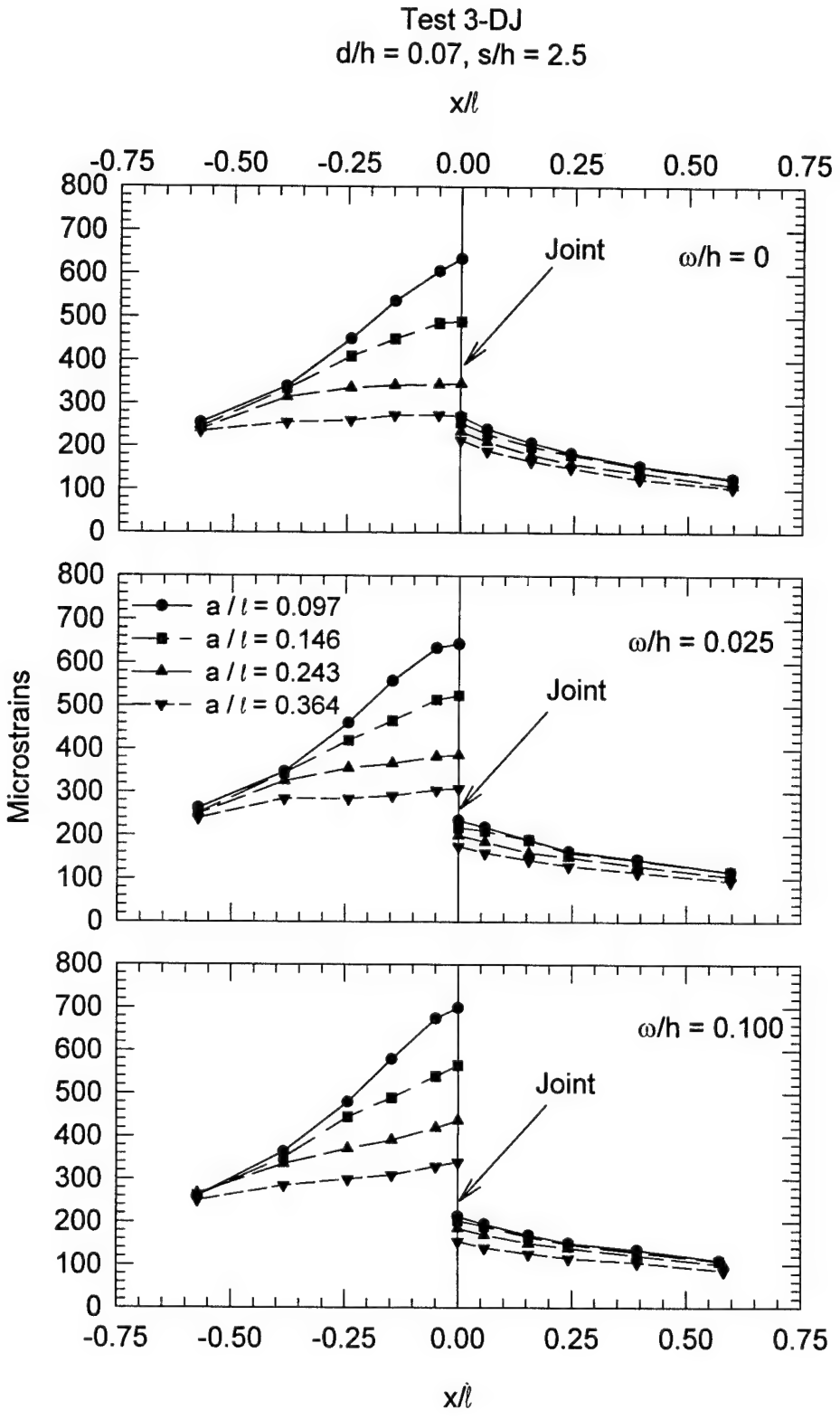

PLATE A1

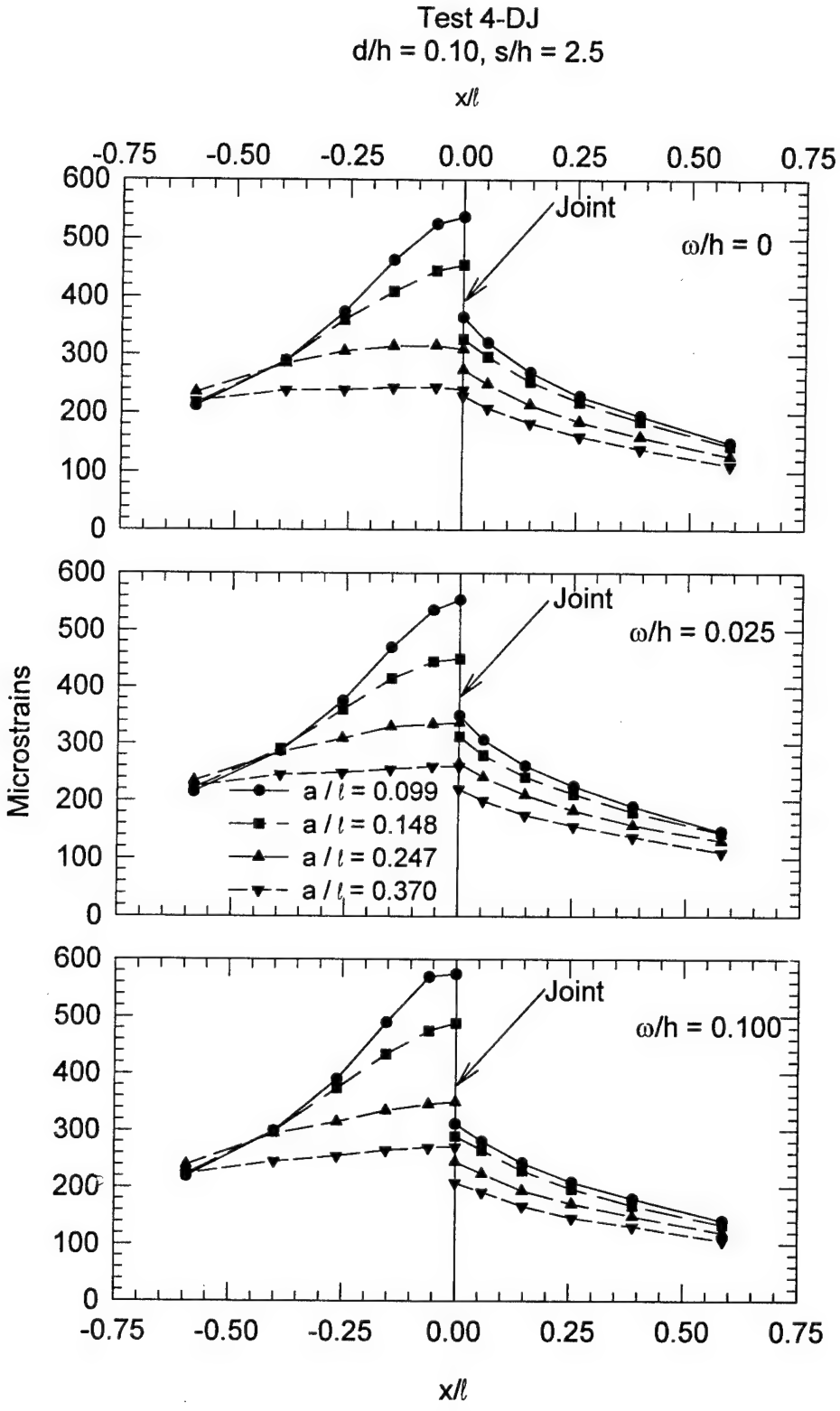
Test 4-DJ
d/h = 0.10, s/h = 2.5
x/ℓ
-0.75
-0.50
-0.25
0.00
0.25
0.50
0.75
Joint
ω/h = 0
ω/h = 0.025
ω/h = 0.100
Microstrains
a / ℓ = 0.099
a / ℓ = 0.148
a / ℓ = 0.247
a / ℓ = 0.370
0
100
200
300
400
500
600

PLATE A2

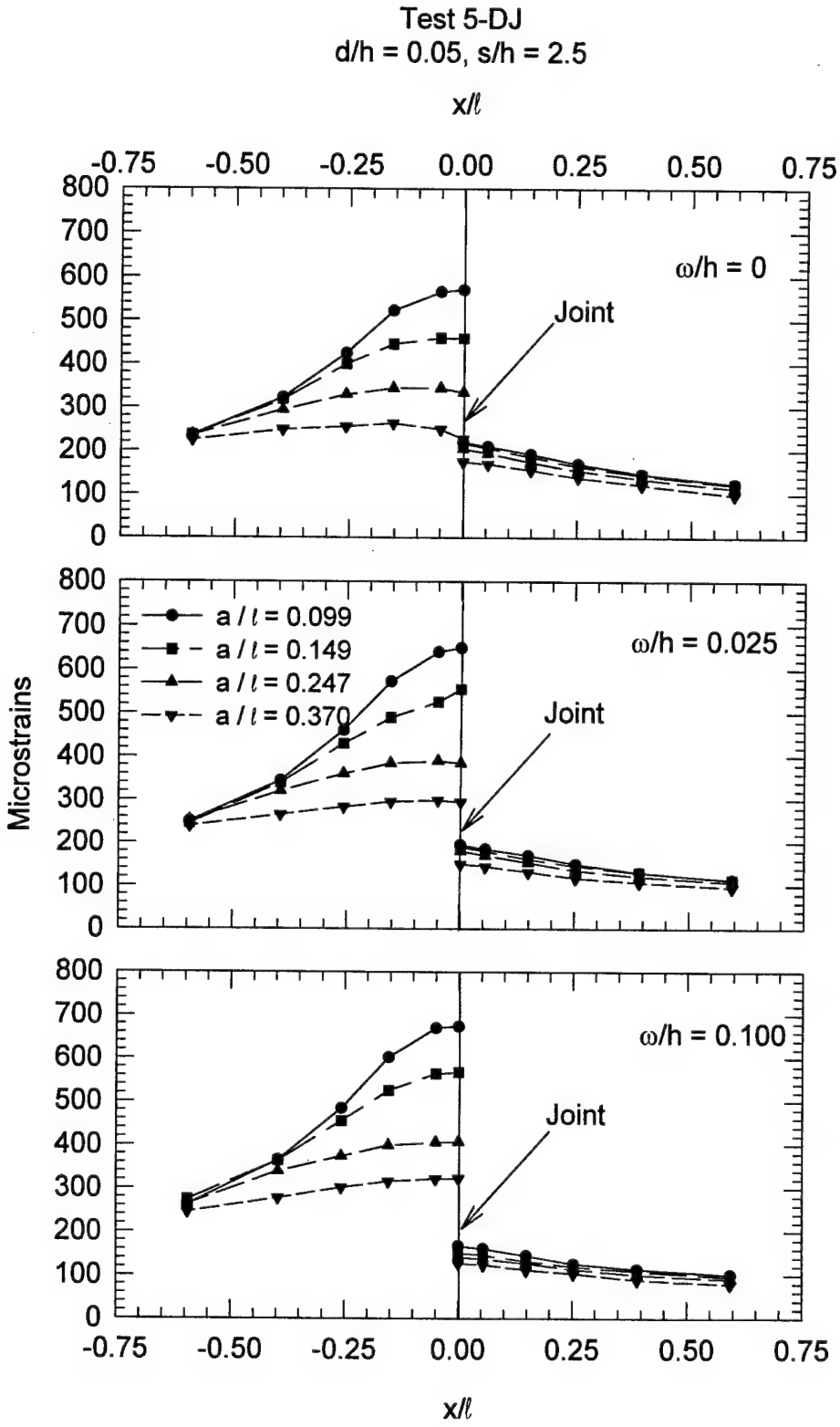
Test 5-DJ
d/h = 0.05, s/h = 2.5
x/ℓ
-0.75
-0.50
-0.25
0.00
0.25
0.50
0.75
800
700
600
500
400
300
200
100
0
ω/h = 0
Joint
a / ℓ = 0.099
a / ℓ = 0.149
a / ℓ = 0.247
a / ℓ = 0.370
ω/h = 0.025
Joint
ω/h = 0.100
Joint
Microstrains
x/ℓ

PLATE A3

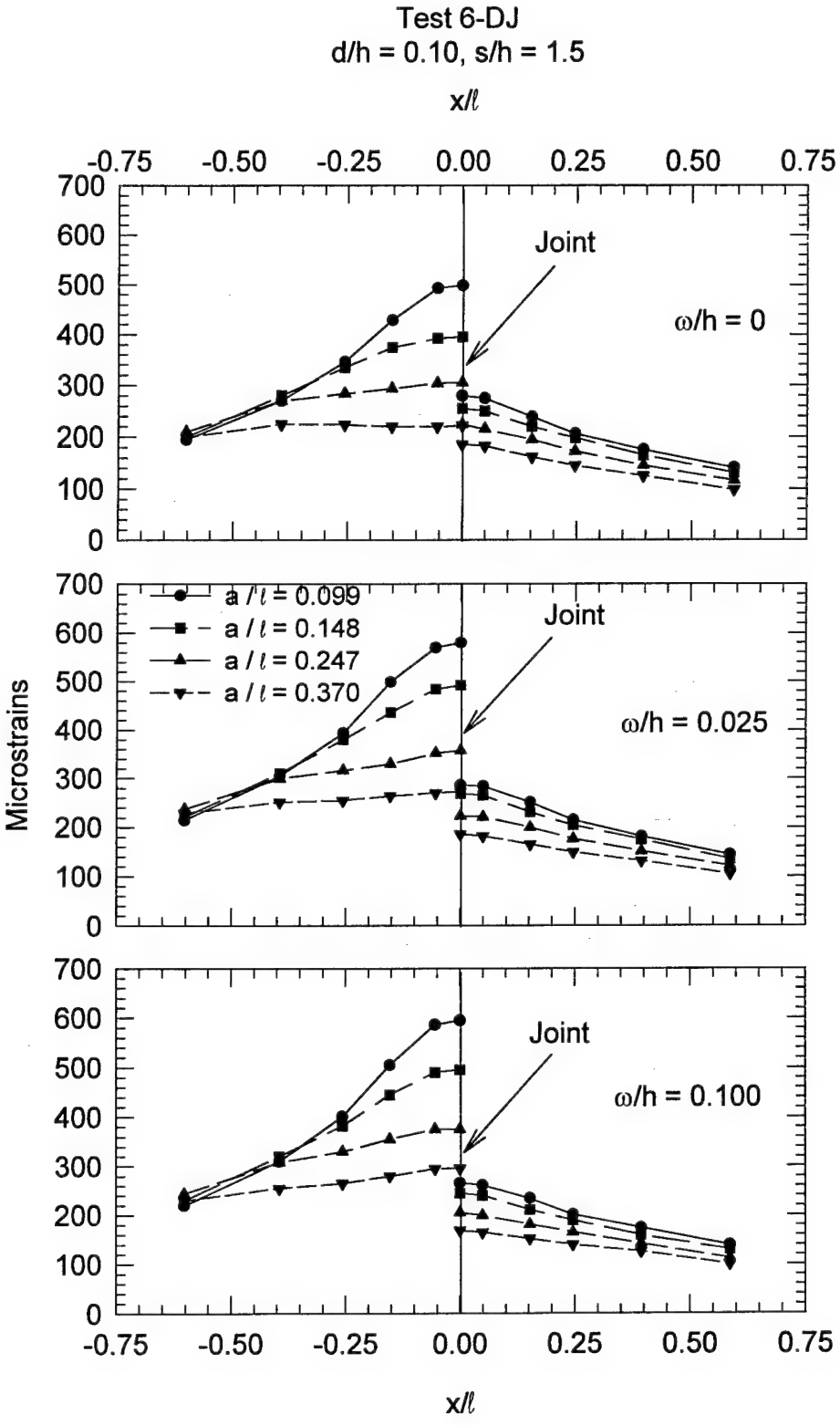
Test 6-DJ
d/h = 0.10, s/h = 1.5
x/ℓ
-0.75
-0.50
-0.25
0.00
0.25
0.50
0.75
Joint
ω/h = 0
ω/h = 0.025
ω/h = 0.100
a / ℓ = 0.099
a / ℓ = 0.148
a / ℓ = 0.247
a / ℓ = 0.370
Microstrains
0
100
200
300
400
500
600
700

PLATE A4

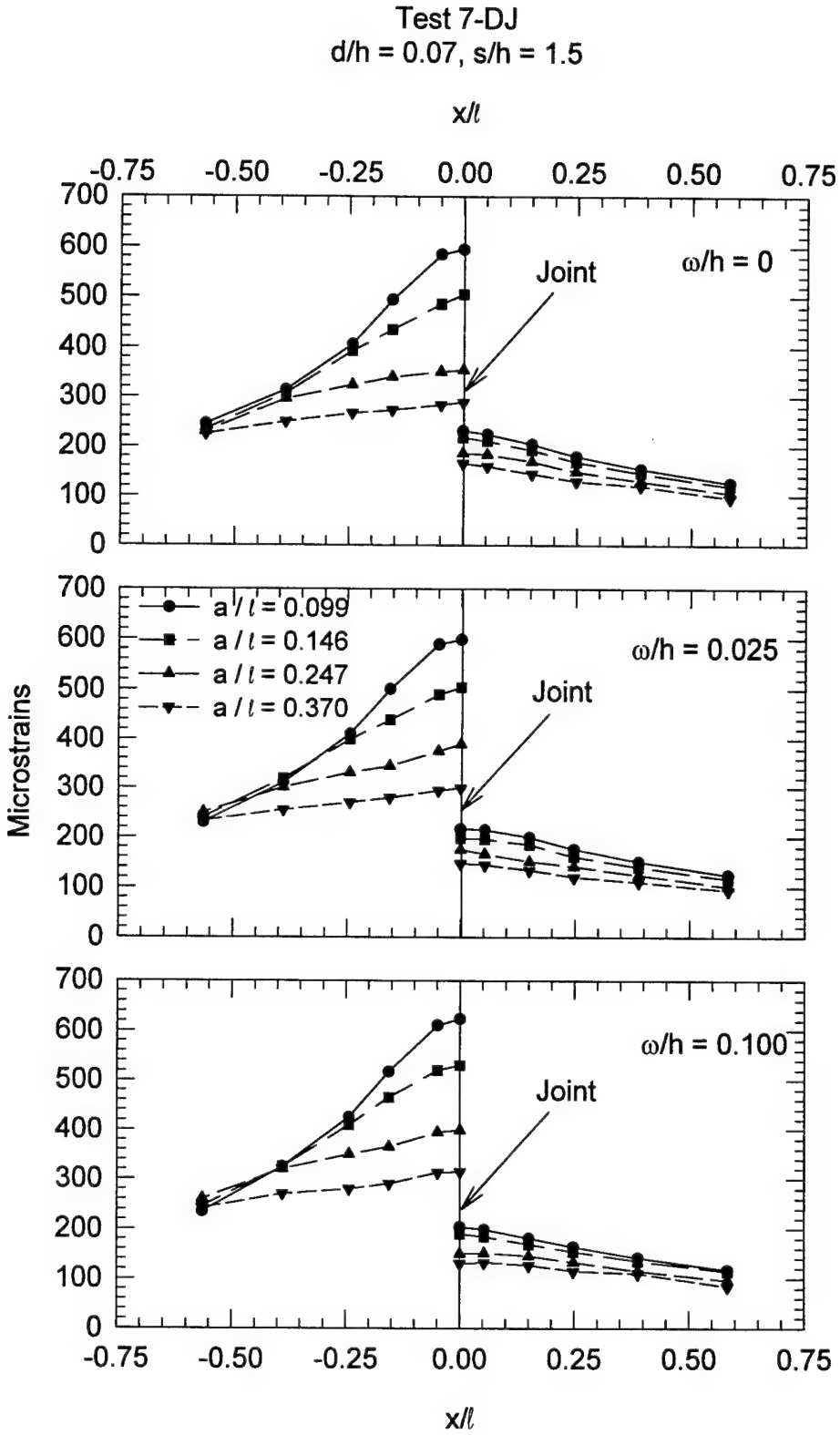
Test 7-DJ
d/h = 0.07, s/h = 1.5
x/ℓ
-0.75
-0.50
-0.25
0.00
0.25
0.50
0.75
700
600
500
400
300
200
100
0
Joint
ω/h = 0
a / ℓ = 0.099
a / ℓ = 0.146
a / ℓ = 0.247
a / ℓ = 0.370
ω/h = 0.025
Microstrains
ω/h = 0.100

PLATE A5

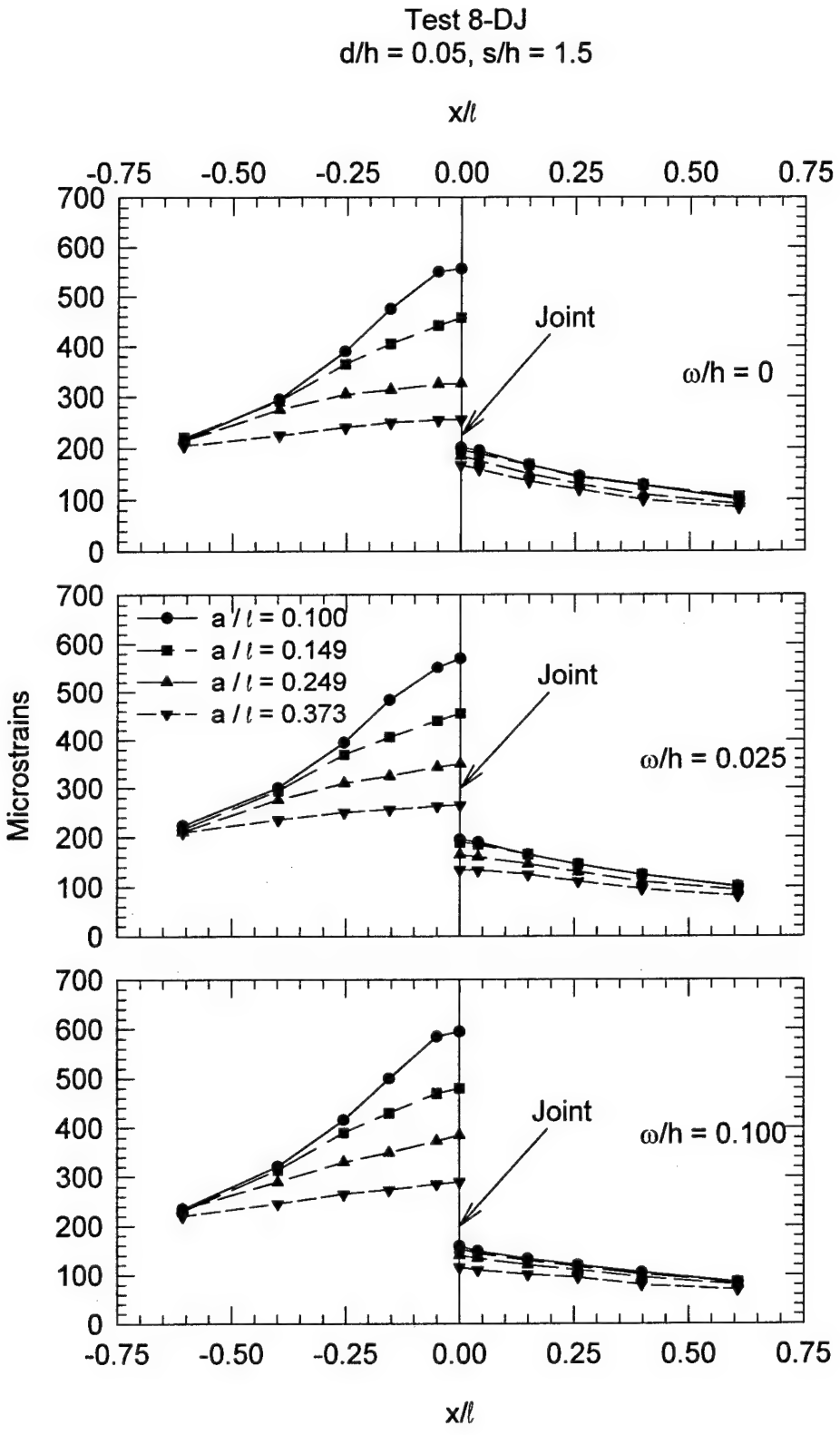
Test 8-DJ
d/h = 0.05, s/h = 1.5
x/ℓ
-0.75
-0.50
-0.25
0.00
0.25
0.50
0.75
700
600
500
400
300
200
100
0
Joint
ω/h = 0
a / ℓ = 0.100
a / ℓ = 0.149
a / ℓ = 0.249
a / ℓ = 0.373
Microstrains
ω/h = 0.025
ω/h = 0.100

PLATE A6

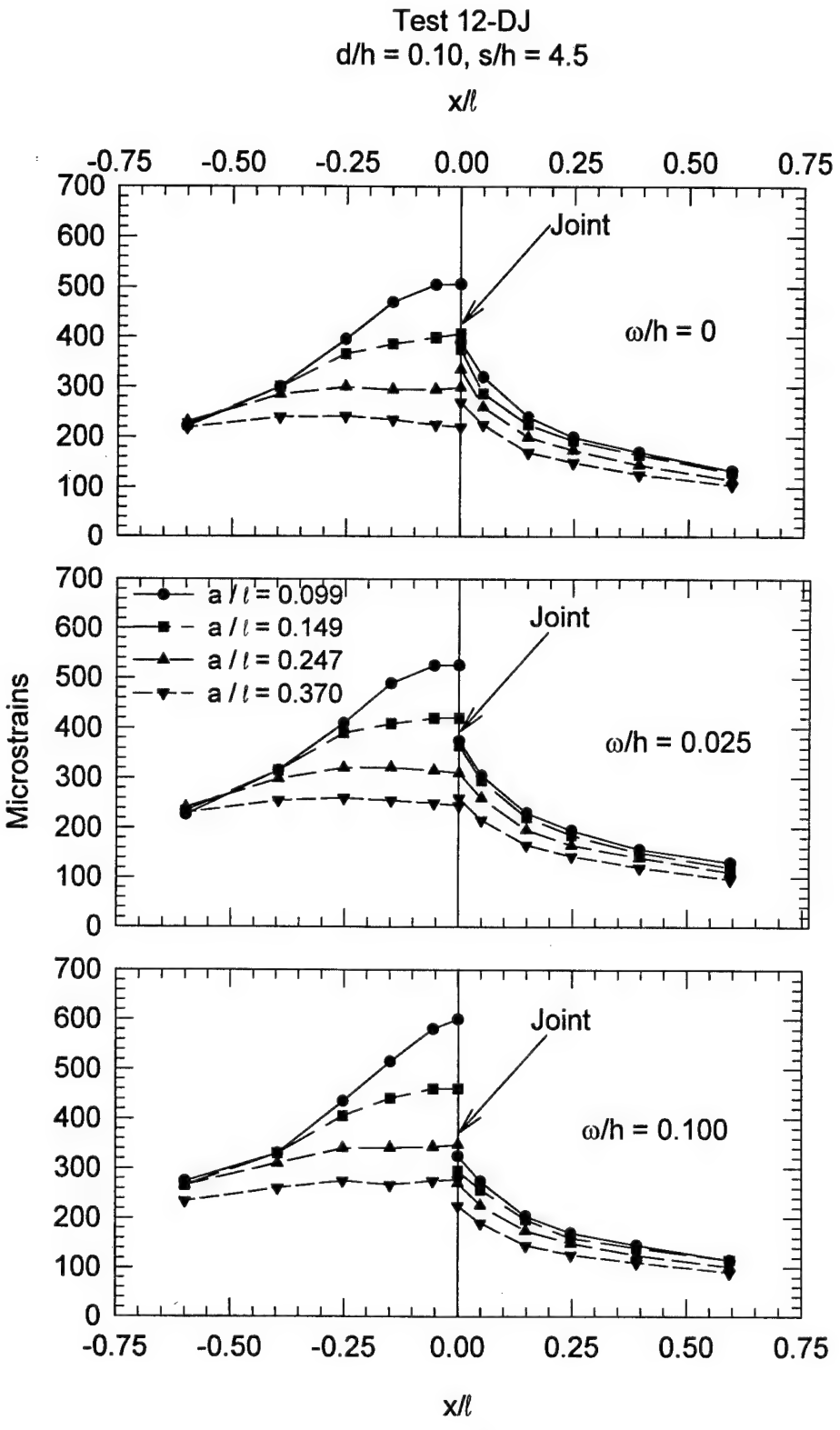
Test 12-DJ
d/h = 0.10, s/h = 4.5
x/ℓ
-0.75
-0.50
-0.25
0.00
0.25
0.50
0.75
Microstrains
0
100
200
300
400
500
600
700
Joint
ω/h = 0
a / ℓ = 0.099
a / ℓ = 0.149
a / ℓ = 0.247
a / ℓ = 0.370
ω/h = 0.025
ω/h = 0.100

PLATE A7

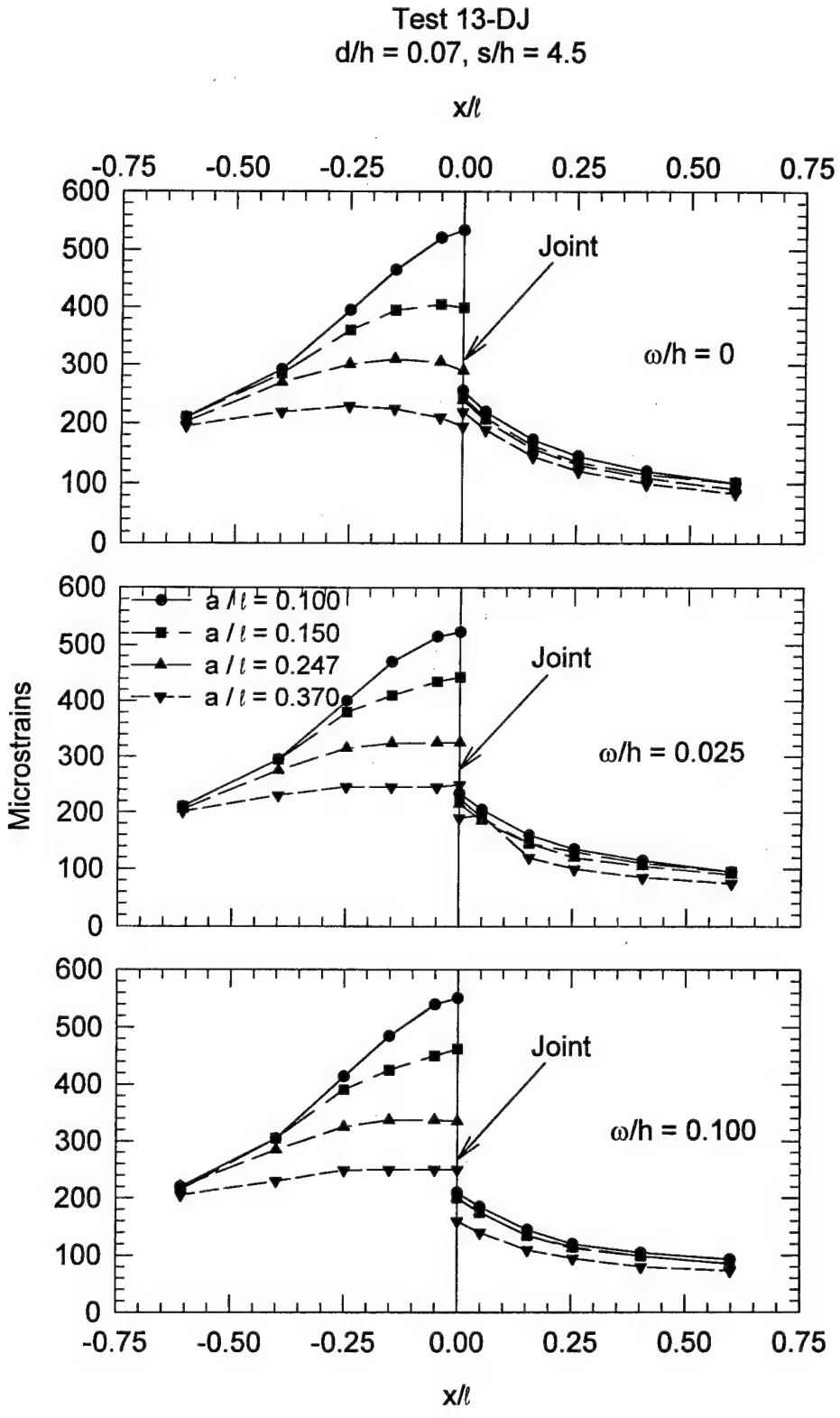
Test 13-DJ
d/h = 0.07, s/h = 4.5
x/ℓ
-0.75
-0.50
-0.25
0.00
0.25
0.50
0.75
600
500
400
300
200
100
0
Joint
ω/h = 0
a / ℓ = 0.100
a / ℓ = 0.150
a / ℓ = 0.247
a / ℓ = 0.370
Microstrains
Joint
ω/h = 0.025
Joint
ω/h = 0.100
x/ℓ

PLATE A8

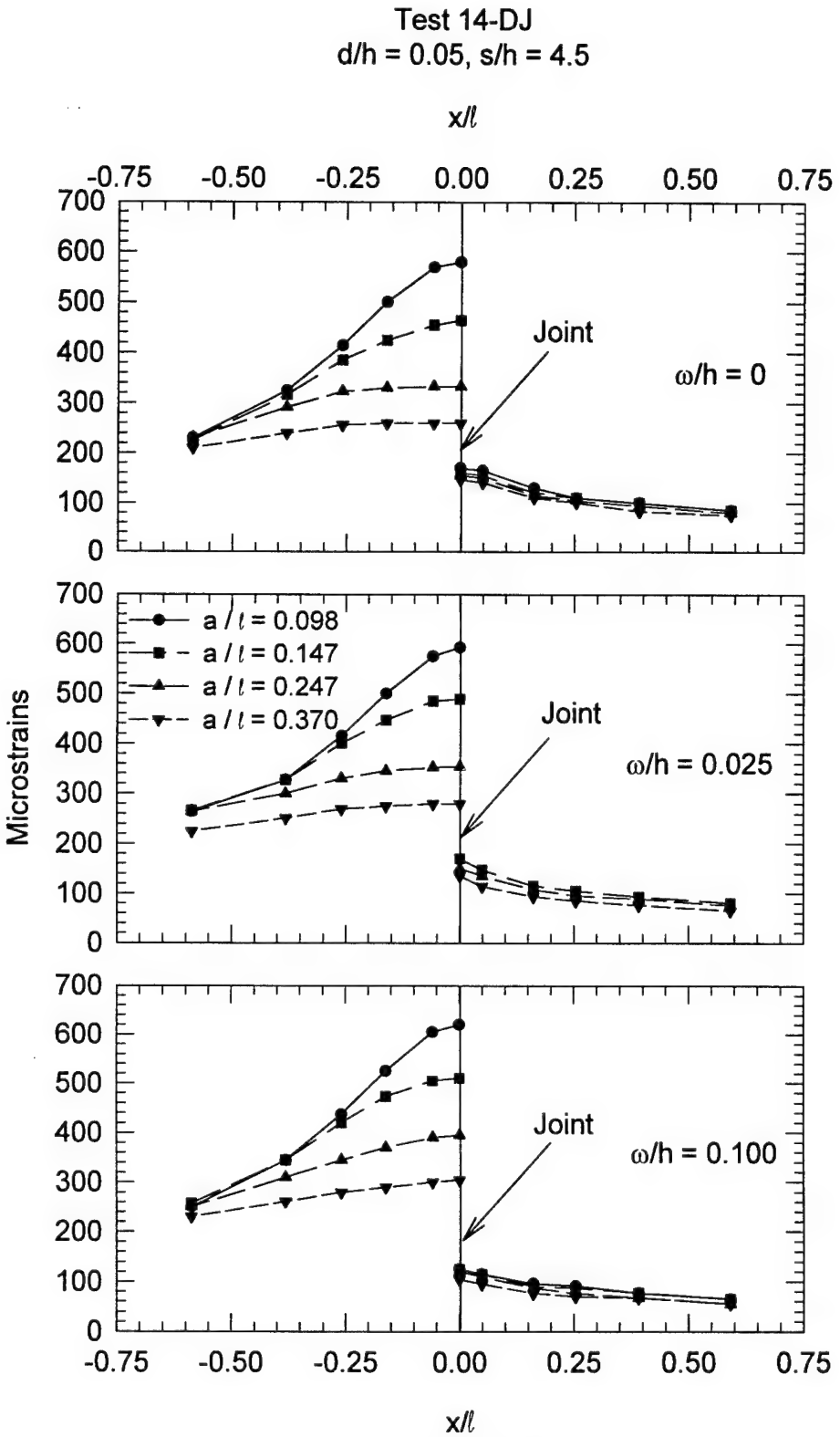
Test 14-DJ
d/h = 0.05, s/h = 4.5
x/ℓ
-0.75
-0.50
-0.25
0.00
0.25
0.50
0.75
Microstrains
0
100
200
300
400
500
600
700
Joint
ω/h = 0
ω/h = 0.025
ω/h = 0.100
a / ℓ = 0.098
a / ℓ = 0.147
a / ℓ = 0.247
a / ℓ = 0.370

PLATE A9

APPENDIX B

TABULATED JOINT RESPONSES FROM SMALL-SCALE MODEL TESTS

Table B1

Percent Load Transfer at Doweled Joint, Test 3-DJ

Footprint Radius *a* mm (in.)	Load Ratio *a/l*	Based on Strains 3 mm (0.12 in.) from Edge (by interpolation)			Based on Strains at Edge (by extrapolation)		
		Joint Opening, mm (in.)					
		0	0.127 (0.005)	0.508 (0.020)	0	0.127 (0.005)	0.508 (0.020)
At Dowels							
Load on Bonded-Dowel Side of Joint							
19 (0.75)	0.364	43.2	38.4	33.9	46.7	40.4	37.2
13 (0.50)	0.243	39.8	35.6	32.2	42.6	38.3	33.9
7.6 (0.30)	0.146	36.1	32.8	29.2	39.0	35.2	30.8
5.1 (0.20)	0.097	31.5	28.7	24.7	34.2	30.4	26.1
Load on Unbonded-Dowel Side of Joint							
19 (0.75)	0.364	41.0	34.2	30.3	44.2	36.0	31.3
13 (0.50)	0.243	37.3	32.9	29.1	40.4	34.1	29.7
7.6 (0.30)	0.146	33.4	29.9	26.6	35.6	30.9	26.8
5.1 (0.20)	0.097	27.5	24.8	22.1	28.6	25.2	22.5
Between Dowels							
Load on Bonded-Dowel Side of Joint							
19 (0.75)	0.364	36.7	34.4	32.6	36.2	34.3	32.1
13 (0.50)	0.243	34.9	32.5	29.8	33.9	32.3	28.7
7.6 (0.30)	0.146	33.8	29.2	27.1	32.9	28.1	26.1
5.1 (0.20)	0.097	29.5	25.8	24.3	28.3	24.2	23.9
Load on Unbonded-Dowel Side of Joint							
19 (0.75)	0.364	37.6	34.5	29.6	37.6	34.3	28.9
13 (0.50)	0.243	35.4	31.8	27.5	35.2	31.8	26.5
7.6 (0.30)	0.146	31.9	28.3	24.8	31.6	27.4	24.2
5.1 (0.20)	0.097	27.3	24.4	21.1	26.8	23.8	20.6

0.356-mm (0.014-in.) diameter dowels spaced at 12.7 mm (0.50 in.)

Bonded-dowel side 5.28 mm (0.208 in.) thick.

Unbonded-dowel side 5.41 (0.213 in.) thick.

Table B2
Percent Load Transfer at Doweled Joint, Test 4-DJ

Footprint Radius *a* mm (in.)	Load Ratio *a/l*	Based on Strains 3 mm (0.12 in.) from Edge (by interpolation) Joint Opening, mm (in.) 0	0.127 (0.005)	0.508 (0.020)	Based on Strains at Edge (by extrapolation) Joint Opening, mm (in.) 0	0.127 (0.005)	0.508 (0.020)
At Dowels							
Load on Bonded-Dowel Side of Joint							
19 (0.75)	0.370	47.0	44.3	41.2	50.0	47.1	42.6
13 (0.50)	0.247	44.9	42.1	39.7	48.3	45.3	42.0
7.6 (0.30)	0.148	40.9	39.3	36.2	43.8	42.8	38.4
5.1 (0.20)	0.099	38.0	36.5	33.3	41.0	39.1	35.4
Load on Unbonded-Dowel Side of Joint							
19 (0.75)	0.370	45.7	43.4	41.3	48.9	45.7	43.3
13 (0.50)	0.247	43.8	41.7	38.9	47.0	44.0	41.2
7.6 (0.30)	0.148	39.8	38.5	35.6	41.9	40.9	37.3
5.1 (0.20)	0.099	37.8	36.1	33.1	40.3	38.7	35.2
Between Dowels							
Load on Bonded-Dowel Side of Joint							
19 (0.75)	0.370	40.3	38.0	35.8	40.2	38.5	34.5
13 (0.50)	0.247	37.9	36.0	33.9	37.6	35.3	33.7
7.6 (0.30)	0.148	33.9	32.8	30.2	33.5	33.0	29.6
5.1 (0.20)	0.099	31.0	30.0	28.0	30.3	29.7	27.7
Load on Unbonded-Dowel Side of Joint							
19 (0.75)	0.370	38.3	34.5	32.6	37.9	33.8	31.7
13 (0.50)	0.247	36.2	33.6	30.9	35.3	33.0	30.1
7.6 (0.30)	0.148	32.9	30.7	28.8	32.1	29.7	28.0
5.1 (0.20)	0.099	30.7	28.7	26.6	29.4	27.8	25.3

0.508-mm (0.020-in.) diameter dowels spaced at 12.7 mm (0.50 in.)
Bonded-dowel side 5.18 mm (0.204 in.) thick.
Unbonded-dowel side 5.28 mm (0.208 in.) thick.

Table B3
Percent Load Transfer at Doweled Joint, Test 5-DJ

Footprint Radius *a* mm (in.)	Load Ratio *a/l*	Based on Strains 3 mm (0.12 in.) from Edge (by interpolation)			Based on Strains at Edge (by extrapolation)		
		Joint Opening, mm (in.)					
		0	0.127 (0.005)	0.508 (0.020)	0	0.127 (0.005)	0.508 (0.020)
At Dowels							
Load on Bonded-Dowel Side of Joint							
19 (0.75)	0.371	40.9	31.0	26.1	42.8	31.8	26.7
13 (0.50)	0.248	32.4	28.4	22.4	32.2	29.8	22.5
7.6 (0.30)	0.149	27.2	23.8	19.4	26.0	24.3	19.3
5.1 (0.20)	0.099	23.6	20.9	17.3	22.7	21.3	17.2
Load on Unbonded-Dowel Side of Joint							
19 (0.75)	0.371	40.3	32.3	27.4	43.4	33.6	28.4
13 (0.50)	0.248	35.9	30.0	25.0	38.1	31.8	25.7
7.6 (0.30)	0.149	30.9	26.1	20.5	32.1	26.9	21.0
5.1 (0.20)	0.099	27.0	21.8	19.4	27.8	23.0	20.0
Between Dowels							
Load on Bonded-Dowel Side of Joint							
19 (0.75)	0.371	34.2	30.7	24.7	33.8	29.0	23.8
13 (0.50)	0.248	30.2	27.9	21.8	29.9	27.0	20.7
7.6 (0.30)	0.149	26.1	24.1	18.4	25.6	23.3	17.2
5.1 (0.20)	0.099	22.7	20.5	17.0	20.9	19.3	15.9
Load on Unbonded-Dowel Side of Joint							
19 (0.75)	0.371	34.1	28.7	23.0	34.4	28.2	21.6
13 (0.50)	0.248	30.7	27.2	21.0	30.8	26.9	20.1
7.6 (0.30)	0.149	27.2	23.5	16.6	26.7	22.8	16.0
5.1 (0.20)	0.099	22.7	19.3	15.8	22.2	18.3	15.4

0.254-mm (0.010-in.) diameter dowels spaced at 12.7 mm (0.50 in.)
Bonded-dowel side 5.16 mm (0.203 in.) thick.
Unbonded-dowel side 5.26 mm (0.207 in.) thick.

Table B4
Percent Load Transfer at Doweled Joint, Test 6-DJ

Footprint Radius *a* mm (in.)	Load Ratio *a/l*	Based on Strains 3 mm (0.12 in.) from Edge (by interpolation) Joint Opening, mm (in.) 0	0.127 (0.005)	0.508 (0.020)	Based on Strains at Edge (by extrapolation) Joint Opening, mm (in.) 0	0.127 (0.005)	0.508 (0.020)
At Dowels							
Load on Bonded-Dowel Side of Joint							
19 (0.75)	0.370	47.2	44.5	42.4	51.0	46.7	43.8
13 (0.50)	0.247	44.3	42.7	40.4	47.2	44.7	42.6
7.6 (0.30)	0.148	41.5	39.2	36.5	45.1	40.1	37.9
5.1 (0.20)	0.099	38.4	36.2	33.9	40.1	37.2	33.9
Load on Unbonded-Dowel Side of Joint							
19 (0.75)	0.370	45.3	40.3	36.0	45.6	40.7	36.3
13 (0.50)	0.247	41.3	38.5	34.5	42.2	38.4	35.2
7.6 (0.30)	0.148	38.8	35.2	32.7	39.2	35.3	33.2
5.1 (0.20)	0.099	35.7	33.2	30.8	36.0	33.0	30.9
Between Dowels							
Load on Bonded-Dowel Side of Joint							
19 (0.75)	0.370	44.6	41.8	40.2	45.7	42.7	41.6
13 (0.50)	0.247	42.2	39.6	37.5	43.3	40.0	39.4
7.6 (0.30)	0.148	39.1	36.9	35.4	40.2	37.2	36.9
5.1 (0.20)	0.099	35.4	34.0	32.4	35.1	34.4	31.9
Load on Unbonded-Dowel Side of Joint							
19 (0.75)	0.370	44.4	40.1	36.8	45.3	39.6	36.4
13 (0.50)	0.247	42.1	38.8	35.0	42.9	38.7	34.8
7.6 (0.30)	0.148	38.7	35.5	32.7	39.0	35.5	32.5
5.1 (0.20)	0.099	36.3	32.7	30.7	36.0	32.3	30.6

0.508-mm (0.020-in.) diameter dowels spaced at 7.62 mm (0.30 in.)
Bonded-dowel side 5.26 mm (0.207 in.) thick.
Unbonded-dowel side 5.21 mm (0.205 in.) thick.

Table B5
Percent Load Transfer at Doweled Joint, Test 7-DJ

Footprint Radius *a* mm (in.)	Load Ratio *a/l*	Based on Strains 3 mm (0.12 in.) from Edge (by interpolation)			Based on Strains at Edge (by extrapolation)		
		Joint Opening, mm (in.)					
		0	0.127 (0.005)	0.508 (0.020)	0	0.127 (0.005)	0.508 (0.020)
At Dowels							
Load on Bonded-Dowel Side of Joint							
19 (0.75)	0.365	39.8	36.7	34.8	40.4	37.8	35.1
13 (0.50)	0.243	36.4	35.1	33.5	37.0	35.9	33.6
7.6 (0.30)	0.146	32.5	32.2	30.3	33.8	33.1	30.5
5.1 (0.20)	0.097	29.6	29.5	27.3	30.1	31.0	27.1
Load on Unbonded-Dowel Side of Joint							
19 (0.75)	0.365	36.2	32.8	29.7	36.6	33.0	29.2
13 (0.50)	0.243	34.2	30.8	27.8	34.6	31.0	27.5
7.6 (0.30)	0.146	30.5	28.8	26.0	30.1	28.2	26.2
5.1 (0.20)	0.097	27.8	26.8	24.5	28.2	26.7	24.5
Between Dowels							
Load on Bonded-Dowel Side of Joint							
19 (0.75)	0.365	34.9	31.4	31.1	35.1	31.4	31.4
13 (0.50)	0.243	31.9	29.9	28.6	31.4	30.0	28.1
7.6 (0.30)	0.146	28.5	27.5	25.9	27.9	28.0	25.9
5.1 (0.20)	0.097	25.7	25.4	23.0	25.2	25.5	22.7
Load on Unbonded-Dowel Side of Joint							
19 (0.75)	0.365	41.1	36.2	33.3	42.2	37.3	33.8
13 (0.50)	0.243	38.3	34.8	30.6	38.7	35.3	30.3
7.6 (0.30)	0.146	34.0	31.8	28.6	34.8	31.6	28.0
5.1 (0.20)	0.097	30.6	29.6	26.7	31.3	30.3	26.1

0.356-mm (0.014-in.) diameter dowels spaced at 7.6 mm (0.30 in.)
Bonded-dowel side 5.33 mm (0.210 in.) thick.
Unbonded-dowel side 5.33 mm (0.210 in.) thick.

Table B6
Percent Load Transfer at Doweled Joint, Test 8-DJ

Footprint Radius *a* mm (in.)	Load Ratio *a/l*	Based on Strains 3 mm (0.12 in.) from Edge (by interpolation) Joint Opening, mm (in.) 0	0.127 (0.005)	0.508 (0.020)	Based on Strains at Edge (by extrapolation) Joint Opening, mm (in.) 0	0.127 (0.005)	0.508 (0.020)
At Dowels							
Load on Bonded-Dowel Side of Joint							
19 (0.75)	0.373	35.1	32.9	30.6	35.5	32.3	31.5
13 (0.50)	0.249	31.9	31.5	27.4	31.6	30.9	27.3
7.6 (0.30)	0.149	28.6	28.8	23.9	27.8	28.8	23.7
5.1 (0.20)	0.100	25.2	24.6	20.5	25.2	24.1	21.3
Load on Unbonded-Dowel Side of Joint							
19 (0.75)	0.373	37.8	33.5	27.6	39.2	33.7	28.6
13 (0.50)	0.249	34.3	31.9	26.2	36.1	31.9	26.8
7.6 (0.30)	0.149	30.1	29.7	23.6	30.7	30.2	24.8
5.1 (0.20)	0.100	25.2	24.9	19.5	26.1	25.0	20.4
Between Dowels							
Load on Bonded-Dowel Side of Joint							
19 (0.75)	0.373	33.3	31.1	28.4	32.7	31.0	28.7
13 (0.50)	0.249	29.8	29.6	25.4	29.3	29.2	25.0
7.6 (0.30)	0.149	26.7	26.1	21.9	25.8	25.8	21.0
5.1 (0.20)	0.100	22.5	22.3	18.6	21.4	21.4	17.8
Load on Unbonded-Dowel Side of Joint							
19 (0.75)	0.373	33.1	28.2	24.4	33.0	28.5	23.9
13 (0.50)	0.249	29.6	27.7	23.0	29.2	27.4	22.4
7.6 (0.30)	0.149	26.5	25.2	20.7	25.4	24.8	20.2
5.1 (0.20)	0.100	21.2	20.3	17.0	20.2	19.4	16.1

0.254-mm (0.010-in.) diameter dowels spaced at 7.6 mm (0.30 in.)
Bonded-dowel side 5.05 mm (0.199 in.) thick.
Unbonded-dowel side 5.28 (0.208 in.) thick.

Table B7
Percent Load Transfer at Doweled Joint, Test 12-DJ

Footprint Radius *a* mm (in.)	Load Ratio *a/l*	Based on Strains 3 mm (0.12 in.) from Edge (by interpolation) Joint Opening, mm (in.) 0	0.127 (0.005)	0.508 (0.020)	Based on Strains at Edge (by extrapolation) Joint Opening, mm (in.) 0	0.127 (0.005)	0.508 (0.020)
At Dowels							
Load on Bonded-Dowel Side of Joint							
19 (0.75)	0.371	47.2	43.2	40.0	53.1	49.0	44.9
13 (0.50)	0.248	42.9	40.9	37.4	50.2	47.4	41.7
7.6 (0.30)	0.149	39.2	38.2	33.9	44.4	44.0	37.8
5.1 (0.20)	0.099	34.2	33.0	28.8	39.3	37.9	31.5
Load on Unbonded-Dowel Side of Joint							
19 (0.75)	0.371	48.9	45.5	40.1	54.3	51.3	39.7
13 (0.50)	0.248	46.1	44.1	38.6	51.5	49.9	38.6
7.6 (0.30)	0.149	41.2	40.5	35.1	45.1	46.4	35.0
5.1 (0.20)	0.099	38.0	36.1	31.4	42.5	41.6	30.6
Between Dowels							
Load on Bonded-Dowel Side of Joint							
19 (0.75)	0.371	35.0	34.0	31.9	33.7	34.1	32.8
13 (0.50)	0.248	32.0	31.1	28.4	31.4	30.3	27.5
7.6 (0.30)	0.149	29.2	27.6	25.4	28.7	27.5	25.0
5.1 (0.20)	0.099	24.6	24.2	22.0	24.0	23.2	20.8
Load on Unbonded-Dowel Side of Joint							
19 (0.75)	0.371	37.4	33.9	30.5	36.9	33.3	30.4
13 (0.50)	0.248	33.2	31.6	28.1	32.9	30.8	28.1
7.6 (0.30)	0.149	32.8	27.8	25.1	32.0	27.2	23.9
5.1 (0.20)	0.099	27.0	24.9	22.1	26.5	24.4	21.7

0.020-in. diameter dowels spaced at 0.90 in.
Bonded-dowel side 0.203-in. thick.
Unbonded-dowel side 0.207-in. thick.

Table B8

Percent Load Transfer at Doweled Joint, Test 13-DJ

Footprint Radius *a* mm (in.)	Load Ratio *a/l*	Based on Strains 3 mm (0.12 in.) from Edge (by interpolation)			Based on Strains at Edge (by extrapolation)		
		Joint Opening, mm (in.)					
		0	0.127 (0.005)	0.508 (0.020)	0	0.127 (0.005)	0.508 (0.020)
At Dowels							
Load on Bonded-Dowel Side of Joint							
19 (0.75)	0.374	50.3	43.1	40.5	58.6	48.5	46.4
13 (0.50)	0.249	44.9	40.6	37.1	52.4	47.2	42.0
7.6 (0.30)	0.150	39.3	36.0	32.1	45.8	40.5	36.1
5.1 (0.20)	0.100	35.0	33.8	29.2	40.8	37.7	32.4
Load on Unbonded-Dowel Side of Joint							
19 (0.75)	0.374	46.3	36.7	35.6	52.8	40.0	39.7
13 (0.50)	0.249	39.3	35.5	33.5	45.0	39.8	37.3
7.6 (0.30)	0.150	33.5	29.6	27.5	36.8	33.6	30.2
5.1 (0.20)	0.100	29.4	28.3	25.2	31.6	31.2	27.5
Between Dowels							
Load on Bonded-Dowel Side of Joint							
19 (0.75)	0.374	31.7	28.5	26.7	30.9	26.9	25.5
13 (0.50)	0.249	28.5	26.5	24.3	27.2	25.4	22.6
7.6 (0.30)	0.150	24.4	22.7	20.7	23.1	20.8	19.8
5.1 (0.20)	0.100	21.3	20.8	18.4	20.2	19.8	17.4
Load on Unbonded-Dowel Side of Joint							
19 (0.75)	0.374	32.2	28.2	25.1	29.1	26.9	23.7
13 (0.50)	0.249	27.3	25.6	22.6	25.3	24.2	20.6
7.6 (0.30)	0.150	24.0	22.5	18.9	22.2	19.4	18.1
5.1 (0.20)	0.100	19.8	20.6	17.3	18.0	18.5	16.1

0.356-mm (0.014-in.) diameter dowels spaced at 22.9 mm (0.90 in.)
Bonded-dowel side 5.11 mm (0.201 in.) thick.
Unbonded-dowel side 5.21 mm (0.205 in.) thick.

Table B9
Percent Load Transfer at Doweled Joint, Test 14-DJ

Footprint Radius *a* mm (in.)	Load Ratio *a/l*	Based on Strains 3 mm (0.12 in.) from Edge (by interpolation) Joint Opening, mm (in.) 0	0.127 (0.005)	0.508 (0.020)	Based on Strains at Edge (by extrapolation) Joint Opening, mm (in.) 0	0.127 (0.005)	0.508 (0.020)
At Dowels							
Load on Bonded-Dowel Side of Joint							
19 (0.75)	0.367	38.6	30.4	24.7	41.3	34.5	26.4
13 (0.50)	0.244	32.0	28.0	23.3	34.0	31.6	24.6
7.6 (0.30)	0.147	26.9	23.1	19.2	28.0	26.8	20.3
5.1 (0.20)	0.098	22.5	21.5	17.1	23.2	24.3	18.0
Load on Unbonded-Dowel Side of Joint							
19 (0.75)	0.367	34.9	28.4	23.6	36.0	32.3	25.5
13 (0.50)	0.244	30.2	27.3	22.4	31.6	30.5	23.9
7.6 (0.30)	0.147	26.2	21.5	17.5	26.8	24.8	18.9
5.1 (0.20)	0.098	20.9	19.9	15.4	21.7	22.8	16.4
Between Dowels							
Load on Bonded-Dowel Side of Joint							
19 (0.75)	0.367	26.5	24.3	18.9	24.4	24.2	17.8
13 (0.50)	0.244	22.7	21.8	16.6	21.0	21.3	15.7
7.6 (0.30)	0.147	19.3	17.7	14.5	17.9	16.6	13.8
5.1 (0.20)	0.098	15.0	16.1	12.9	14.0	15.3	11.8
Load on Unbonded-Dowel Side of Joint							
19 (0.75)	0.367	25.8	21.8	17.2	24.3	20.7	16.5
13 (0.50)	0.244	22.4	20.1	15.4	21.5	19.0	14.6
7.6 (0.30)	0.147	17.9	15.8	11.5	16.9	15.2	10.9
5.1 (0.20)	0.098	13.6	13.9	11.7	12.8	13.0	11.1

0.254-mm (0.010-in.) diameter dowels spaced at 0.90 in.
Bonded-dowel side 5.26 mm (0.207 in.) thick.
Unbonded-dowel side 5.33 mm (0.210 in.) thick.